EFFECT OF CONCRETE TYPE ON FLEXURAL BEHAVIOR OF CONCRETE

BEAMS REINFORCED WITH HSS BARS

by

Saif Maad Aldabagh

A Thesis Presented to the Faculty of the
American University of Sharjah
College of Engineering
in Partial Fulfillment
of the Requirements
for the Degree of

Master of Science in
Civil Engineering

Sharjah, United Arab Emirates

March 2016

Approval Signatures

We, the undersigned, approve the Master's Thesis of Saif Maad Aldabagh.

Thesis Title: Effect of Concrete Type on Flexural Behavior of Concrete Beams Reinforced with HSS Bars

Signature   **Date of Signature**
                                                                  (dd/mm/yyyy)

_____   _____
Dr. Farid H. Abed
Associate Professor, Department of Civil Engineering
Thesis Advisor

_____   _____
Dr. Sherif Yehia
Professor, Department of Civil Engineering
Thesis Co-Advisor

_____   _____
Dr. Adil Al-Tamimi
Professor, Department of Civil Engineering
Thesis Committee Member

_____   _____
Dr. Basil Darras
Associate Professor, Department of Mechanical Engineering
Thesis Committee Member

_____   _____
Dr. Ali Osman Akan
Head, Department of Civil Engineering

_____   _____
Dr. Mohamed El Tarhuni
Associate Dean, College of Engineering

_____   _____
Dr. Leland Blank
Dean of Engineering

_____   _____
Dr. Khaled Assaleh
Interim Vice Provost for Research and Graduate Studies

Acknowledgment

Dedication

To my beloved parents,

Without whom I wouldn't make it up to here

Abstract

High-Strength Steel (HSS) bars can be a promising alternative to commonly used mild steel since they have the potential of making more efficient use of high-performance concrete and reducing the required number and size of the reinforcement. The main shortcomings associated with utilizing HSS bars in concrete beams are related to the cracking behavior of these beams at service load and the possibility of concrete crushing prior to steel yielding. This research investigates the effect of using high-strength concrete, fiber-reinforced concrete and compression reinforcement to enhance the flexural behavior of HSS-RC beams. Twenty four beams singly and doubly reinforced with high-strength steel bars were cast using plain concrete, steel fiber and synthetic fiber-reinforced concrete. In addition, concrete compressive strength of 50 and 80 MPa were used in the investigation. Four-point loading flexure tests were conducted on all beams. The flexure test results showed that increasing the concrete compressive strength contributes the most to the flexural capacity in steel fiber-reinforced concrete specimens. The concrete compression strain at mid-span's top surface of steel fiber-reinforced specimens reached up to 0.0039 prior to ultimate loading which, in turn, enhanced the flexural capacity. Results also indicated that highest curvature ductility was achieved by synthetic fiber-reinforced concrete beams with $f'c = 80$ MPa. The deep propagation of cracks was noticeably restrained at service and steel yielding load in fiber-reinforced specimens. In addition, the applicability of ACI ITG-6R-10 recommendations was evaluated using the results of plain concrete specimens and then extended to cover fiber-reinforced concrete beams. A nonlinear finite element model was developed and verified to evaluate the effect of utilizing different reinforcement ratios on the flexural behavior of the HSS-bar reinforced concrete beams.

Search Terms: High-strength reinforcing steel; High-strength concrete, Fiber reinforced concrete; Flexural strength; Cracking behavior, Non-linear finite element

Table of Contents

List of Figures

List of Tables

List of Abbreviations

A_s = area of nonprestressed longitudinal tension reinforcement, mm^2

a = depth of equivalent rectangular stress block as defined in section 10.2.7.1 of ACI 318-08, mm

C = force in the compression zone of a beam, N

T = force in the tension reinforcement of a beam, N

f_y = specified yield strength of tension reinforcement, MPa

$f_c{}'$ = specified compressive strength of concrete, MPa

ε_s = strain in tension reinforcement

$c_b = C_{min} + 0.5d_b$, mm

C_{max} = maximum value of C_S or C_{bb}, mm

C_{min} = minimum value of C_S or C_{bb}, mm

C_s = minimum value of $C_{si} + 6.35$ mm or $S_{so,}$ mm, S_{si} may be used in lieu of $S_{si} + 6.35$ mm

C_{si} = one-half of average clear spacing between bars or lap splices in a single layer, mm

C_{So} = clear cover of reinforcement being developed or lap spliced, measured to side face of member, mm

ω = factor reflecting benift of large cover/spacing perpendicular to controlling cover/spacing = $0.1\,(C_{max}/C_{min}) + 0.9 \leq 1.25$

d_b = bar diameter, mm

k_{tr} = transverse reinforcement index

A_{tr} = total cross-sectional area of all transverse reinforcement, mm

t_d = bar diameter factor, mm

t_r = term representing the effect of relative rib area

β_1 = factor relating depth of equivalent rectangular compressive stress block to neutral axis depth

Chapter 1: Introduction

As technology advances, reinforcing steel bars made of new steel grades are being introduced to the construction industry. High-strength steel (HSS) which is characterized by a yield strength of 689 MPa is expected to be one of the promising alternatives to the commonly used mild steel, particularly in heavily reinforced members. As per the ASTM specifications, HSS can be specified as A1035 CS Grade 689 based on its chemical composition and tensile properties [1]. The 689 MPa yield strength allows designers to use smaller cross-sectional area of reinforcement when compared to the traditional 414 MPa reinforcing bars. This may result in reducing the number of reinforcing bars in a certain concrete section, i.e., less bar congestion, leading to an improved placement productivity and workability of the concrete. Moreover, since ASTM A1035 bar-reinforced concrete members require less amount of reinforcement, the total required tonnage of reinforcement is susceptible to substantial reductions, resulting in reducing labor cost and the time required for placing the reinforcing bars. By investigating the productivity benefits of using the ASTM A1035 Grade 689 steel versus ASTM A615 Grade 414 steel, a 36% reduction in the weight of reinforcement in beams was reported [2]. However, insignificant benefit was noticed when using ASTM A1035 Grade 689 reinforcement in slabs, post-tensioned girders and columns. The same study also recommended substituting ASTM A615 Grade 414 with ASTM A1035 Grade 689 in expensive labor market in order to offset the material cost by substantial reduction in labor costs. ASTM A1035 Grade 689 is more corrosion resistant than conventional ASTM A615 Grade 414 which can be beneficial to structures located in harsh environments with severe exposure conditions. ASTM A1035 can be between two and ten times more capable of resisting corrosion than the commonly used ASTM A615 Grade 414 [3].

Promoting the use of High-strength steel in the construction industry, specifically as longitudinal reinforcement in flexural members, allows designers to make use of its above mentioned potential advantages. However, the current ACI code (ACI 318-14) permits the use of ASTM A1035 rebars as lateral support of longitudinal bars but not as longitudinal bars in flexural members [4]. This indicates that more research needs to be done in order to overcome the main shortcomings associated with utilizing HSS rebars in flexural members. Since HSS rebar yields at higher stress than

that of conventional mild steel rebar, HSS rebars in flexural members undergo higher strains which can result in: the possibility of concrete crushing prior to the yielding of HSS reinforcement, high target strain limit for the section to be classified as tension-controlled and the development of excessively wide cracks.

Adopting concrete mixes with enhanced properties in flexural members reinforced with HSS bars can be an approach to overcome the aforementioned drawbacks. High-strength concrete (HSC) and fiber reinforced concrete (FRC) are two of the promising concrete types whose effects on the flexural behavior of concrete beams reinforced with HSS bars have not yet been investigated. Therefore, this study is mainly intended to evaluate the effect of utilizing different HSC and FRC mixes on the moment capacity, curvature ductility, cracking behavior and crack widths of HSS-RC beams. In addition, it evaluates the applicability of current design recommendations to accommodate the use of HSS rebars in flexure using plain concrete as well as fiber-reinforced concrete specimens.

1.1 Problem Statement

In August 2010, the American Concrete Institute (ACI) released the *Design guide for the use of ASTM A1035/A1035M Grade 100 (690) steel bars for structural concrete* (ACI innovation Task group 6 2010) (henceforth ACI-ITG-6R-10) which provided comprehensive design recommendation for concrete members reinforced with HSS bars [5]. However, practicing structural designers have commonly used it only as confinement steel in structural members located in active seismic regions. This could be attributed to certain behaviors found in concrete beams reinforced with Grade 689 steel. As discussed earlier, Grade 689 steel yields at higher strain than that of Grade 414 which makes the concrete more susceptible to compression failure prior to steel yielding. Furthermore, strain in the tension steel is one of the main variables affecting the crack widths; therefore, in HSS bar-reinforced beams where the reinforcing bars are subjected to high strains, the crack widths can be another concern, particularly at service load. Introducing either HSC, FRC, or compression reinforcement can delay the crushing of concrete by strengthening the concrete compression zone and thus allow the HSS reinforcement to engage efficiently in the section. In addition, the capability of fibers in FRC to bridge between cracks can be highly effective in controlling the crack depths and widths, particularly at service load levels.

1.2 Significance of the project

The capability of HSS reinforcement to reduce the required cross-sectional area of longitudinal reinforcement in flexural members can lead to substantial reductions in the cost of concrete structures which are normally comprised of several flexural members. However, this will not be possible unless building design codes such as the ACI 318 permits the use of such reinforcement in flexural applications. Although the ACI-ITG-6R-10 provides the necessary guidelines for structural designers to utilize HSS reinforcing bars in flexural members, local municipalities might not approve them since they have not been incorporated into the ACI 318 design codes.

In this study, the effect of varying the concrete compressive strength, concrete type and reinforcement arrangement on the overall flexural performance of concrete beams reinforced with HSS bars is evaluated. This results in determining an optimum section in which the HSS reinforcing bars are capable of developing the highest moment capacity and are characterized with a controlled cracking behavior.

In addition, the adequacy of ACI-ITG-6R-10 recommendations are initially evaluated in case of specimens with plain concrete and then extended to cover specimens with fiber reinforced concrete. Documenting the behavior of HSS-RC beams cast with different types of concrete with concrete compressive strengths is expected to reduce the uncertainty associated with using HSS as longitudinal reinforcement in flexural members. This, in turn, could encourage building codes reporting committees such as the ACI Committee 318 to consider ASTM A1035 Grade 689 rebars to be applicable for flexural applications if being coupled with certain type of concrete.

1.3 Objectives

This research aims at evaluating the effect of adopting different concrete mixes with enhanced properties on the flexural performance of concrete beams reinforced with HSS bars. To achieve this main objective, the following approaches are proposed:

1. Improve concrete properties by:
   A. Using two types of concrete; one with compressive strength $f'_c = 50$ MPa that is commonly used in the Gulf region and another with high compressive strength of 80 MPa.

B. Introducing fibers (steel and synthetic) within the concrete mix, resulting in a concrete mix characterized by high strength, high ductility and better crack control, which are considered common features of FRC.

2. Enhance the capacity of the section through the addition of compression steel

The proposed solutions are evaluated from the following different perspectives:

1. Material testing: Investigate the mechanical properties of different concrete mixes to evaluate their performances at the martial level. Study the effects of adding fibers to the mix on the concrete properties.

2. Flexural test: Understand the flexural behavior of sections reinforced with high-strength steel under four-point loading setup. Capture any improvements in the ultimate compression strain at mid-span at the top fibers of the concrete. Monitor the cracking behavior and crack widths at different stress levels in the HSS reinforcing bars.

3. Pull-out test: Investigate the bond behavior of HSS with different concrete mixes for further understanding of its surface contact behavior and the required development length. In order for the concrete to resist the flexural compressive forces or for the reinforcement to provide the flexural tensile forces, there has to be sufficient bond between the two materials.

4. Analytical program: Evaluate the applicability of the ACI-ITG-6R-10 recommendations to calculate the flexural capacity of HSS bar-reinforced specimens cast with plain and FRC. In addition, the accuracy of the modified version of Forsch equation in predicating the crack widths in HSS-RC beams at loads corresponding to different stresses in the reinforcing steel is evaluated.

5. Finite Element analysis: Develop a non-linear finite element (FE) model to capture more details on the effect of adopting concrete having higher compressive strength on the flexural behavior of members having single and doubly HSS bar-reinforced sections. The FE model will be verified based on the experimental results. The verified model will be used to conduct a parametric study investigating the effect of varying the tension and compression reinforcement ratios on the flexural capacity.

1.4 Thesis Structure

The thesis starts with the introduction chapter which introduces HSS material and its potential advantages when being utilized as longitudinal reinforcing bars in flexural members. The chapter also states the problem being investigated and significance of the study. The second chapter provides the necessary background to build up sufficient knowledge to understand the properties of different materials used in the research, such as: HSS, HSC and FRC. Chapter 2 also introduces and discusses research outcomes of others who studied the effect of utilizing the concrete types considered on the behavior of flexural members reinforced with materials exhibiting high tensile strength (similar to HSS) such as fiber reinforced plastic (FRP) and prestressing steel. Chapter 3 describes the adopted experimental program in details. It states the test setup and instrumentation for flexure and pullout tests. The results of the experimental program are presented in Chapter 4 and then discussed in Chapter 5 to capture the main contributions of using high concrete compressive strength, compression steel, and steel and synthetic fibers in FRC to the overall flexural behavior. Chapter 6 evaluates the current design recommendations based on the experimental results and then examines crack widths prediction models. Chapter 7 provides detailed description of the development and verification of the FE model. The thesis ends with Chapter 8 which presents main conclusions and provides several recommendations for structural designers.

Chapter 2: Background and Literature Review

2.1. High-Strength Steel

High-strength steel reinforcing rebars exhibit higher yield strength than that of commonly used mild steel. The HSS reinforcing bars, commercially known as ChrōmX 9000 (formally $MMFX_2$), used in this research are adopted by the American Society for Testing and Materials (ASTM) through its A1035 CS Grade 690 standard [1]. The commonly used mild steel exhibits a plateau in its post-yielding response; therefore, its yield strength can be easily determined using the 0.2 % method suggested by ACI 318-14 [4]. For example, the yield strength of the conventional 414 MPa steel determined using the suggested 0.2 % offset method is found to be 420 MPa with a corresponding slope (Young's Modulus) of 200 GPa. On the contrary, HSS exhibits neither a well-defined yield point nor a yielding plateau in its stress-strain response, which leads to some variability in the established yield strength. The uncertainty associated with defining the yield strength of HSS reinforcing bars was one of the main reasons behind limiting their strength capabilities when utilized in flexural members. Figure 1 shows stress-strain relationships for different types of high-strength steels compared with the stress-strain relationship for conventional Grade 414 MPa [6].
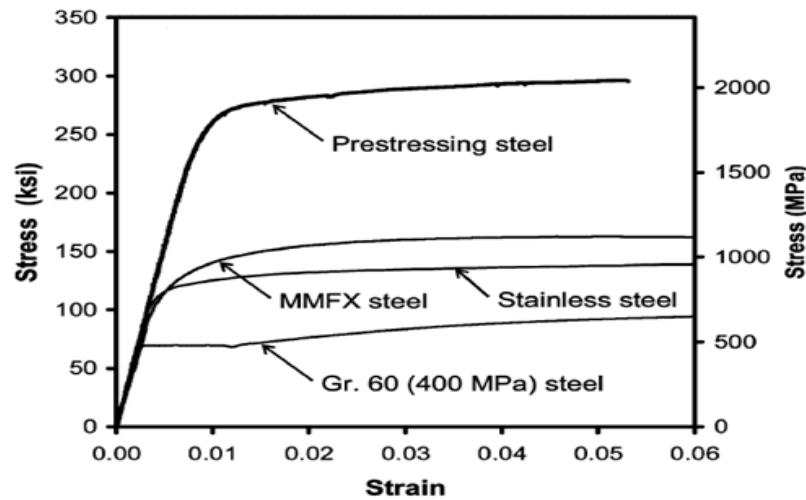
Figure 1: Stress-strain responses of different types of reinforcing steel [6]

Different approaches that can be used to capture the yield strength of bars without a well-defined yield plateau were found in the literature. These approaches are: (1) the 0.35 % extension under load (EUL) method, (2) the 0.5 % EUL method and (3) the 0.2 % offset method [7]. Figure 2 illustrates how the aforementioned approaches can be used to establish the yield strength of bars without a well-defined yield plateau.
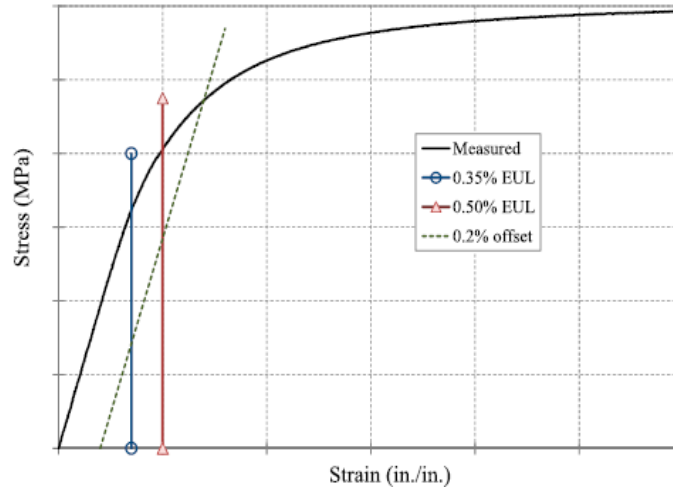
Figure 2: Various approaches to determine the yield strength [7]

In any strain compatibility and equilibrium analysis of a reinforced concrete beam's section, an equivalent concrete stress block model is assigned to the concrete while an elastic perfectly-plastic design model is assigned to the reinforcing steel. Such analysis is part of a common procedure that is used to compute section's design capacity. Due to the uncertainty associated with capturing the yield strength of HSS, previous design codes (up to the ACI-318-08) limited the yield strength of HSS bars to 551 MPa in any strain compatibility and equilibrium analysis [8]. However, the yield strength of the high-strength reinforcing steel used in design was increased to 689 MPa based on a simplified stress-strain model proposed by Mast et al. [6]. The simplified model with yield strength of 689 MPa was incorporated into the ACI-ITG-6R-10 but not into the ACI-318 design codes [5]. The simplified model assumes elastic perfectly-plastic stress-strain relationship consisting of a linear portion with a slope of 200 GPa, followed by a yielding plateau with a yielding stress of 689 MPa. Figure 3 demonstrates how the simplified model is making more use of the HSS strength when compared to the previous ACI limitations [6].
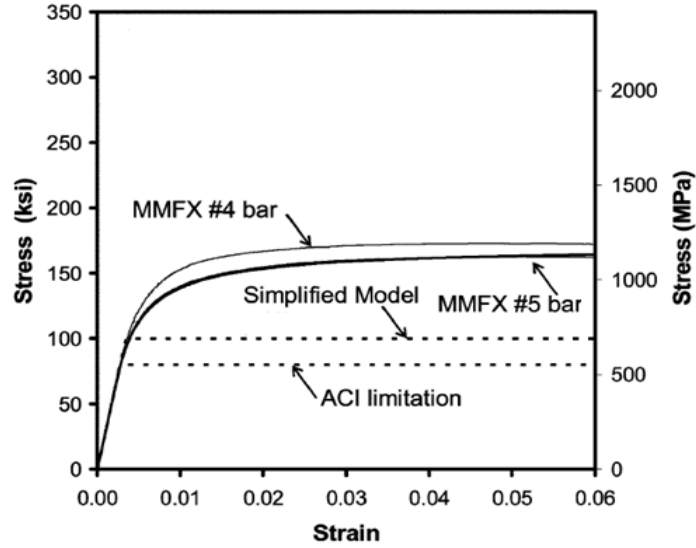
Figure 3: Previous and current limitations and material models [6]

The proposed simplified design model is found to be conservative when computing the nominal flexural capacities of members with different steel ratios as illustrated in Figure 4 [6]. It can be seen form Figure 4 that when the steel reinforcement ratio exceeds 3.95 %, the nominal moment capacity is equal for all of the different material models as the failure of heavily reinforced sections is governed by the crushing of concrete regardless of the adopted model. The figure also illustrates experimental results of beams reinforced with HSS tested at the Florida Department of Transportation (DOT) and at the University of North Florida (UNF).
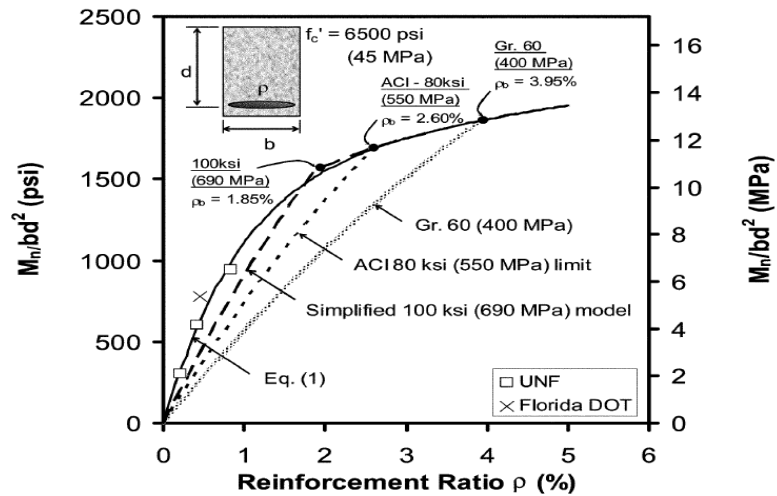
Figure 4: Nominal moment capacity as a function of steel reinforcement ratio [6]

20

Similar to the ACI design codes and up to 2012, the American Association of State Highway and Transportation Officials (AASHTO) had an upper limit of 515 MPa yield strength for HSS bars when utilized as flexural reinforcement. In 2007, the National Cooperative Highway Research Program (NCHRP) initiated a project to reevaluate the AASHTO design provisions related to the use of HSS in structural applications. Based on the findings of Shahrooz et al. [7], a number of sections in the AASHTO were modified to allow reinforcing bars with yield strength up to 689 MPa to be used in design. In the AASHTO (2013) edition, it is advised to adopt an elastic perfectly-plastic model in which the yield strength is established using a stress value that corresponds to a strain equal to 0.0035 or 0.005 [9]. Adopting an elastic-perfectly plastic stress-strain relationship for a yield strength of 689 MPa, which approximately corresponds to a strain of 0.004, was found to be conservative when computing the flexural capacity of flexural members reinforced with ASTM A1035. However, the yield strength of HSS reinforcing rebars used in the analysis is still restricted to the strain corresponding to 0.0035 under two conditions which are: (1) reinforcement ratio exceeding 0.026 and (2) concrete compressive strength exceeding 69 MPa to ensure conservative predictions of flexural nominal capacities when using strain compatibility and equilibrium analysis [7]. ASTM A1035 reinforcing bars are excluded from the aforementioned limitation, and their yield strength at strain of 0.0035 may be taken as 689 MPa.

As for the chemical composition, HSS is composed of a low carbon micro-composite Fe-C-Cr-Mn alloy which is characterized by an average chromium content of 9 %. The chemical compositions of a typical ChrōmX 9000, as provided by the manufacturer, are shown in Table 1.

Table 1: Chemical compositions (weight %)

Element	Carbon	Chromium	Manganese	Nitrogen	Phosphorous	Sulfur	Silicon
Typical ChrōmX 9000	0.08	9	0.5	0.05	0.035	0.045	0.5

Since the chromium content is less than 10.5 %, ChrōmX 9000 cannot be referred to as "stainless steel", yet it still exhibits considerably higher corrosion resistance

capabilities compared to traditional reinforcing steel. High-strength steel can be up to 10 times more corrosion resistant than the commonly used ASTM A615 reinforcing steel [3].

2.2 High-Strength Concrete

According to the ACI 363R-10 [10], high strength concrete (HSC) is characterized by a compressive strength (f'_c) greater than 55 MPa. Previous research on HSC shows that the stress-strain response of HSC is characterized by a strain at maximum compressive strength that increases as the maximum compressive strength increases [11]. Figure 5 shows this phenomenon in the stress-strain responses of concrete with different compressive strengths. Experimental tests show that as the compressive strength of concrete increases, it exhibits more brittle behavior [11].
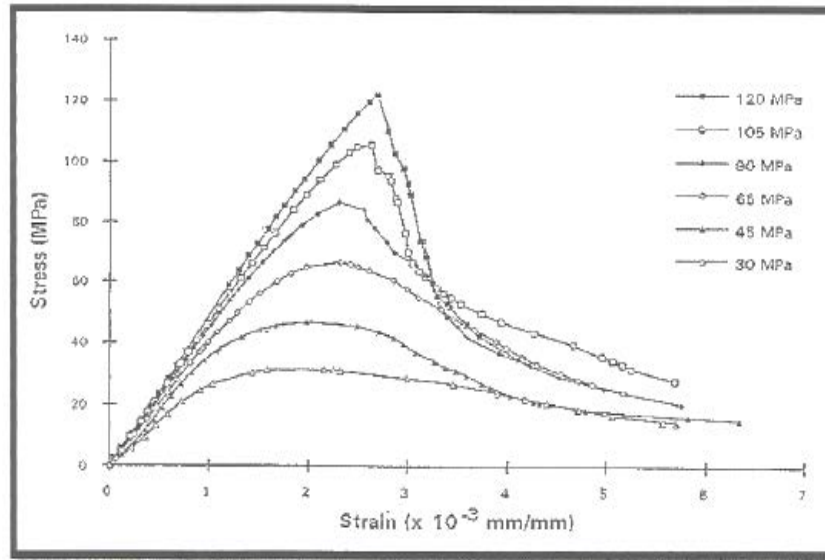
Figure 5: Stress-strain responses of concrete with different compressive strengths [11]

Since the Young's modulus of concrete varies in its compressive strength, ACI 318-14 permits the use of Equation (1) to compute the modulus of elasticity for normal strength concrete [4].

$$E_c = 4700\sqrt{f'_c} \tag{1}$$

where f'_c in MPa. As for concrete with f'_c ranging from 25 to 85 to MPa, ACI 363R-10 permits the use of Equation (2) to compute the modulus of elasticity of the concrete [10].

$$E_c = 9500 \, (f'_c)^{0.3} \tag{2}$$

where f'_c in MPa. To avoid sudden failure in RC members utilizing HSC, it is essential to investigate the strain capacity of HSC. The NCHRP project conducted both pure flexure and combined axial and flexure loading tests on beams with compressive strengths up to 124 MPa and found that the recorded strain values in concrete at ultimate ranged between 0.003 and 0.004 [12]. It was, therefore, recommended that the concrete compression strain must be set to 0.003 in any strain compatibility analysis to ensure the conservativeness of the results. Figure 6 shows the proposed value of concrete compression strain of 0.003 which provides a lower bound for all the recorded ultimate strain limits. However, the NCHRP report suggests that proposing a strain of 0.004 to be used as the concrete compression strain in a compatibility analysis is still appropriate [12].
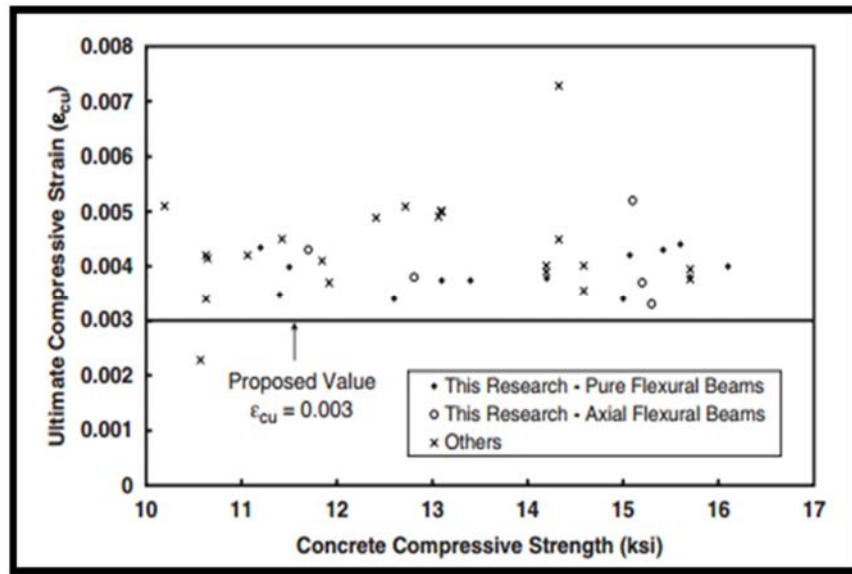
Figure 6: Ultimate strain limits from experimental tests [12]

2.3 Fiber Reinforced Concrete

Fiber-reinforced concrete (FRC) with high concrete compressive strength is also a recommended type of concrete in structural applications associated with the use of HSS. According to tests carried out on concrete mixes containing different types of fibers such as smooth, hooked and twisted fibers, the existence of such fibers enhances the strain hardening and cracking properties of the concrete [13]. The addition of steel

23

fibers to the concrete mix significantly improves the ultimate flexural strength, flexural toughness and ductility of RC beams reinforced with normal strength steel [14]. However, the utilization of fibers in concrete mixes has not only proven its efficiency in improving the flexural behavior of concrete members reinforced with normal strength steel, but also in fir concrete members reinforced with fiber-reinforced polymer (FRP) and prestressing steel. FRP and prestressing steel share similar stress-strain response with HSS, yet they are characterized by even higher strength capabilities than that of HSS. The adoption of fibers in RC beam reinforced with FRP bars results in increasing the first-cracking load, nominal flexural strength and ductility and also minimizing the large crack widths at ultimate loads [15]. According to [16] which investigated the effect of using ultra-high performance concrete (UHPC) on the flexural behavior of a 24.4 m long AASHTO Type II girder reinforced with 26 prestressing strands, UHPC I-girder had larger flexural capacity compared to the capacity of the conventional concrete girder. The idea of coupling HSS with UHPC has been adopted recently by some researchers who investigated the effect of such coupling on the shear behavior of beams reinforced with HSS rebars [17]. It was found that through utilizing UHPC and providing adequate rebar anchorage, members without transverse reinforcement showed an acceptable ductile shear failure with shear resistance comparable with the one exhibited by members reinforced with transvers reinforcement. It should be noted that no research work has yet investigated the effect of using fiber-reinforced concrete on the performance of flexural members reinforced with HSS.

2.4 Design Considerations

When designing a flexural member reinforced with conventional Grade 414 steel, ACI 318-14 [4] provides certain limits for target strains in the tension steel which can be used to classify the section of the member to be a tension- or compression-controlled. Sections with target strains computed through strain compatibility analysis greater than 0.005 are referred to as tension-controlled sections; whereas, sections with target strain less than 0.002 are referred to as compression-controlled sections. Such classification significantly reflects the behavior of the member. The behavior of flexural members with a tension-controlled section is considered desirable. Under service load, it is characterized by small deflections and minimal cracks; while under ultimate loads, it is characterized by excessive deflections and large cracks, indicating clear warnings

24

prior to failure. As a result, the ACI 318-14 permits using a resistance factor of 0.9 when computing the design flexural capacity of flexural members with tension-controlled section. On the other hand, members with compression-controlled sections exhibits less ductility and are characterized by sudden failure. Therefore, the ACI 318-14 limits the resistance factor to 0.65 when computing the design capacity of members with compression-controlled section due to the uncertainty associated with its behavior. The ACI-318-14 does not permit the design of flexural members with compression-controlled sections. For sections falling within the transition between the aforementioned two zones, their resistance factors can be computed through interpolation [4].

A recent study by Mast et al. [6] proposes modified tension- and compression-control strain limits to determine the adequate design resistance factors for flexural members reinforced with HSS bars. These proposed limits are suggested based on an extensive analytical work which captured the strain, curvature and deflection deformability ratios of 8 concrete beams with a 300 mm × 760 mm cross section through strain compatibility and equilibrium principles. Three of the analyzed beams were reinforced with conventional steel while the remaining five were reinforced with HSS. Beams reinforced with conventional steel were designed to achieve target strain in the tension steel corresponds to the limiting strain of the tension-controlled section to capture the control deformability ratios. The concrete compressive strengths of the beams reinforced with HSS were varied from 27 MPa to 70 MPa. For various concrete compressive strengths, it was found that the deformability ratios are comparable when tension-controlled strain in the HSS is taken as 0.0066. However, the 0.0066 tensions-controlled limit is based on a strain compatibility and equilibrium analysis in which the stress-strain relationship of HSS was modeled using actual responses and not the elastic-perfectly plastic model. Therefore, in order to utilize the simplified design model (discussed earlier) in design applications, the tensions controlled limit was modified to 0.009. The compression-controlled limit; on the other hand, was found to be 0.004, which was determined using the same approach. The aforementioned tension- and compression-controlled limits were later adopted by the ACI-ITG-6R-10 [5]. Figure 7 shows how the resistance factor φ is varied at different strains ε_t.
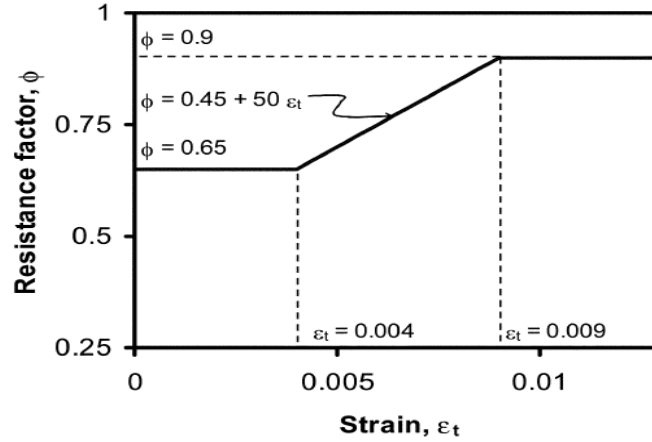
Figure 7: Resistance factor as a function of the tension steel strain [5]

The NCHRP project also conducted a study to propose tension- and compression-controlled limits for members reinforced with HSS [12]. The study consisted of an analytical program which aimed at developing the tension- and compression limits by comparing the curvature ductility of members reinforced with conventional Grade 414 steel with others reinforced with HSS at different steel strains. Curvature ductility is defined as the ratio of the curvature at the target strains in the extreme tension steel to the curvature computed at service load. Service load condition is reached when the stress in the reinforcing steel is equal to $0.6f_y$, where f_y is the yield stress of the steel reinforcement. The analysis was based on strain-compatibility and equilibrium principles, where the actual stress-strain response of the HSS was modeled using the Ramberg-Osgood (R-O) equation [7]. The study considered different cases to capture the effect of a number of parameters such as concrete compressive strength, longitudinal tension reinforcement ratio and compression longitudinal reinforcement ratio. For all the considered cases, the strains in the ASTM A1035 Grade 689 required to obtain curvature ductility corresponding to that for the ASTM A615 Grade 414 at the strain limits of 0.002 and 0.005 were recorded. Based on the aforementioned analytical program, it was recommended that a steel strain of 0.008 will provide the lower bound of tension-control behavior, and a strain limit of 0.004 will provide the upper bound of the compression-control behavior. Figure 8 provides a comparison between strain limits for ASTM A615 Grade 414 and ASTM A1035 Grade 689. The suggested tension- and compression-controlled limits were incorporated into the AASHTO (2013) LFRD bridge design specifications.
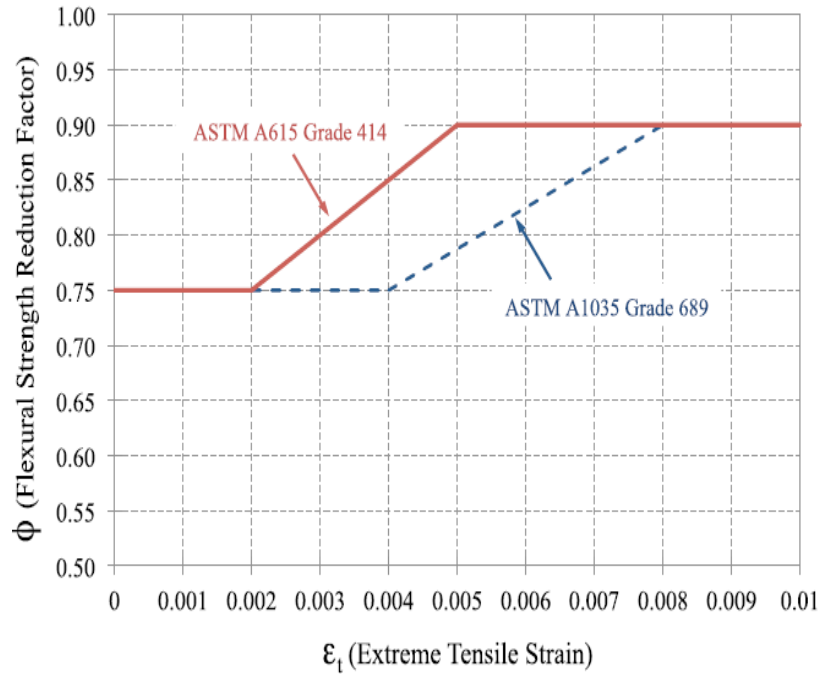
Figure 8: Resistance factor of ASTM A615 Grade 414 and ASTM A1035 Grade 689 as a function of tension steel strain [7]

2.5 Serviceability Challenges

In order to promote the use of HSS in flexural applications, a number of challenges associated with its uses in flexural members have to be addressed and investigated. One of the challenges is the large absolute mid-span deflections when compared with the mid-span deflections of members reinforced with conventional steel at service loads [6]. Therefore, it is recommended that, for serviceability purposes, deeper sections must be utilized in flexural members reinforced with HSS to minimize the mid-span deflections. Furthermore, another challenge is the large crack width of flexural members reinforced with HSS at service loads [18]. In case of ASTM A1035 rebars where the f_y is taken to be 689 MPa, the stresses in these rebars and, consequently, strains are expected to be greater than the ones found in ASTM A615/A615M with f_y equal to 414 MPa. Since crack widths at the tension face is a function of the strain in the reinforcing bars, large cracks widths are expected to develop in ASTM A1035 bar-reinforced beams. This could be a great concern for designers, particularly at service-condition. The NCHRP project has research work of Harries et al. [18] who studied the flexural crack width in concrete girders with high-strength reinforcement at loads corresponding to reinforcing bar stresses of 248, 414 and 496

27

MPa, which represent service load conditions for steel having f_y equal to 414, 690 and 827 MPa, respectively. The measured crack widths were compared with the AASHTO de facto limits for class 1 and class 2 exposures [0.43 and 0.33 mm, respectively]. Similar to Grade 414 reinforcement, the aforementioned tension- and compression-controlled limits for HSS were based on the assumption that the stresses in HSS at service loads do not exceed the limit of $0.6f_y$, where f_y is the yield stress. Based on their experimental program which had three specimens with different reinforcement ratio, it was found that up to a stress level of 496 MPa (about 0.718 fy), which is beyond the limiting service stress of 414 MPa [appropriate for bars having f_y 690 MPa], all the measured average crack widths were below the AASHTO de facto limits for class 1 and class 2 exposures. Such results indicate that the conservativeness of existing ACI and ASSHTO crack control provisions allow current specifications to be extended to higher service loads associated with the use of high-strength steel. On the other hand, the majority of the maximum measured crack widths fell below class 1 threshold only through bar stresses of 496 MPa. The analytical program which adopted a modified version of Frosch equation [19] to predict the crack width based on center-to-center reinforcement spacing indicated that at $f_s = 414$ MPa, class 1 exposure crack width limit [0.43mm] is met for all cases except when two #11 bars are used in a 305 mm web, which is an impractical case. On the other hand, class 2 exposure crack width limit was violated by all bars larger than #7. As a result, to meet the crack width limits when using AASHTO LFRD in design of RC, Shahrooz et al. suggested two solutions: (1) limit $f_s < 345$ MPa $(0.5f_y)$ to meet the class 2 requirements for all cases or (2) limit $f_s < 414$ MPa $(0.6y)$ and remove class 2 limit when utilizing the high-strength reinforcing steel [7]. Equation (3), which is a modified version of Frosch equation, can be used to predict maximum probable crack width at loads corresponding to different stresses in the reinforcing steel.

$$w = 2\frac{f_f}{E_f}\beta\sqrt{d_c{}^2 + \left(\frac{s}{2}\right)^2} \qquad (3)$$

where f_f is the stress in longitudinal bars, E_f is the modules of elasticity of steel, d_c is the minimum concrete cover measured to center of reinforcing bar, s is the bar spacing, and

$$\beta = 1 + \frac{d_c}{0.7\,(h - d_c)} \qquad (3\text{-}1)$$

28

where h is the overall depth of the concrete section. According to previous research [20], crack widths ranging from 0.15 to 0.30 mm under service load are considered unacceptable from the aesthetic point of view as they are visible by the naked eye which generates senses of discomfort and structural insecurity.

Therefore, in order to address the challenges associated with crack width limits from the standpoint of aesthetics and exposure, a crack control approach must be adopted. One of the proposed crack control approaches is the coupling of HSS and concrete with improved properties such as FRC. Introducing fiber-reinforced concrete (FRC) can be an effective solution to overcome the problem of crack widths in HSS bar-reinforced beams at service load levels. Since fibers are capable of bridging between cracks, it was reported by several researchers that flexural members cast with fiber-reinforced concrete and longitudinally reinforced with ordinary steel or fiber-reinforced plastic (FRP) exhibited an enhanced cracking behavior [15, 21, 22]. However, to the best of the researcher's knowledge, there are still no studies carried out on evaluating the effect of adopting FRC on the flexural crack width of ASTM A1035 bar-reinforced members.

2.6 Bond Strength Characteristics

Sufficient anchorage will result in developing the required stress to reach the ultimate capacity of the member. When bars are loaded for the first time, the bond transfer mechanisms are the adhesion and friction between the bar and the concrete. However, with increasing loads, the aforementioned bond transfer mechanisms are quickly lost, resulting in a bond being transferred through bearing on the deformations of the bar as shown in Figure 9-a. As a result, forces equal in magnitude and opposite in direction are exerted on the concrete as shown in Figure 9-b. Figure 9-c shows the radial and longitudinal components of the bond forces on the concrete.

The radial forces will result in circumferential tensile stresses in the concrete surrounding the rebar. Failure occurs when the concrete splits in a direction parallel to the rebar, and the concrete cracks propagate out radially to the surface of the beam. This failure is referred to as splitting failure and is illustrated in Figure 10.

(a) Forces on bar.

(b) Forces on concrete.

Longitudinal — Radial

(c) Components of force
on concrete.
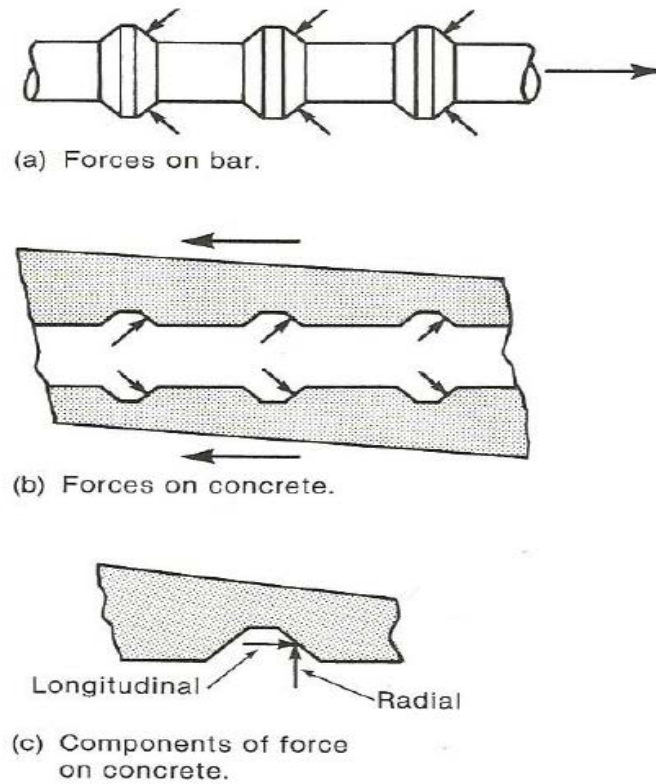
Figure 9: Bond-transfer mechanisms [23]
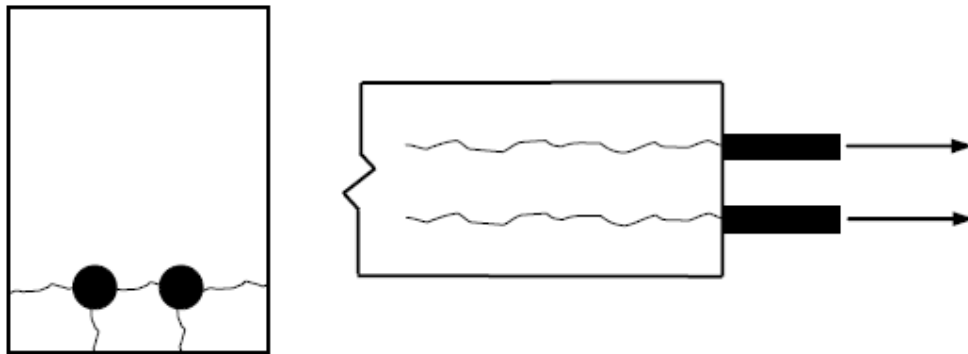
Figure 10: Splitting failure [24]

The load at which the splitting failure occurs can be increased by controlling the opening of the splitting crack [23]. Moreover, it is found that splitting failure load is a function of the minimum distance from the bar to the surface of the concrete or the next bar, the tensile strength of concrete and average bond stress. Therefore, it is expected that the utilization of concrete with improved tensile properties and crack control capabilities through the introduction of fibers in the concrete mix will result in

increasing the splitting failure load and thus improving the bond strength characteristics. Alternatively, another bond failure could occur because of the shearing of concrete around the rebar. This failure mode is defined as pullout failure which occurs when the concrete cover and bar spacing are large compared to the bar diameter [23]. Figure 11 demonstrates the pullout failure.
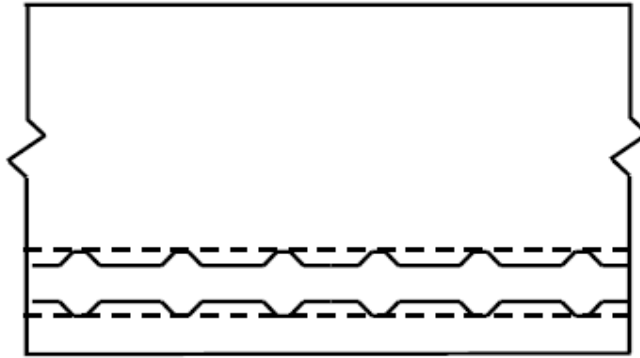
Figure 11: Pullout failure [24]

Recent research work [25] investigating bond properties between corrosion resistant steel reinforcement and concrete indicates that concrete splitting failure occurs when the tensile stresses coming from the uplift forces on the bars exceed the tensile modulus of rapture of concrete. Figure 12 illustrates how the tensile stresses created cracks parallel to the steel reinforcement that propagated along the depth of the specimen.
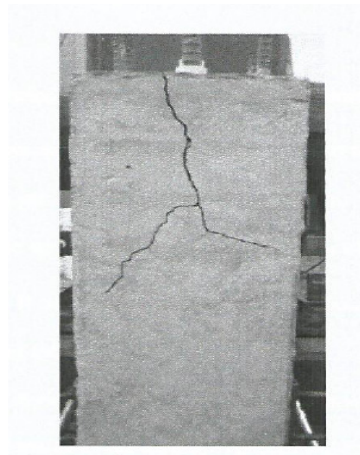
Figure 12: splitting failure in a specimen after a pullout test [25]

Pullout failure mode may also be attributed to the high yield stress of the HSS rebar with respect to Grade 50 reinforcement. Based on studies investigating the load-slip behavior between the corrosion resistant reinforcing (CRR) bar types, it was found that relative rib-area was the most influential factor affecting the load-slip responses [25]. In direct pullout test, it is necessary to embed the reinforcing bars in concrete block in which sufficient concrete is surrounding the reinforcing bar in order to reduce the tensile stress and consequently reduce the probability of having splitting failure mode. The accuracy of the pullout tests in capturing the actual bond strength between the reinforcing bar and the concrete is questionable because pullout tests do not reflect the realistic loading conditions found in structural members. Therefore, Equation (4), which is used to calculate the average bond stress between reinforcing bar and concrete in a flexural member, can be used to evaluate the accuracy of measured bond strengths from the pullout tests.

$$u = \frac{V}{0.87\, d\, \sum o} \tag{4}$$

where u is the average bond stress, V is the shear force, d is the depth of the section, and $\sum o$ is the sum of perimeters of the bars at tension side of the section.

Chapter 10 of the ACI ITG-6R-10 [5] design guide provides recommendations related to the development and lap splice length of HSS bar embedded in normal concrete. The ACI ITG-6R-10 design guide suggests that Equation (12-1) of the ACI 318-08 (Equation 5) can be used only to predict the strength of confined splices whereas a modified version of the equation proposed by ACI 408R-03 (Equation 6) [26] can be used to estimate the strength of both confined and unconfined splices [5]. The strength reduction factor $\emptyset$ in the ACI408R-03 equation was slightly modified as it was set to 0.80, instead of 0.82.

$$l_d = \left(\frac{f_y}{1.1\lambda\sqrt{f'_c}} \cdot \frac{\Psi_t \Psi_e \Psi_s}{\frac{c_b + K_{tr}}{d_b}} \right) d_b \tag{5}$$

where Ψ_t is a modifier for reinforcement location (1.3 for top bars, 1.0 for other bars), Ψ_e is a modifier for epoxy coated bars (1.5 when cover $< 3d_b$ or clear spacing $< 6d_b$, 1.2 for other epoxy coated reinforcing, and 1.0 for non-epoxy coated reinforcing), and Ψ_s

is modifier for bar size (0.8 for #6 and smaller and 1.0 for #7 and larger), and λ is a term reflecting the type of concrete (1.0 for normal weight concrete).

$$K_{tr} = \frac{40A_{tr}}{sn} \tag{5-1}$$

The ACI ITG-6R-10 suggests using Equation 6 to compute the development length in SI units (mm) of both confined and unconfined HSS bars.

$$l_d = \frac{\left(\frac{f_y}{4\sqrt{f'_c}} - \emptyset 57.4\omega\right)\alpha\beta_c\lambda}{\emptyset 1.83\left(\frac{c_b\omega+k_{tr}}{d_b}\right)} (d_b) \tag{6}$$

where $\emptyset$ is the strength reduction factor, 0.82, α is the bar location factor (1.3 for top reinforcement and 1.0 for all other locations), β_c is the coating factor (1.5 for coated bars and 1.0 for uncoated bars), and

$$K_{tr} = \left(\frac{6.26t_r t_a A_{tr}}{sn}\right)\sqrt{f'_c} \tag{6-1}$$

$$t_r = 9.6R_r + 0.28 \leq 1.72 \tag{6-2}$$

$$t_d = 0.03d_b + 0.22 \tag{6-3}$$

$$\left(\frac{c_b\,\omega+K_{tr}}{d_b}\right) \leq 4.0 \tag{6-4}$$

It is essential to understand the effect of improving concrete properties on the bond strength between the HSS reinforcing bar and the concrete. Improving the bond strength characteristics is mainly dependent on how the proposed concrete mixes are going to improve load transfer and slip resistance capabilities. Previous work has indicated that increasing the concrete compressive strength results in increasing bond strength between conventional steel and concrete [27]. Furthermore, in case where ultra-high-strength concrete is utilized, very high bond strength and stiffness were observed due to the high compressive strength and modulus of elasticity of the ultra-high strength concrete [28]. According to [29], based on pullout tests performed on the uncorroded specimens, it was found that increasing the concrete compressive strength for a given concrete cover depth results in higher bond strength than increasing the concrete cover for a given concrete strength. The contribution of the compressive strength on the bond strength between HSS and concrete is determined by the term $\sqrt{f'_c}$.

However, with increasing compressive strength, the use of the aforementioned term is questionable due to the nonlinear behavior of the bond strength and the concrete compressive strength. ACI committee 408 suggests the use of the term $f_c'^{1/4}$ to capture the contribution of concrete compressive strength to bond strength as shown in equation (4) which is, as mentioned earlier, a modified version of the ACI 408R-03 [26] equation. Another type of concrete that previous research has proven its efficiency in improving the bond strength characteristics is the fiber reinforced concrete. It was found that fibers limit crack width through bridging and confinement which consequently results in higher bond strength and more ductile failure in concrete containing fibers when compared to plain concrete [30]. Another research indicated that adding up to 2.5 % fibers by volume fraction to a concrete mix resulted in increasing its bond strength by 60 % [31].

A recent study investigated the effect of utilizing ultra-high performance concrete on the bond strength characteristics between HSS and concrete [32]. The research aimed to determine the development lengths of #10 (#3) and #22 (#7) HSS rebar embedded in UHPC. Because this work was part of a larger research project, which aimed to develop a lightweight bridge deck system for movable bridges, all the dimensions of their specimens were kept small, resulting in a clear cover of only 13 mm. The experimental program consisted of a series of pullout and beam tests. Beam tests were adopted in their experimental program to refine the results of the pullout tests because the limited concrete cover of 13 mm resulted in not fully utilizing the steel rebar in pullout tests, particularly when bar #22 is used. Based on the pullout and beam tests, the development lengths for bars #10 and #22 were found to be $12d_b$ and $18d_b$, respectively, where d_b is the diameter of the bar. Beside the experimental program, an analytical program was adopted to assess the accuracy of ACI 318-08, ACI 408R-03 and AASHTO equations in recommending development lengths. Based on comparisons between recommended and experimental development lengths of HSS rebar embedded in UHPC, it was found that the values suggested by ACI 408R-03 are in accordance with the experimental data while the ACI 318-08 and AASHTO overestimated the development lengths. Further research was suggested to be done in order to propose an equation that can be used to accurately estimate the development length of HSS embedded in UHPC. In addition to investigating the effect of improving concrete properties on the flexural behavior of RC beams, bond strength characteristics and bond

failure mechanisms should be assessed when adopting concrete mixes with improved properties. The set of pullout tests conducted in this study provides a better understating of the bond strength between HSS and different types of concrete having different f'_c and provides results that can be used in future research to develop an equation that can accurately estimate the development length of HSS embedded in FRC.

2.7 Summary

HSS exhibits a yield strength that is considerably higher than that of conventional mild steel; however, it lacks a well-defined yield point and yielding plateau. The simplified design stress-strain relationship for HSS consists of a linear portion with a slope of 200 GPa (Young's modules), followed by a yielding plateau with a yielding strength of 689 MPa. HSC and FRC are characterized by higher compression strain corresponding to the peak stress when compared to normal plain concrete. This would allow HSS reinforcing bars to develop higher strains and stresses and engage more in the section. Adopting HSC and FRC may enhance the flexural behavior of beams reinforced with conventional steel, FRP, or prestressing steel. The ACI-ITG-6R-10 and the NCHRP established the target strain limits for the section to be classified as tension-controlled or compression-controlled. Due to the high strains developed in HSS reinforcement at service load conditions, crack widths can be a considerable concern to designers. It was found analytically that meeting the AASHTO de facto limits for class 2 exposure is not applicable except in cases where bars smaller than #8 are utilized. The bond strength between HSS and concrete differs from that between concrete and conventional steel. Therefore, the ACI-ITG-6R-10 suggests using a modified version of ACI408R-03 equation to compute the development length of HSS reinforcement. Previous studies have proven that adopting HSC or FRC significantly increases the bond between the reinforcing bars and surrounded concrete.

Chapter 3: Experimental Program

The main objective of this research is to evaluate the flexural performance of concrete beams reinforced with HSS bars when coupled with concrete exhibiting enhanced properties. Initially, the properties of the proposed concrete mixes and the HSS reinforcing bars used in this study are evaluated. Then, a series of flexure tests is conducted to evaluate the effect of the proposed concrete mixes on the flexural behavior of concrete beams reinforced with HSS. Lastly, the bond strength between the proposed concrete mixes and the HSS reinforcing bars is studied through a series of pullout tests.

3.1 Material Properties

3.1.1 High-strength steel. The high-strength steel reinforcing bars used in this study were manufactured by MMFX Technologies Corporation and are commercially known as ChrōmX 9000 (formally $MMFX_2$). As per the ASTM specifications, these bars can be specified as A1035 CS Grade 689 based on their chemical composition and tensile properties (ASTM 2010). Because the ASTM A1035 Grade 689 steel lacks a well-defined yield point and yielding plateau, the yield strength was established based on two different approaches: the 0.2 % offset method and the 0.35 % Extension Under Load (EUL) method. Consequently, the yield strength for MMFX bars was found to be 800 MPa for the former and 610 MPa for the latter, as illustrated in Figure 13. The ultimate tensile strength for this HSS bar exceeded 1000 MPa, and the measured Young's Modulus was around 200 GPa.
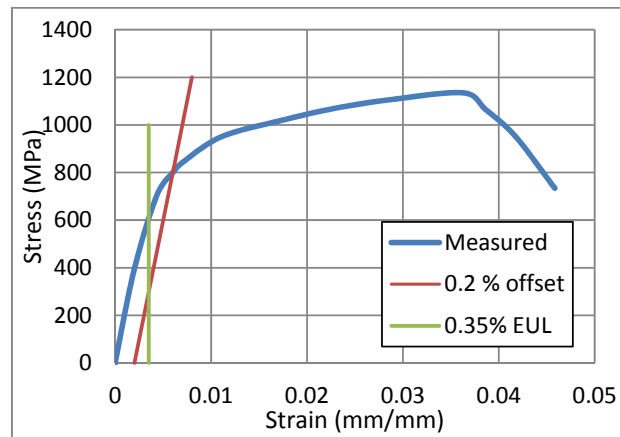

Figure 13: Different methods for establishing the yield strength of the ASTM A1035 reinforcing bar

3.1.2 Concrete mixes. Two types of concrete are evaluated in the current study; the first one has f'_c of 50 MPa, and the second has f'_c of 80 MPa. For each type of concrete, three different concrete mixes are developed which are plain, steel fiber-reinforced and synthetic fiber-reinforced concrete. Table 2 lists the mixes used in this study, along with their designations.

Table 2: Proposed Concrete Mixes

Types of concrete	Compressive strength f'c , (MPa)	Designation
Plain concrete	80	80 NS
Plain concrete	50	50 NS
Steel fiber reinforced concrete	80	80 SF
Steel fiber reinforced concrete	50	50 SF
Synthetic fiber reinforced concrete	80	80 SYF
Synthetic fiber reinforced concrete	50	50 SYF

The two mixes of plain concrete with compressive strengths of 50 MPa and 80 MPa are given in Table 3. In case of FRC, the plain concrete mix design was slightly modified by the addition of 0.65 % per volume of either steel or synthetic fibers. The geometry and properties (provided by manufacturers) of these fibers are summarized in Table 4.

Table 3: Proportions of Plain Concrete (f'_c = 50 MPa and f'_c = 80 MPa) Constituent Material

Constituent Material		f'_c (MPa)	
		50	80
Unit weight (kg/m³)	10mm Aggregate	340	360
	20mm Aggregate	650	550
	Washed Sand	570	600
	Dune Sand	320	350
	Cement	420	440
	Water	164	154
	Silica Fume	-	9.6
%	Crushed Ice	71	60

Table 4: Properties of Fibers

Type of fiber	Steel	Synthetic
ASTM	A820	C1116
Length l_f (mm)	35	40
Dimensions(mm × mm)	Φ 0.55	1.4×0.11
Aspect Ratio (l_f/d_f)	65	111
Density (kg/m^3)	7850	0.92 (SG)
Tensile Strength (MPa)	1345	620
Young's Mod (GPa)	210	9.5

3.2 Flexure Test

The experimental program consisted of flexure tests on a total of 24 full-scale concrete beams reinforced with high-strength steel (HSS) bars. As mentioned earlier, 6 different concrete mixes were used, considering plain concrete, synthetic fiber-reinforced concrete and steel fiber-reinforced concrete with 50 MPa and 80 MPa compressive strengths. In addition, single and double-reinforcement arrangements were considered for each of the six different concrete mixes. Two identical beams were constructed for each of the proposed specimens in the test matrix to ensure the repeatability of results. The combination effect of the different mixes and reinforcement arrangements on the flexural behaviors of HSS-reinforced concrete beams is carefully investigated. The schematic diagram shown in Figure 14 summarizes the test matrix as well as the labeling system used in this study. The samples are labeled to indicate reinforcement arrangements, concrete strength, concrete type and specimen number. For example, D80-SYF-1 refers to specimen 1 with a double-reinforcement, 80 MPa compressive strength and synthetic fiber-reinforced concrete.

3.2.1 Specimens configuration. All of the twenty four beams were 2.6 m long, with a cross-section of 200 mm × 400 mm. A layer of three 12 mm ASTM A1035 Grade 689 reinforcing bars was used for the tension reinforcement of all concrete beams. An additional layer of two 12 mm ASTM A1035 Grade 689 reinforcing bars was placed in the compression zone for the doubly-reinforced beams. To avoid the possibility of shear failure, 8 mm diameter closed stirrups were provided as shear reinforcement along the beam's span. Section details of the single and doubly reinforced sections are shown in Figure 15.

Figure 14: Details of test beams

Test Matrix

$f'_c = 50\ MPa$

$f'_c = 80\ MPa$

Single Reinforced (S)

Doubly Reinforced (D)

Single Reinforced (S)

Doubly Reinforced (D)

- S50-NS-(1,2)
- S50-SF-(1,2)
- S50-SYF-(1,2)

- D50-NS-(1,2)
- D50-SF-(1,2)
- D50-SYF-(1,2)

- S80-NS-(1,2)
- S80-SF-(1,2)
- S80-SYF-(1,2)

- D80-NS-(1,2)
- D80-SF-(1,2)
- D80-SYF-(1,2)
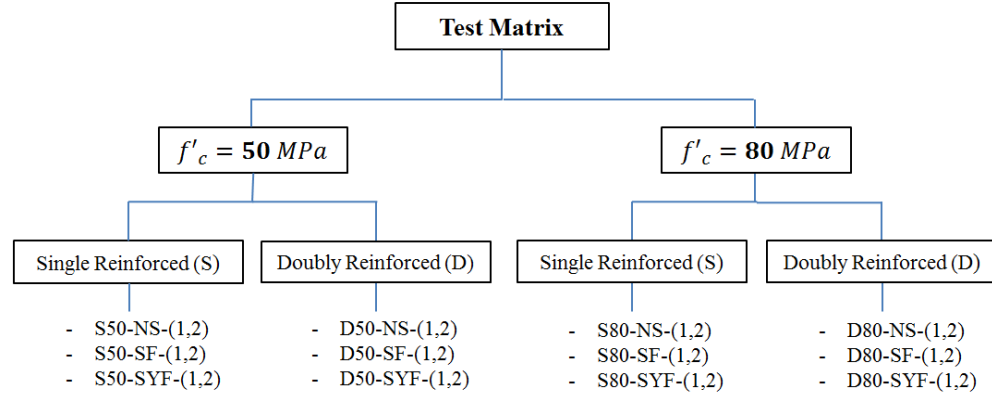
f'_c = Concrete Compressive Strength
NS = Plain Concrete
SF = Steel fiber-reinforced Concrete
SYF = Synthetic Fiber-reinforced Concrete

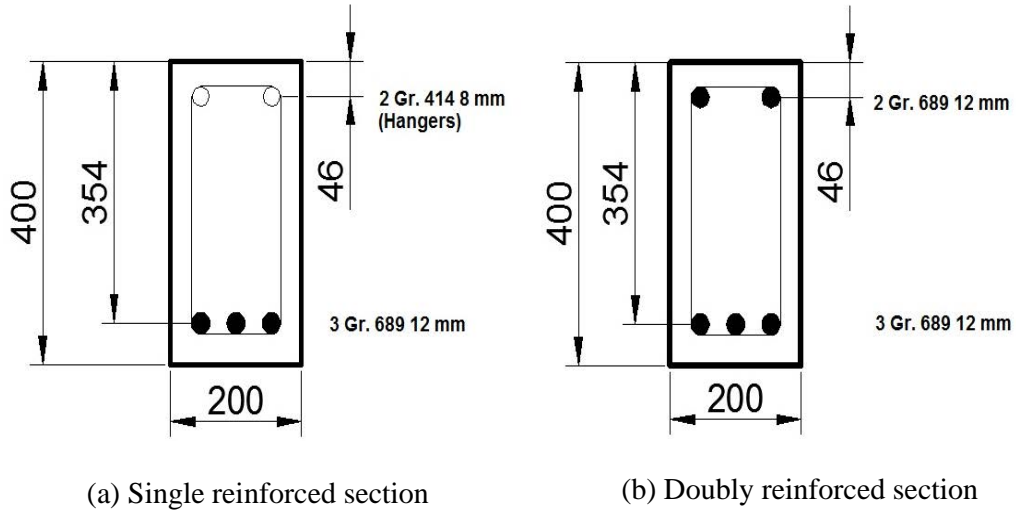(a) Single reinforced section   (b) Doubly reinforced section

Figure 15: Section details (Dimensions in mm)

3.2.2 Test setup and instrumentation. All specimens were tested over a 2.3 m clear span in a four-point loading setup with a constant moment region of 0.5 m, as shown in Figure 16. The load was induced using a hydraulic jack attached to a reaction frame and transferred to two loading points on the specimen through a spreader beam. Four quantities were electronically measured during the flexure test: load, deflection, crack widths and strains in concrete and in steel bars at mid-span. In addition, the specimens were continuously observed to mark the crack patterns and note any signs of distress during the loading process. The load was measured using a 500kN load cell that was placed at mid-span above the spreader beam. The deflection of the specimens

was measured at mid-span and one-fourth of the span length using position transducers. Displacement transducers were utilized to record crack widths of the first three cracks at the depth of the reinforcing steel. In order to capture strain distribution along the concrete depth throughout the test, four strain gauges were installed on one side of the beam at mid-span. The first strain gauge was located at a distance of 20 mm form the top surface while the remaining three were mounted below it at 50 mm interval. Strains in the tension reinforcement were recorded using strain gauges mounted at mid-span. Additional strain gauges were mounted on the compression reinforcement for specimens with doubly reinforced sections. The load, mid-span deflection, crack widths and strains were recorded every 0.1 second using a high-speed data acquisition system.
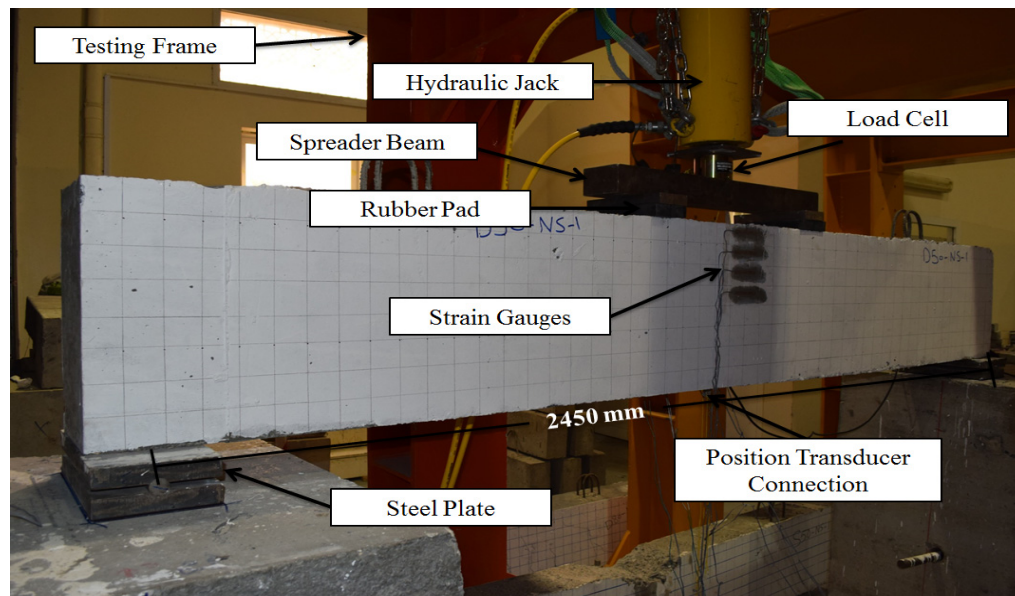
Figure 16: Test setup and instrumentations used in the investigation

3.2 Pullout Tests

One pullout block was cast for each of the six proposed concrete mixes. Table 5 lists the mix type of each block and its corresponding designation. For example, PO1 pullout block is cast with plain concrete and having f'_c of 50 MPa. Pullout tests played a crucial role in developing sufficient understanding of the bond strength between the ASTM A1035 rebrs and the different types of concrete considered. In addition, the

results of these tests were used to verify the accuracy of the development lengths computed based on Equation (5).

Table 5: Pull-out specimens types and their designations

Pull-out blocks	Concrete type
PO1	50 NS
PO2	80 NS
PO3	50 SF
PO4	80 SF
PO5	50 SYF
PO6	80 SYF

3.2.1 Specimens configurations. In each block, three HSS bars were embedded by a length equal to the development length which was calculated based on the development length equitation of the ACI 318-11 (ACI committee 318 2011) (Equation 5). The development length varied with the concrete compressive strength. HSS rebars embedded in specimens cast with concrete having $f'_c = 50$ MPa had a development length of 465 mm; whereas, the ones embedded in concrete having $f'_c = 80$ MPa had a development length of 367 mm. The results of calculating the final depth of the block are summarized in Table 6. All of the pullout blocks had the same longitudinal cross-section (1050 mm × 450 mm). In order to ensure that the conic failure plane of each rebar does not coincide with the adjacent ones, the rebars were spaced at 300 mm. In addition, sufficient clear cover below the bars was provided to ensure that the failure plane will occur without interruption.

Table 6: Pull-out block depth calculations

	Concrete mix $f'c = 50$ MPa	Concrete mix $f'c = 80$ MPa
Embedment Length (cm)	46.5	36.7
Bottom concrete depth (cm)	28.5	28.3
Depth of the block (cm)	75	65

Finally, the total length of the bars had to be determined according to the embedment length required for each concrete mix in addition to the length required for the test setup, knowing that the pull-out test will consist of hydraulic jack, two loading plates, load cell, and locking nuts to secure the testing mechanism. Table 7 summaries the procedure of calculating the total required length of HSS bars.

Table 7: Bar length calculations for pull-out test

	Concrete mix $f'c = 50$ MPa	Concrete mix $f'c = 80$ MPa
Embedment Length (cm)	46.5	36.7
Hydraulic Jack (cm)	25	25
Two loading plates (cm)	5	5
6" Load cell (cm)	15.25	15.25
Thread for nuts (cm)	7	7
Final length of rebar (cm)	~ 100	~ 90

3.2.2 Test setup and instrumentation. Photograph of the pullout test setup is shown in Figure 17. The rebars were extended through a hollow hydraulic jack placed above the pullout concrete block. Threaded nuts and steel plates were utilized to fix the hydraulic jack and the load cell to the concrete block, as shown in Figure 17. A Linear Variable Differential Transformer (LVDT) was installed near the end of the rebar to capture its elongation. In addition, strain gauges were mounted on the rebars to measure the tensile strains in the rebars throughout the test. The specimens were loaded until pullout of the rebar is observed and the bond between the steel rebar and concrete is broken. Load, strain and elongation were recorded electronically every 0.1 sec using data acquisition system.
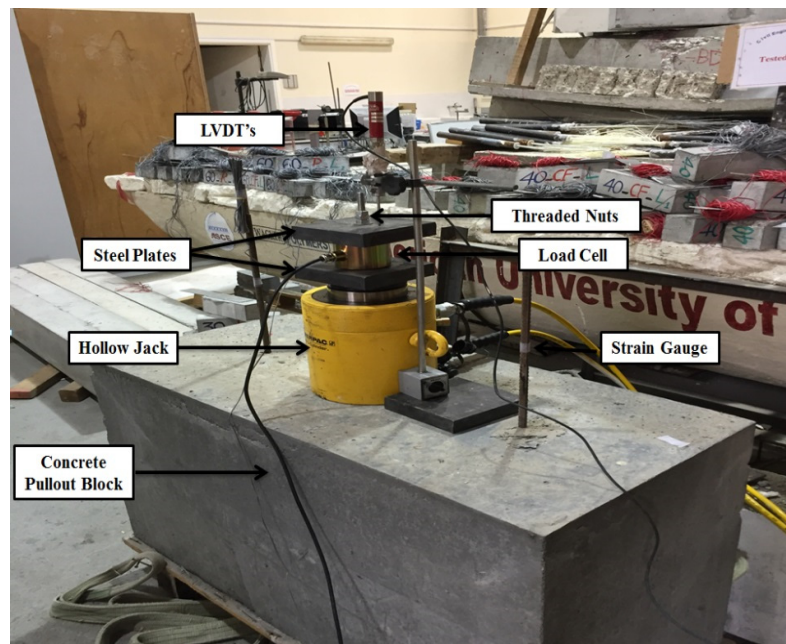

Figure 17: Experimental setup and details of pullout test

Chapter 4: Results

4.1 Material Evaluation

The concrete compressive strength (f'_c) and modulus of elasticity (E) for all types of concrete used in this study were measured to investigate the effect of fibers at material level as given in Table 8. The results indicate that, for the same volumetric ratio of steel and synthetic fibers, the addition of steel fibers increased the concrete compressive strength; whereas, synthetic fibers slightly decreased it. Fibers replace some of the volume of the course aggregate which might result in reducing the concrete compressive strength as was observed in SYF specimens.

Table 8: Mechanical Properties of Concrete

Concrete Type	Modulus of Elasticity (GPa)	Average Compressive Strength f'_c (MPa)
50-NS	30	59
50-SF	30.7	61
50-SYF	26.4	55
80-NS	35.4	75
80-SF	31.1	85
80-SYF	27.8	70

The stress-strain curves for 80 and 50-NS, -SF and -SYF presented in Figure 18 shared relatively similar initial slope which explains the insignificant effect of fibers on the measured Young's modules.
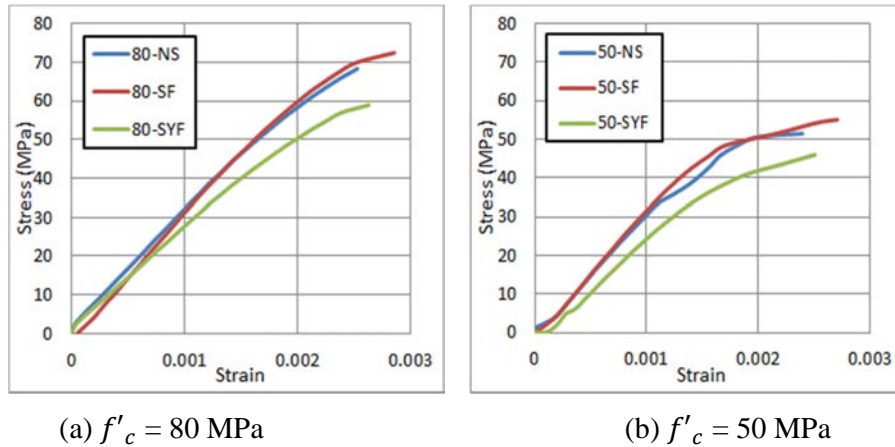

(a) f'_c = 80 MPa   (b) f'_c = 50 MPa

Figure 18: Stress-strain responses for the different types of concrete considered in this study

Similar observations were reported by Afroughsabet et al. [33] with high strength concrete and Hannawi et al. [34] with ultra-high performance concrete. The failure mode of the specimens was noticeably influenced by the existence of fibers. Due to the capability of fibers in bridging between cracks, fiber-reinforced specimens were characterized by less destructive failure modes compared to that of the control specimens, i.e., cast with plain concrete, and almost preserved their original shape, as shown in Figure 19. Furthermore, due to the bridging effect of fibers, both steel and synthetic fiber-reinforced concrete exhibited higher strain corresponding to the peak stress than that of plain concrete, which in turn improved the elastic deformation of the concrete matrix; similar observation was reported by Thomas et al [35]. In addition, both fibers contributed to the ductile behavior by improving the post peak response and enhancing the tensile behavior which led to more strain (deformation) before failure; a similar behavior was reported by Ding and Kusterle [36] and Bencardino et al. [37].
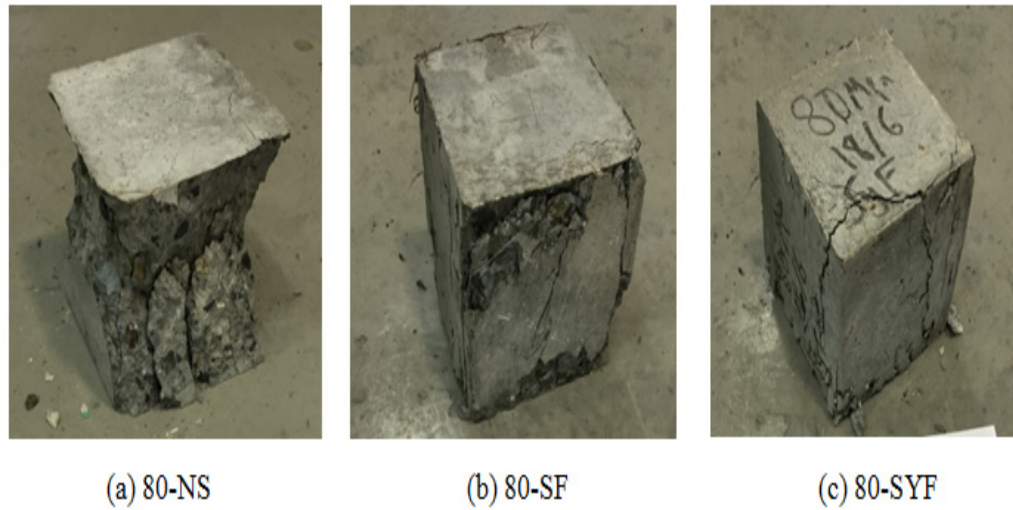

(a) 80-NS   (b) 80-SF   (c) 80-SYF

Figure 19: Concrete cubes failure modes

4.2 Flexure Tests

4.2.1 Load vs mid-span deflection. Figure 20 shows the load vs mid-span deflection responses for twelve different beams. Responses of the load vs mid-span for the second set of specimens were very similar to their identical counterparts (see Appendix A). The maximum measured loads, moment capacities and mid-span deflections, first cracking loads and curvature ductility for all of the 24 specimens are given in Table 9.
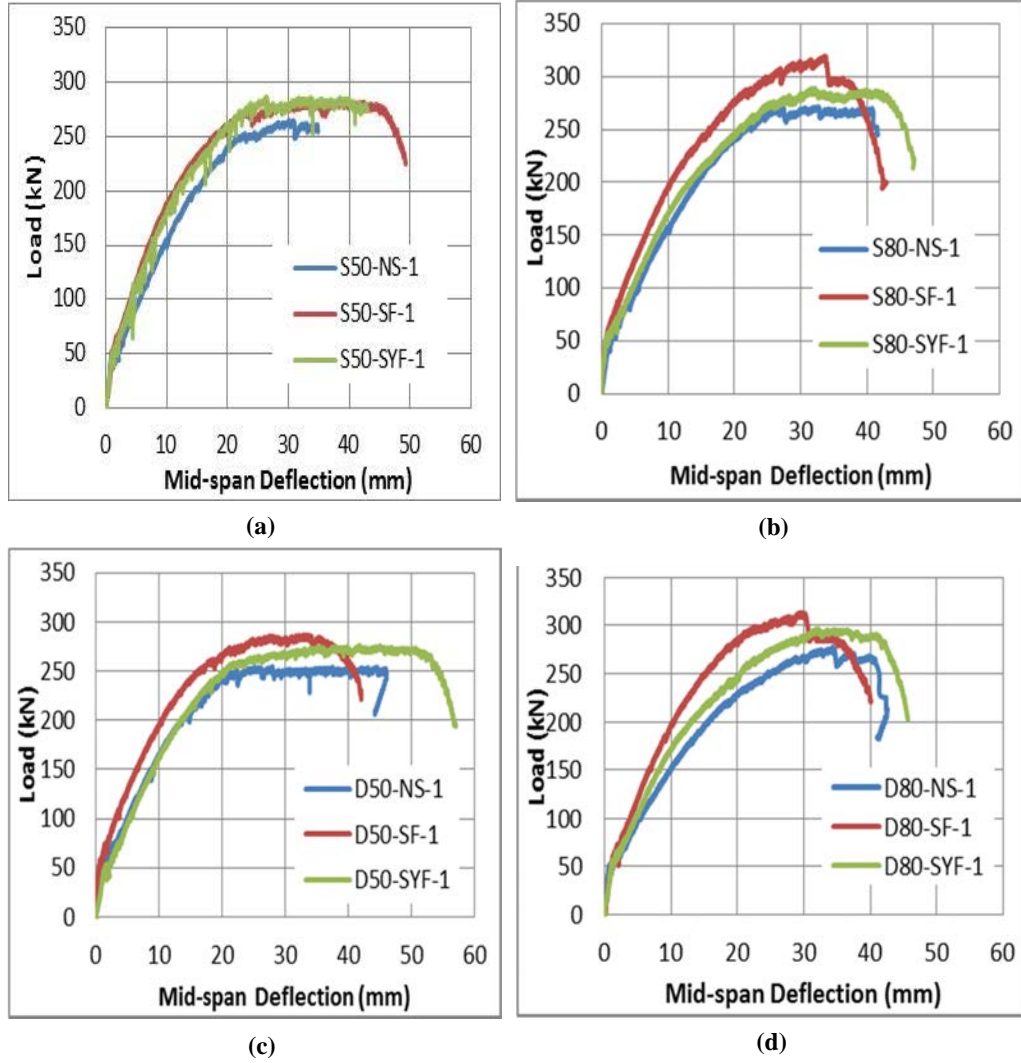
Figure 20: Load versus mid-span deflection responses for the tested beams: (a) S50-(NS, SF, and SYF)-1; (b) S80-(NS, SF, and SYF)-1; (c) D50-(NS, SF, and SYF)-1; (d) D80-(NS, SF, and SYF)-1

The curvature ductility is defined as the ratio of the curvature at ultimate load to the curvature at steel yielding load. The curvature was measured using the section strain distribution which was developed based on a linear connection of two points of strains at the two cross-sections extremes. However, in some specimens, the steel strain gauges were damaged during casting, and therefore, capturing their curvature ductility was not possible, as shown in Table 9.

The results of the identical specimens were consistent, and therefore measured load capacities, nominal moment capacities, maximum mid-span deflections, first

cracking loads and curvature ductility for each pair of identical specimens were averaged, as shown in Table 10.

Table 9: Summary of flexure tests results

Specimen type	Load capacity (kN)	Nominal moment capacity (kN.m)	Maximum mid-span deflection (mm)*	First cracking load (kN)	Curvature ductility
S50-NS-1	265	129	35.0	50	3.57
S50-NS-2	258	126	34.0	52	3.27
S50-SF-1	282	137	46.3	57	3.09
S50-SF-2	276	135	48.3	66	3.11
S50-SYF-1	286	139	42.9	50	3.71
S50-SYF-2	287	140	39.9	38	3.92
D50-NS-1	255	124	46.0	48	3.25
D50-NS-2	244	119	43.5	41	-
D50-SF-1	287	140	38.5	63	3.31
D50-SF-2	286	139	47.5	57	-
D50-SYF-1	276	135	53.2	47	3.85
D50-SYF-2	277	135	47.5	42	-
S80-NS-1	272	133	41.6	47	3.39
S80-NS-2	282	137	46.1	52	3.1
S80-SF-1	319	156	34.0	57	-
S80-SF-2	325	158	31.0	67	3.44
S80-SYF-1	289	141	43.5	72	4.24
S80-SYF-2	301	147	47.4	54	4.19
D80-NS-1	278	136	40.4	45	3.16
D80-NS-2	283	138	38.5	47	3.21
D80-SF-1	313	153	30.6	60	3.24
D80-SF-2	320	156	30.5	70	3.27
D80-SYF-1	297	145	41.6	57	3.67
D80-SYF-2	299	146	42.2	61	3.85

* Mid-span deflection corresponds to the load at failure, i.e., 5 % drop in the load capacity

For selected beams, the section strain distribution at three loading stages: initiation of the first crack, yielding of steel bars and 95 % of the ultimate load were scrutinized to clearly identify the effect of concrete compressive strength, compression reinforcement, and steel and synthetic fibers on the flexural behavior of HSS-RC beams. The load vs mid-span deflection for S80-NS-1 beam, along with the established strain distributions at the aforementioned loading stages are shown in Figure 21. Some strain gauges became highly unstable at ultimate load, and therefore, their readings were considered only up to 95 % of the ultimate load.

Table 10: Average load capacity, nominal moment capacity, maximum mid-span deflection, first cracking load, and curvature ductility for each pair of identical specimens

Specimen type	Avg. Load capacity (kN)	Avg. Nominal moment capacity (kN.m)	Avg. Maximum mid-span deflection (mm)	Avg. First cracking load (kN)	Avg. Curvature Ductility
S50-NS	262	127	34.5	51	3.42
S50-SF	279	136	47.3	62	3.1
S50-SYF	287	140	41.4	44	3.82
D50-NS	250	122	44.8	45	3.25
D50-SF	287	140	43	60	3.31
D50-SYF	277	135	50.4	45	3.85
S80-NS	277	135	43.9	50	3.25
S80-SF	322	157	32.5	62	3.44
S80-SYF	295	144	45.5	63	4.22
D80-NS	281	137	39.5	46	3.19
D80-SF	317	154	30.6	65	3.26
D80-SYF	298	145	41.9	59	3.85
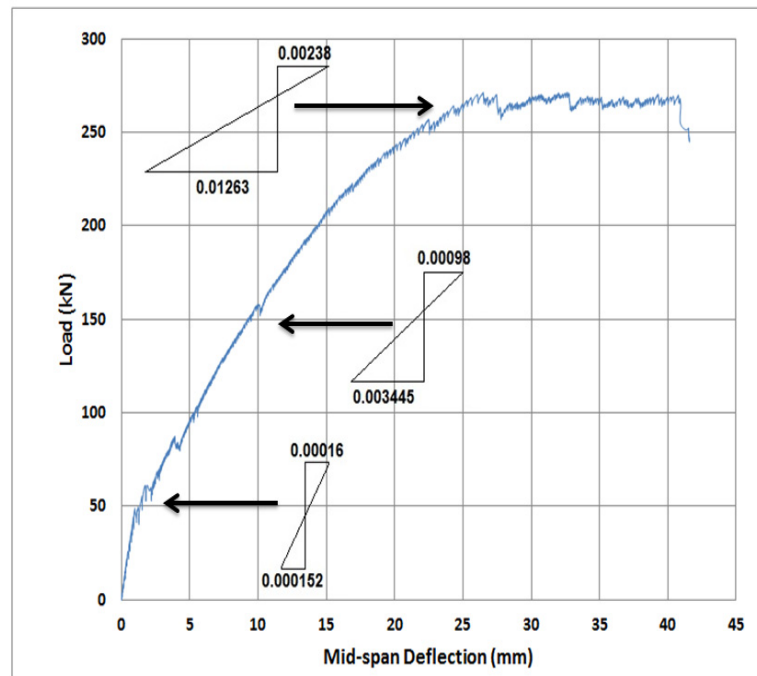
Figure 21: Load vs mid-span deflection relationship, and the established section strain distributions at: first cracking load, steel yielding load, and 95 % of the ultimate load capacity

47

4.2.1 Moment vs curvature relationships. The measured deflection at one-fourth of the span length was utilized to measure the angle at which the beam was deflecting, i.e., the curvature. Figure 22 shows the measured moment-curvature relationships for twelve of the tested beams.
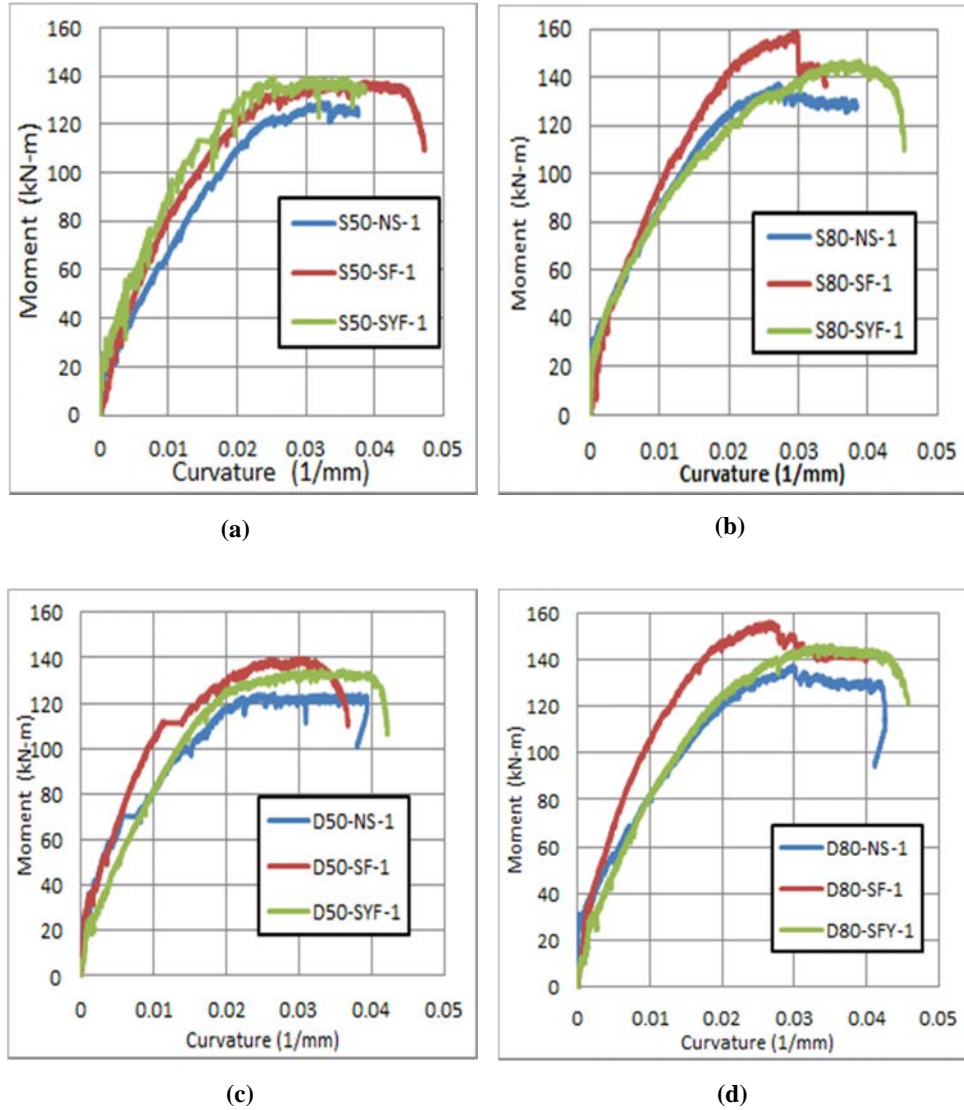

(a)   (b)

(c)   (d)

Figure 22: Moment-curvature relationship for the tested beams: (a) S50-(NS, SF, and SYF)-1 beams; (b) S80-(NS, SF, and SYF) beams; (c) D50-(NS, SF, and SYF)-1 beams; (d) D80-(NS, SF, and SYF)-1 beams

4.2.3 Crack patterns. Crack patterns of all of the tested beams were captured at the following loading stages: initiation of the first crack, yielding of steel bars and the ultimate load. In addition, the loads required to develop each crack (up to crack

48

No.7) were also monitored, as illustrated in Table 11. Figures 23 and 24 illustrate the crack patterns for S-(NS, SF and SYF)-1 specimens having f'_c of 80 and 50 MPa, respectively. The crack patterns of the reaming 18 beams at the same loading conditions are provided in Appendix B.

Table 11: Required loads to develop the cracks (up to crack No. 7)

|	Crack No.	Load (kN)						
		1	**2**	**3**	**4**	**5**	**6**	**7**
Specimen Type	S50-NS-1	50	52	55	59	72	80	85
	S50-NS-2	52	61	67	70	76	77	111
	S50-SF-1	57	65	65	70	78	85	95
	S50-SF-2	66	71	79	90	94	103	105
	S50-SYF-1	50	60	61	71	75	88	92
	S50-SYF-2	38	49	53	66	72	74	86
	D50-NS-1	48	57	67	77	79	97	100
	D50-NS-2	41	46	46	61	64	66	72
	D50-SF-1	63	74	75	41	44	46	52
	D50-SF-2	57	72	75	83	95	104	108
	D50-SYF-1	47	48	49	71	75	81	100
	D50-SYF-2	42	50	65	69	76	80	91
	S80-NS-1	47	59	68	83	85	97	-
	S80-NS-2	52	57	62	77	79	100	112
	S80-SF-1	57	66	87	94	96	102	107
	S80-SF-2	67	79	79	94	97	98	102
	S80-SYF-1	72	78	78	79	79	94	100
	S80-SYF-2	54	58	64	70	76	80	83
	D80-NS-1	45	51	56	60	72	90	107
	D80-NS-2	47	54	59	63	75	93	110
	D80-SF-1	60	63	69	79	81	86	112
	D80-SF-2	70	76	80	81	90	97	107
	D80-SYF-1	57	61	67	75	85	93	100
	D80-SYF-2	61	65	69	71	75	90	100

4.2.4 Crack Widths. The widths of the first three cracks were measured at the level of the longitudinal bars for all beams. The measured crack widths versus the flexure load capacity and also versus the stress in the reinforcing bars for the six singly-reinforced specimens are presented in Figures 25 and 26, respectively. Results of the crack width for the other (doubly-reinforced) specimens are provided in Appendix C.
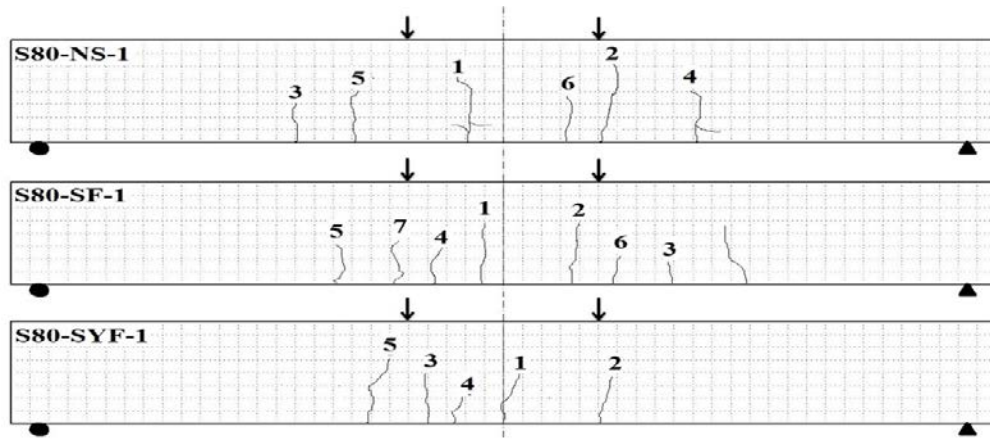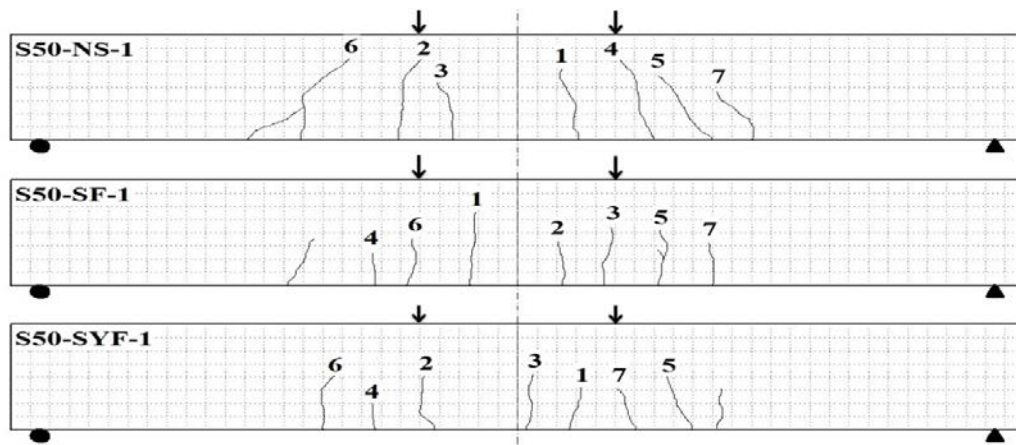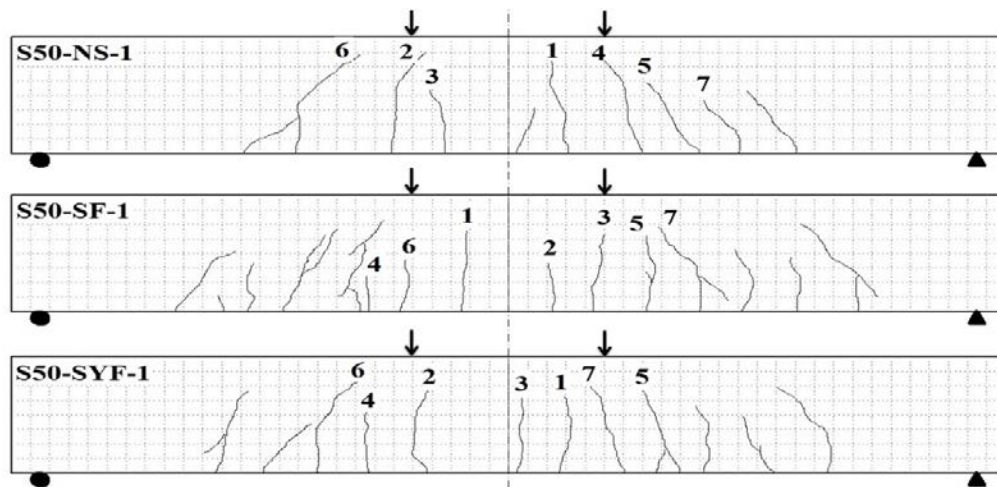
(a)
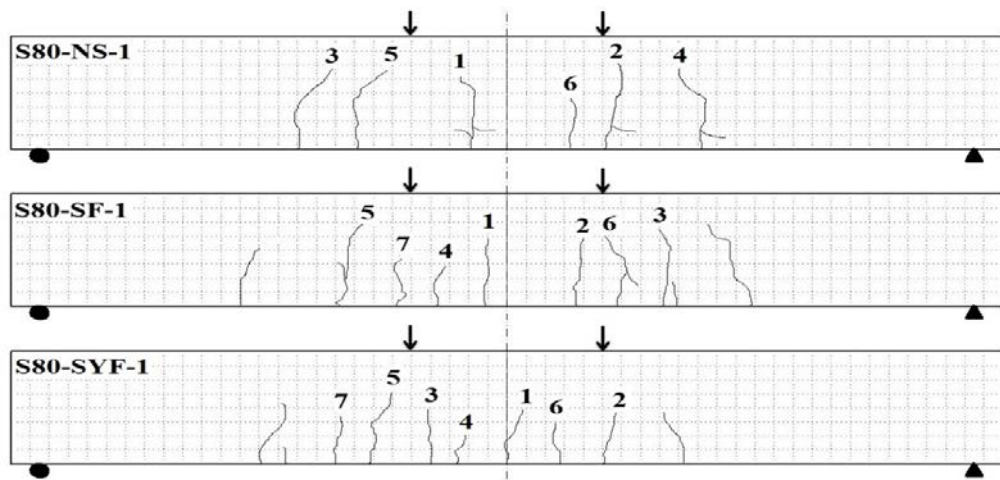
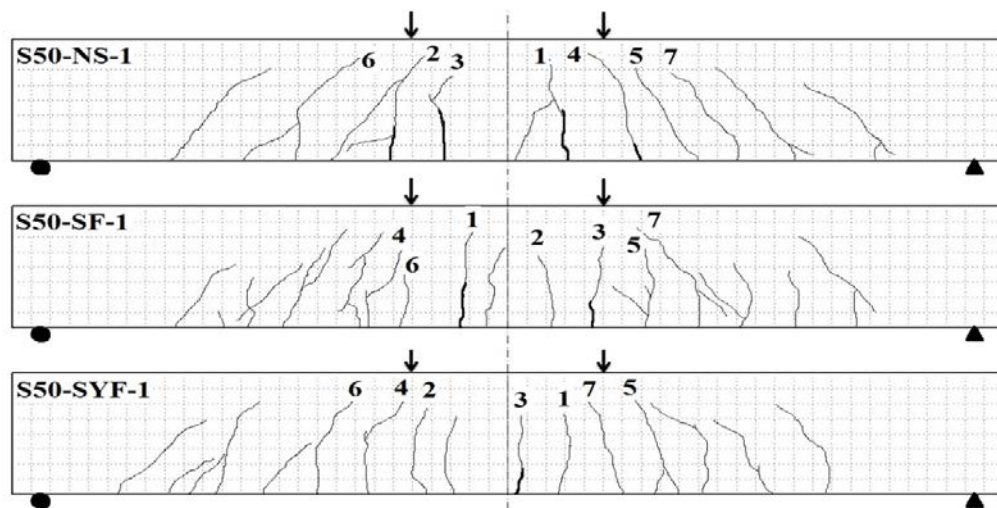**(b)**
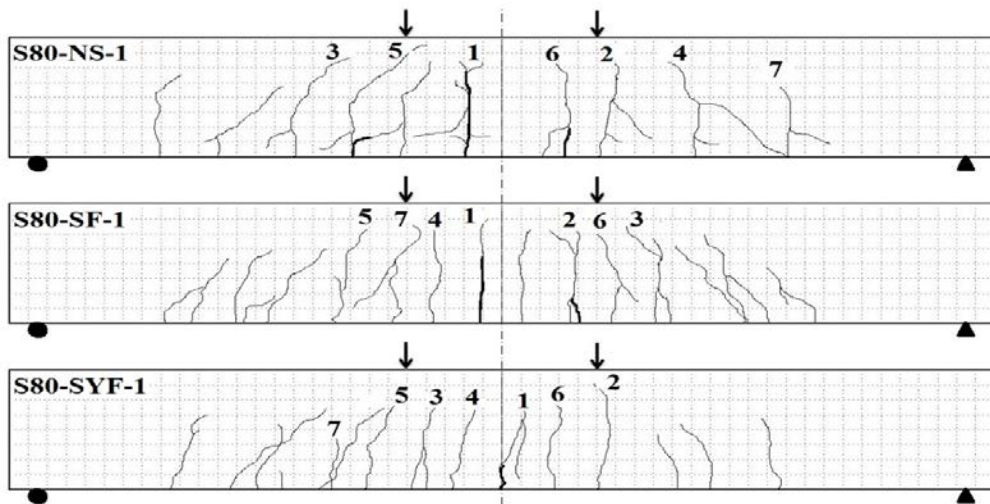
(c)

Figure 23: Crack patterns for S80-(NS, SF, and SYF)-1 at: (a) service load; (b) steel yielding load; (c) ultimate load
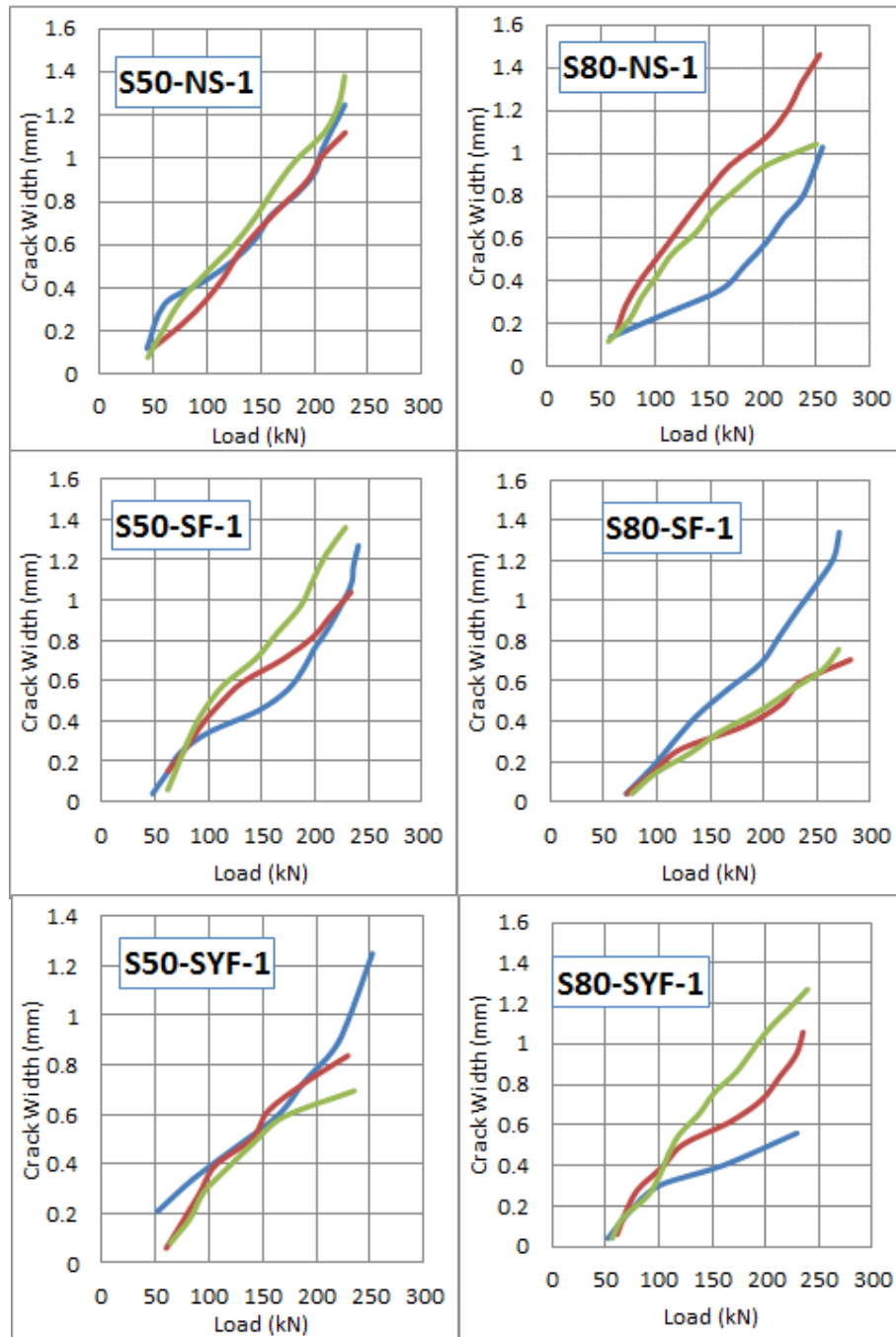
50

(a)

(b)

(c)

Figure 24: Crack patterns for S50-(NS, SF, and SYF)-1 at: (a) service load; (b) steel yielding load; (c) ultimate load

51

4.3 Pullout Tests

In this section, the adequacy of the ACI 318-08 (Equation 5) to compute the development length of HSS rebars embedded in different types of concrete with different concrete compressive strengths is evaluated. The stress-strain responses were established based on strain readings obtained from strain gauges mounted on the rebars. Figure 27 presents the typical stress versus strain responses for the HSS reinforcing bars when being pulled out from blocks cast with the proposed types of concrete. Although three bars were embedded in each concrete block, only a typical response (for each block) is presented in Figure 27 to ease differentiating between the behaviors of the bars when the type of concrete is being varied. The stress-strain responses for all other bars embedded in the different types of concrete are provided in Appendix D. The maximum tensile stress developed in each bar and the average maximum tensile stresses for the different blocks are given in Table 12.

Table 12: Summary of the pullout tests

Pullout block type	Bar No.	Maximum tensile stress (MPa)	Avg. tensile maximum Stress (MPa)
50-NS	1	957	
	2	762	895
	3	967	
50-SF	1	980	
	2	968	963
	3	941	
50-SYF	1	937	
	2	899	934
	3	965	
80-NS	1	901	
	2	860	886
	3	896	
80-SF	1	886	
	2	896	890
	3	886	
80-SYF	1	927	
	2	881	910
	3	923	

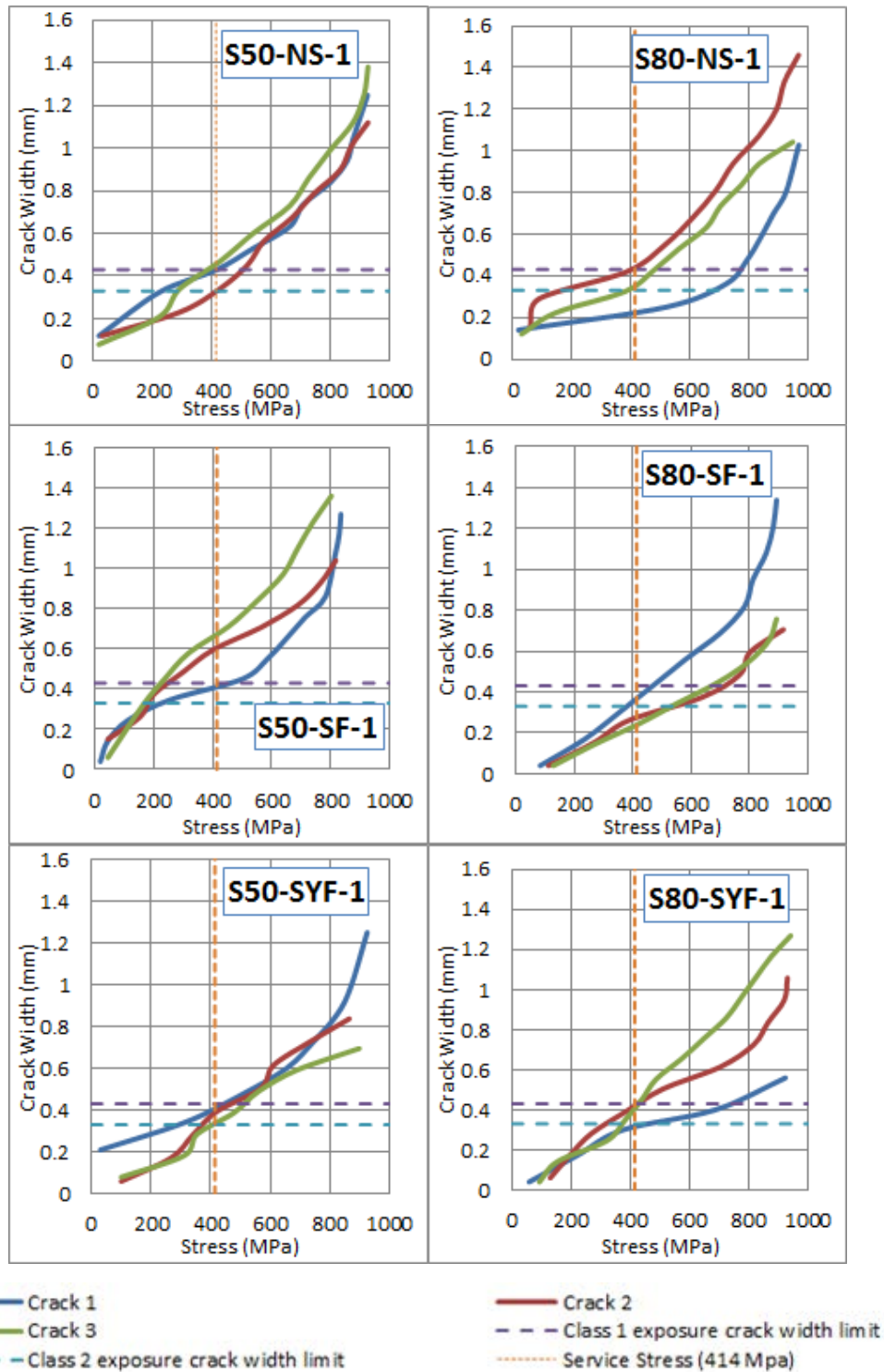**Figure 25: Crack width versus load responses**

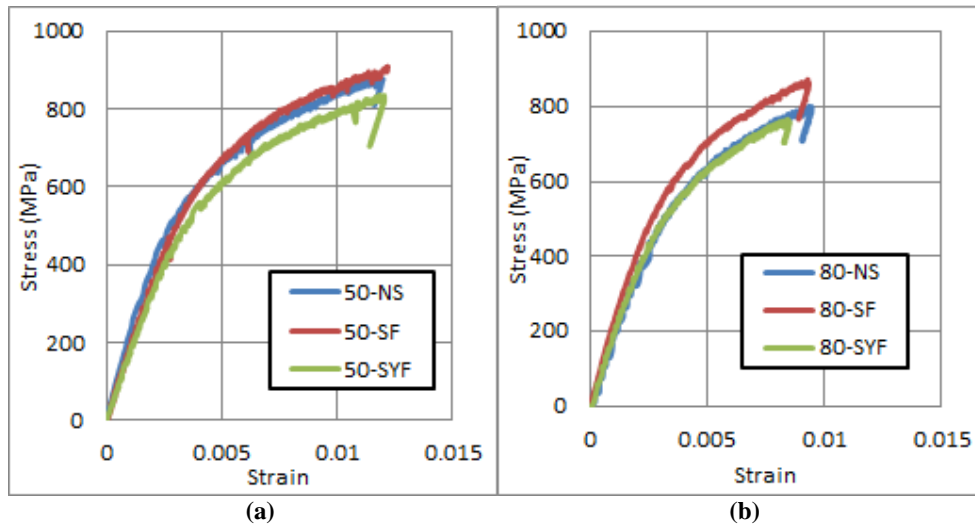**Figure 26: Crack width versus longitudinal bar stress responses**

Figure 27: Typical stress versus strain relationships for bars embedded in: (a) 50-(NS, SF, and SYF) pullout blocks (b) 80-(NS, SF, and SYF) pullout block

Chapter 5: Results Discussions

5.1 Flexure Tests

5.1.1 The effect of concrete compressive strength (f'_c). The effect of the concrete compressive strength on the load vs displacement behavior varied with the type of concrete used. Negligible differences in the specimens' stiffness were generally observed before the appearance of the first crack, i.e., first cracking load. After the first cracking load, it was found that, for the same type of concrete (NS, SF, and SYF), specimens with $f'_c = 80$ MPa exhibited a slightly higher stiffness than those having $f'_c = 50$ MPa, as shown in Figures 22 (a) and (b). This indicates that increasing the concrete compressive strength has the potential to enhance the stiffness of the specimens, irrespective of the type of concrete being used. It was noticed that, in general, specimens with higher f'_c started cracking at higher loads which indicates that theses specimens were capable of resisting more damage, and thus exhibited higher stiffness (Table 11). Additionally, increasing concrete compressive strength contributed positively to the maximum load carrying capacity; however, the percentage of such increase varied with concrete type. The highest recorded percentage of increase in load capacity due to the increase in concrete compressive strength was found to be 13.4 % in S80-SF specimens; whereas, the least was found to be 2.8 % in S80-SYF specimens, as shown in Table 10. Tables 13 and 14 present the strain values at the two cross-section extremes for S80-(NS, SF and SYF)-1 and S50-(NS, SF and SYF)-1, respectively, at first cracking load, steel yielding load, and 95 % of the ultimate load. In general, irrespective of the type of concrete, the increase in concrete compressive strength led to increase in concrete compression strain at mid-span at top surface prior to reaching the ultimate load. As the ultimate concrete compression strain increases, the strain in tension reinforcement increases, resulting in developing higher stresses and thus enhancing the section capacity.

Increasing the concrete compressive strength in case of specimens with plain concrete did not enhance the curvature ductility. In fact, the increase in concrete compressive strength reduced the curvature ductility of S80-NS beam by 5 % when compared to that of S50-NS beam (see Table 10). The increase in concrete compressive strength in specimens with plain concrete resulted in delaying the yielding of the HSS reinforcement, which in turn increased the curvature at steel yielding load, as shown in

Tables 13 and 14. Therefore, such increase in the curvature at steel yielding load resulted in decreasing the curvature ductility. In addition, it was found that increasing the concrete compressive strength for specimens cast with the same type of concrete had insignificant effect on the cracking behavior at service, steel yielding and ultimate load (see Figures 23 and 24).

Table 13: section strain distribution for S80-(NS, SF, and SFY)-1 at three loading stages: initiation of the first crack, yielding of steel bars, and 95 % of the ultimate load capacity

Table 14: section strain distribution for S50-(NS, SF, and SFY)-1 at three loading stages: initiation of the first crack, yielding of steel bars, and 95 % of the ultimate load capacity
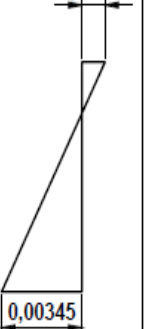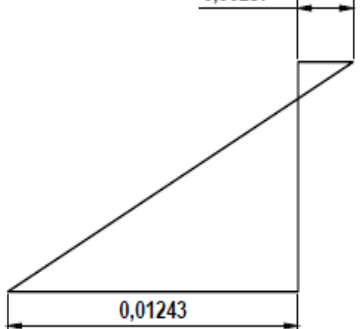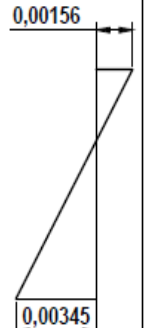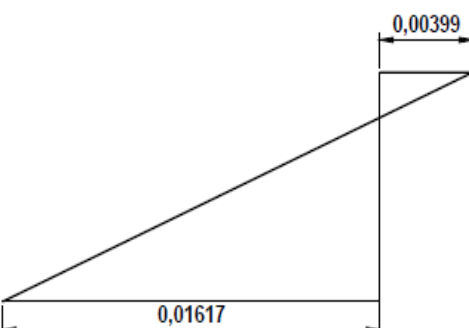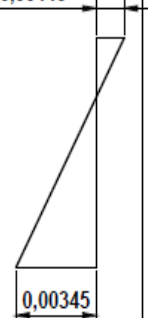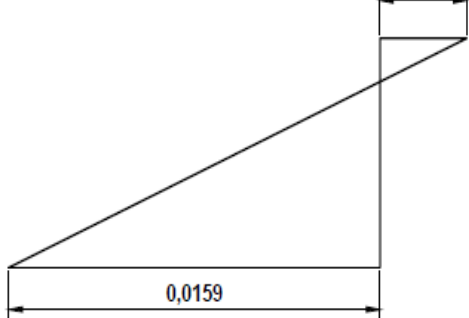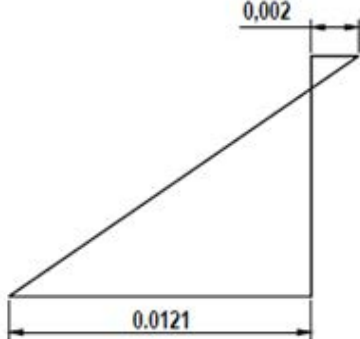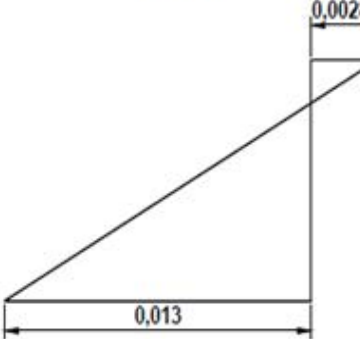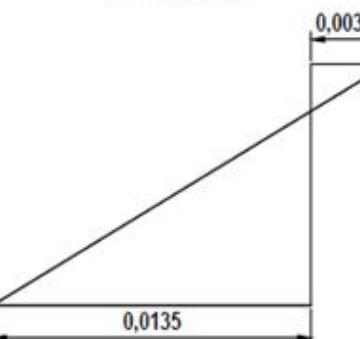
Specimen Type	Cracking Load	Steel Yielding load	0.95 % Ultimate Load Capacity
S50-NS	P = 50 kN 0,00011 0,00008	P = 138 kN 0,0007 0,00345	P = 251 kN 0,002 0.0121
S50-SF	P = 57 kN 0,00022 0,00013	P = 179 kN 0,00146 0,00345	P = 268 kN 0,00281 0,013
S50-SYF	P = 50 kN 0,00024 0,00023	P = 151 kN 0,00107 0,00345	P = 272 kN 0,00326 0,0135

5.1.2 Effect of compression reinforcement. Behavior of the specimens with doubly reinforced sections was compared with their corresponding single reinforced specimens (cast with the same type of concrete) to evaluate the effect of the compression reinforcement on the overall performance of the beams. It can be seen from Figures 20 (c) and (d) that the addition of compression reinforcement had

58

insignificant influence on the load carrying capacity of all single reinforced specimens regardless of the type of concrete used. A 2.9 % increase in the load capacity of D50-SF when compared to that of S50-SF was found to be the highest recorded percentage of increase in the load capacity due to the addition of compression reinforcement (Table 10). The existence of HSS reinforcement in the compression zone had insignificant effect on the load carrying capacity of D50-NS, D50-SYF and D80-SF specimens when compared to their corresponding specimens with single reinforced section. Table 15 shows the locations of the neutral axis, strains and corresponding stresses in the compression reinforcement for the first set of doubly reinforced specimens at 95 % of the ultimate capacity. Prior to reaching the nominal capacity, the neutral axes of all doubly reinforced specimens were located below the compression steel, which indicates that such reinforcement must have enhanced the compression zone in all of the specimens. However, the strains at the level of the compression reinforcement were extremely small to develop sufficient stresses that would noticeably contribute to the section capacity as can be seen in Table 15. This can be attributed to the small distance between the location of the neutral axis and the compression steel prior to reaching the ultimate load.

Table 15: Section properties of the first set of doubly reinforced specimens at 95 % of the ultimate capacity

	Location of neutral axis from top (cm)	Strain in compression steel	Stress in compression steel (MPa)
D50-NS-1	7.24	-0.0001	18.2
D50-SF-1	6.39	-0.0004	83.5
D50-SYF-1	5.28	-0.0002	41
D80-NS-1	6.92	0	0
D80-SF-1	6.82	-0.00018	35.4
D80-SYF-1	7.62	-0.0005	99.5

It is common to provide compression reinforcement in the case of concrete beams reinforced with conventional steel to increase the ductility of the specimens since the addition of such reinforcement causes a reduction in the depth of the compression stress block; "a". Since the stresses developed in the compression reinforcement were small, the effect of these reinforcement on "a" was negligible. Therefore, the

enhancements of the compression reinforcement to the ductile behavior, i.e., the curvature ductility of specimens reinforced with HSS, were small and only observed in D50-SF and D50-SYF specimens. In contrast, the curvature ductility of specimens cast with other types of concrete was reduced due to the addition of the compression reinforcement. Moreover, it was observed that the presence of the HSS reinforcement in the compression zone had no influence on the failure mode of the doubly reinforced specimens.

5.1.3 Effect of Fibers

5.1.3.1 Effect on moment capacity. By comparing the behavior of fiber-reinforced concrete specimens with their corresponding plain concrete specimens, the addition of steel or synthetic fibers resulted in increasing the load capacity and enhancing the cracking and post cracking behavior of fiber-reinforced specimens. Steel and synthetic fibers increased the maximum moment capacity in fiber-reinforced specimens regardless of their concrete compressive strength and reinforcement arrangement. In case of SF specimens, percentage of increase in load capacity was higher for specimens with $f'_c = 80\ MPa$; whereas, in the case of SYF specimens, percentage of increase in load capacity was higher for specimens with $f'_c = 50\ MPa$. Steel fibers in S80-SF and S50-SF increased the load capacity of S80-NS and S50-NS by 16.3 % and 6.5 %, respectively. In contrary, synthetic fibers in S80-SYF and S50-SYF increased the load capacity of S80-NS and S50-NS by 6.5 % and 9.5 %, respectively (see Table 10). The less contribution of synthetic fibers to the load capacity as compared to the contribution of steel fibers can be explained by the difference in strength between the two types of fibers; a similar behavior was reported by Yang et al. [15]. Plastic synthetic fibers exhibited less strength to resist the shearing forces as compared to steel fibers. However, they utilized similar mechanism in enhancing the flexural performance of NS specimens.

In general, the use of fibers helped controlling the compression failure of the concrete by the bridging effect, allowing the HSS reinforcement to reach the strain hardening phase, which can be the main reason for the increase in moment capacities observed in fiber-reinforced specimens. For example, prior to the ultimate load, S80-SF-1 beam had a concrete compression strain near the top surface of mid-span of 0.00399, while S80-NS-1 had a concrete compression strain of 0.00237. The difference

between the two concrete compression strains allowed HSS reinforcing bars to undergo higher strains than that found in NS beams, as shown in Table 13. Similar observation was found in specimens having $f'_c = 50\ MPa$, as given in Table 14. The increase in the strain of the HSS reinforcement does not only contribute to the section capacity, but it also helps meeting the ACI-ITG-6R target strain limit for the section to be classified as tension-controlled; hence, a design reduction factor of 0.9 can be assigned.

5.1.3.2 Effect on curvature ductility. Steel and synthetic fibers also enhanced the curvature ductility in all specimens except for S50-SF beam where curvature ductility was slightly reduced due to steel fibers (Table 10). The highest recorded percentage of increase in the curvature ductility was around 30 % in S80-SYF beam when compared to that of S80-NS beam. Steel-fiber reinforced concrete exhibited an enhanced tensile strength which resulted in delaying the yielding of the HSS rebars. In Table 14, it can be seen that the HSS rebars in S80-SF and S50-SF beams yielded at higher loads than their counterparts in plain concrete specimens. Such delay in the yielding of the reinforcement resulted in having higher curvature at steel yielding load, and thus the curvature ductility was slightly reduced, particularity in S50-SF beam.

It is worth noting that, based on the behavior of NS control specimens, a 5 % drop in load carrying capacity beyond the ultimate was considered to be an indication of beam failure in the current analysis. However, loading was continued until further stages for each test. In this regard, the HSS reinforcing bars in all SF and SYF specimens were ruptured after more than 20 % drop in the maximum load carrying capacity, except for S50-SYF beam where the HSS bars ruptured after 5% drop only (see Figure 20). The use of these fibers in concrete controlled the propagation of cracks at the top compression face which allowed the HSS reinforcement to be strained further. Figure 28 shows the difference in the compression zone at the top of mid-span section in the three S80 specimens after 5 % drop in the load carrying capacity. The figure illustrates how the compression zone at mid-span in S80-NS beams was severely damaged; whereas, in S80-NS and S80-SYF beams, it was well preserved. The capability of SF and SYF specimens to sustain loads after failure confirms that these specimens exhibited an enhanced ductile behavior when compared to NS specimens.
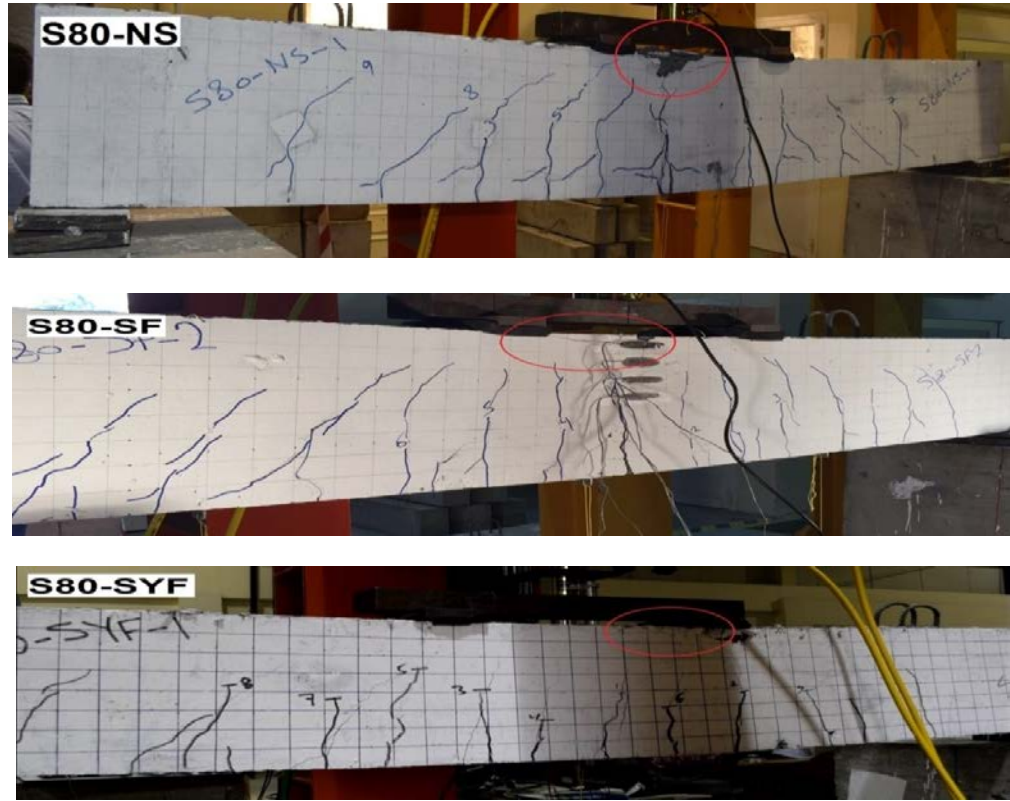
Figure 28: Failure mode of S80-NS, S80-SF and S80-SYF specimens after 5 % in the load capacity

5.1.3.3 Effect on cracking behavior. The bridging effect of the steel and synthetic fibers had a dominant influence on the cracking behavior of fiber-reinforced specimens. The specimens with fibers showed higher first cracking load than those without fibers, except in the case of 50-SYF specimens. The highest first cracking load was observed in S80-SYF-1 beam in which the first crack appeared at a load of 72 kN (Table 9). This implies that the synthetic fibers perform better in controlling the appearance of the first crack in 80 MPa concrete mixes.

At service loading, which is defined as the stage at which $0.6f_y$ stress is developed in the HSS rebars, the number of cracks decreased in S80-SYF-1 specimen but increased in S80-SF-1 specimen when compared to S80-NS-1 specimen (Figure 23 (a)). However, the average depth of the cracks that appeared in S80-SF-1 and S80-SYF-1 was less than that of the cracks that appeared in S80-NS-1. The performance of synthetic fibers in controlling the number of cracks at service loading stage was slightly better than that of steel fibers. Since synthetic fibers are less dense than steel fibers,

more fibers can be uniformly distributed along the beam's cross-section in the case of SYF specimens than that of SF specimens, resulting in a better crack control.

At steel yielding stage, although more cracks were developed in both S80-SF and 80-SYF specimens, the depths of these cracks were noticeably less than those that appeared in S80-NS specimen (see Figure 23 (b)). This indicates that the deep propagation of cracks at service and steel yielding stages can be restrained by the bridging effect of the steel and synthetic fibers. A similar observation was noticed at ultimate loading stage, where the dominant influence of steel and synthetic fibers was the increase in the number of cracks compared to S80-NS, resulting in limiting the development of excessively wide cracks (shown in bold lines in Figure 23 (c)) prior to failure. The same observations regarding the effect of fibers on the cracking behavior at the different considered loading stages were observed in specimens having $f'_c = 50\ MPa$ (see Figure 24).

5.1.3.4 Effect on crack widths. The widths of the first three cracks were monitored during the loading process to investigate their compatibility with the code limitation, particularly at service condition. Figure 29 shows the experimentally measured (for the largest only) and analytically predicted (based on Frosch equation) crack width versus the longitudinal bar stress response for S50-(NS, SF, and SYF) and S80-(NS, SF, SYF) specimens. It can be seen from Figure 29 that plain concrete specimen (S50-NS) was characterized with the maximum crack widths at service load conditions, exceeding AASHTO class 1 and class 2 exposure crack width limits, of 0.43 and 0.33 mm, respectively. The effect of increasing the concrete compressive strength to 80 MPa was minimal as shown in S80-NS specimen. Introducing fibers to the concrete mixes, however, was found to be more effective particularly for the case of SF specimens with $f'_c = 80$ MPa. The crack widths in S80-SF were reduced and thus satisfied both class 1 and 2 exposure crack width limits. On the other hand, synthetic fibers were only effective in reducing the crack widths to meet class 1 exposure crack width limit, but not class 2 exposure limit as illustrated in in Figure 11 for S50-SYF and S80-SYF specimens. The suitability of using the Frosch equation for HSS-RC beams to predict the crack width at service is also investigated. The results presented in Figure 27 Indicated that for FRC specimens, the equation slightly overestimated the

maximum probable crack width for $f'_c = 80\ MPa$, whereas it underestimated the maximum probable crack width for $f'_c = 50\ MPa$.
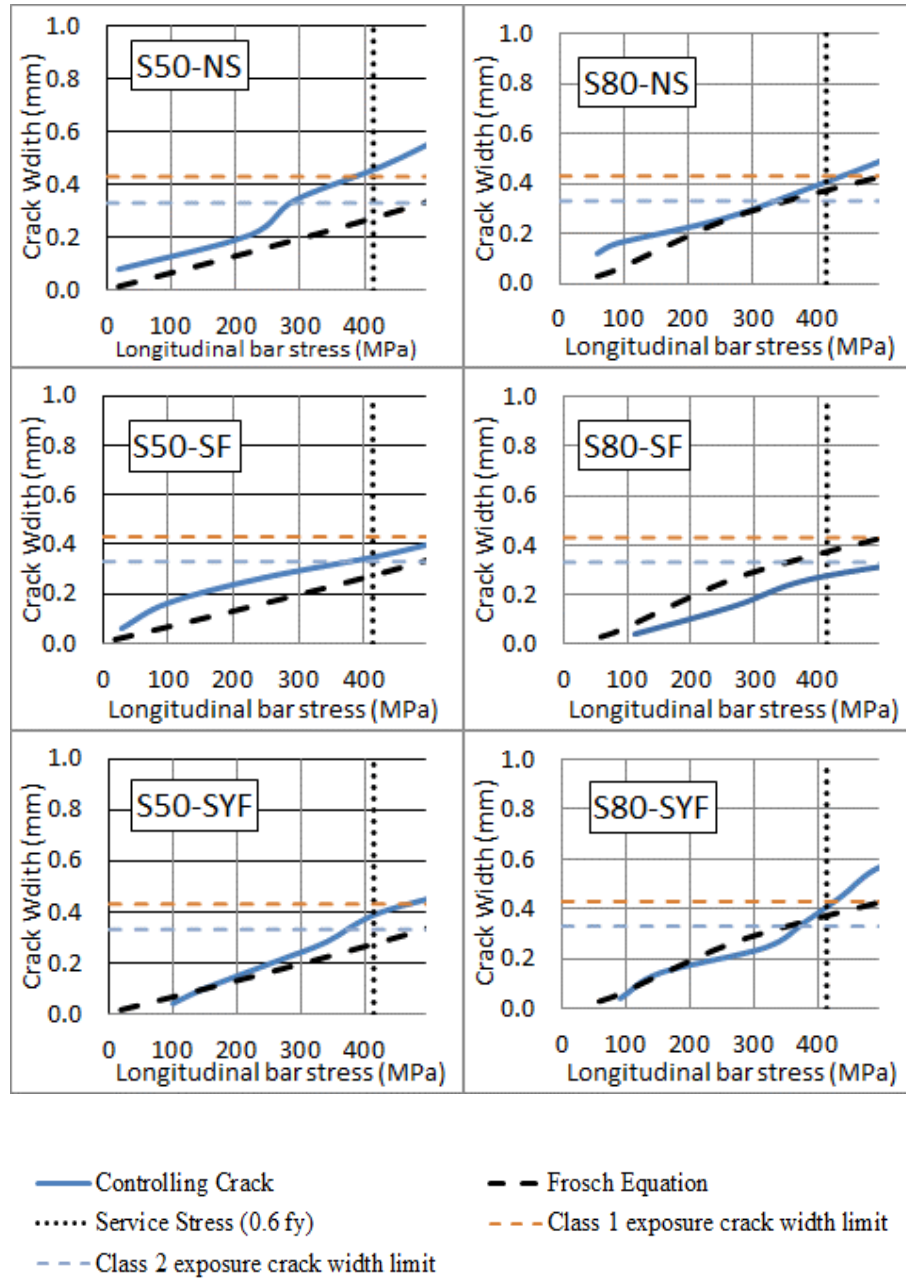

Figure 29: Experimentally measured and analytically predicted (based on Frosch equation) crack width versus longitudinal bar stress responses for S50-(NS, SF and SYF) and S80-(NS, SF and SYF)

5.2 Pullout Tests

It can be seen from the stress-strain responses presented in Figure 27 that the use of Equation 5 to calculate development length for HSS rebars embedded in different types of concrete with different f'_c gives conservative results since it was possible to load the bars till rupture without breaking the bond between the rebars and concrete. The measured average maximum tensile stress in the all of pullout blocks exceeded the yield strength of the HSS rebars (689 MPa), indicating that sufficient development length was provided in all of the blocks. Similar observations were reported by Saleem et al. [32]. In all cases, the HSS rebars were loaded till rupture; however, there were signs of concrete crushing and cracking at concrete surface prior to failure, as shown in Figure 30.

Figure 30: Crushing and cracking of concrete surrounding the rebar at the surface

Chapter 6: Analytical Results

6.1 Evaluation of ACI-ITG Recommendation to measure the moment capacity

Section 4.2 in the ACI ITG-6R-10 design guide provides a simplified design method to compute the nominal and design capacities of flexural members reinforced with ASTM A1035/A1035M bars. The suggested approach is very similar to the one used commonly to compute the capacity of members reinforced with ASTM A615 Grade 414 that is mainly based on an idealized elastic-plastic stress strain curve. The idealized curve of the ASTM A1035/A1035M consists of a linear elastic region with modulus (E) equal to 200 GPa, and a perfectly plastic behavior after reaching a yield stress (f_y) of 690 MPa. In this study, the nominal flexural capacities of the all single-reinforced specimens were computed analytically as per the ACI ITG-6R-10 recommendation and compared with the experimental results. Although different types of concrete mixes were considered in this study, only the concrete compressive strengths were found to affect the analytically computed capacities; thus, nominal capacities were calculated based on f'_c equal to 50 MPa and 80 MPa. The strain in the HSS reinforcement (ε_s) was initially assumed to be more than the yield strain (ε_y) so that f_y can be assumed to be equal to 690 MPa at ultimate to solve for the force equilibrium equation (Equation 7). This assumption has to be verified after finding the location of the neutral axis through strain compatibility analysis.

$$A_s\, f_y = 0.85\, f'_c\, a\, b \tag{7}$$

Here A_s is the area of HSS reinforcement, "a" is the depth of compression zone, and "b" is the width of cross-section. In this analysis, the maximum concrete compression strain was taken to be 0.003 as suggested by the ACI ITG-6R-10. Table 16 summarizes the main parameters used in this analysis and the nominal moment capacities of the two sections considered in the analysis.

In case of NS specimens, the ratio of measured-to-computed nominal moment capacities was found to be approximately 1.65 regardless of the concrete compressive strength. Figure 31 shows how the analytical section strain distribution (based on ACI ITG-6R-10) for S50-NS and S80-NS beams varied from the ones developed experimentally. The analytical approach overestimated the strains in HSS reinforcement and shifted up the location of the neutral axis at ultimate load for both

S50-NS and S80-NS beams. Similar observation was reported by Bernardo et al. [38] who experimentally evaluated the location of neutral axis in high-strength concrete beams. Therefore, the difference between the measured and computed nominal capacities for NS specimens can be attributed to the variability between section properties that are developed experimentally and analytically.

<div align="center">Table 16: Summary of analysis</div>

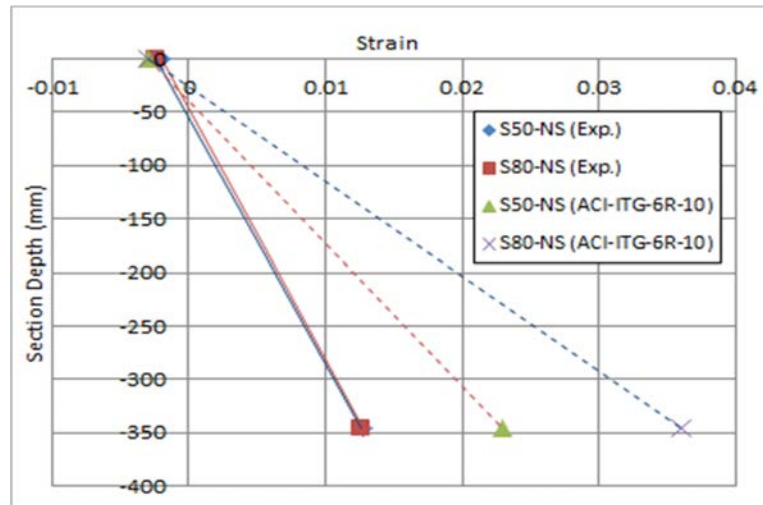| Section type	f'_c (MPa)	A_s (mm^2)	β_1	c (mm)	ε_s	M_n (kN-m)	Measured/ Computed
S50-NS							1.63
S50-SF	50	339	0.693	39.68	0.0238	77.7	1.75
S50-SYF							1.80
S80-NS							1.67
S80-SF	80	339	0.65	26.44	0.0372	80.7	1.95
S80-SYF							1.78

<div align="center">Figure 31: Section strain distributions for NS specimens at ultimate load</div>

Next, the applicability of the ACI ITG-6R-10 was extended to include FRC and its effect on the beam section capacity as compared with experiments. Initially, the validity of the assumption of plane section remains plane was evaluated using two different approaches of section strain distribution at ultimate load. The first approach was developed by linearly connecting the strains of concrete and steel at the mid-span extremes. The other approach, on the other hand, considers actual concrete strains using the strain gauges readings located at different depths along the beam mid-span section (see Figure 32). It can be noticed from Figure 32 that there is a consistency in the

<div align="center">67</div>

locations of the neutral axis when being established using the two different approaches. This indicates that the assumption of plane section remains plane is valid and applicable to FRC beams reinforced with HSS bars.
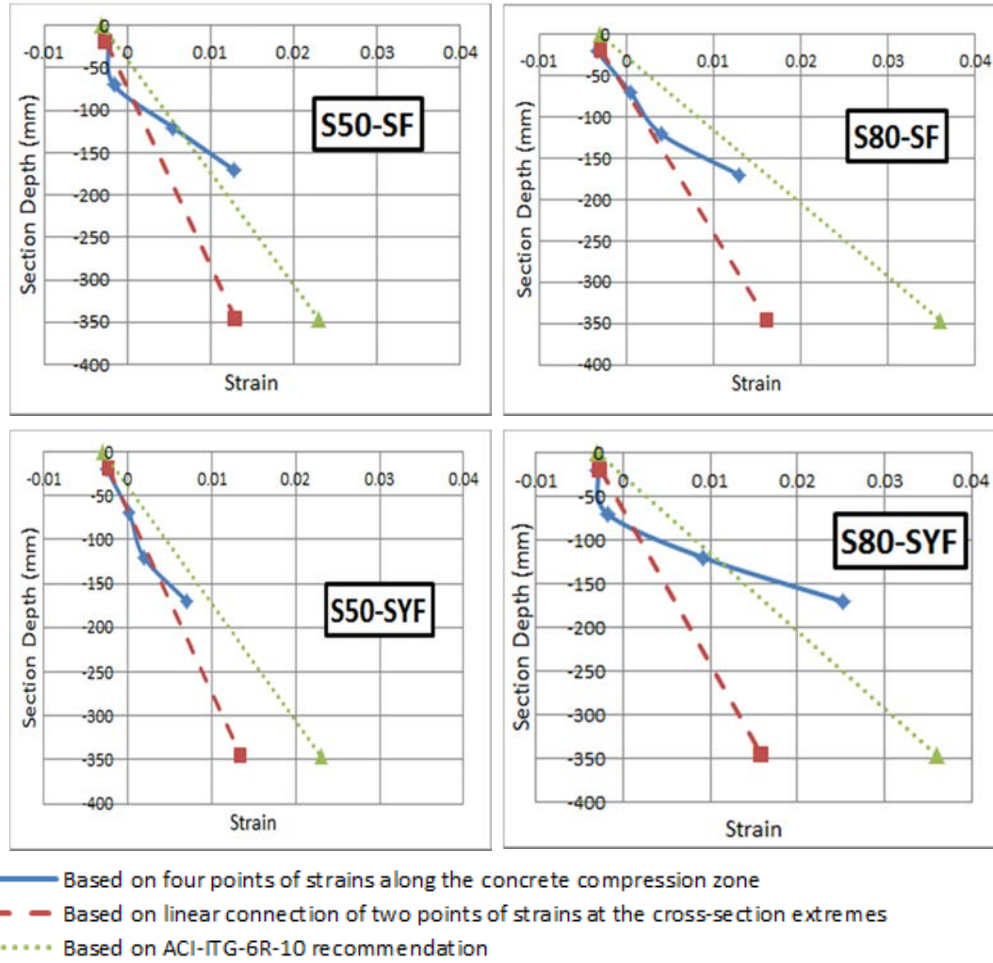

—— Based on four points of strains along the concrete compression zone

– – Based on linear connection of two points of strains at the cross-section extremes

······ Based on ACI-ITG-6R-10 recommendation

Figure 32: Section strain distributions based on different approaches for SF and SYF specimens at ultimate load

Similar to NS specimens, the ACI ITG-6R-10 recommendations were adopted to compute the flexural capacities of SF and SYF specimens. The ratios of measured-to-computed nominal moment capacities for S50-SF and S80-SF beams were 1.75 and 1.95, respectively; whereas, for S50-SYF and S80-SYF, the ratios were 1.80 and 1.78, respectively (Table 16). These high ratios for SF and SYF specimens may be attributed, similar to NS specimens, to the variation of section strain distributions between the ACI ITG-6R-10 and the experiments, as shown in Figure 32.

In addition to the strain distribution, the accuracy of β_1 factor, which relates the depth of the equivalent compression block to neutral axis depth, should be evaluated. The actual depth of the equivalent compressive stress block was determined by

measuring the depth of the compression zone prior to reaching the ultimate load; whereas, the location of the neutral axis was determined by developing the actual strain distribution along the specimen section. As a result, and based on the previous findings, β_1 was computed experimentally. Table 17 presents the measured *a, c,* and β_1 for the first set of specimens with single reinforced sections.

Table 17: Measured Section Properties

	a (mm)	*c* (mm)	β_1
S50-NS-1	37	46.7	0.792
S50-SF-1	33.6	64.2	0.523
S50-SYF-1	41.9	67.2	0.624
S80-NS-1	25.5	54.9	0.464
S80-SF-1	22.47	68.4	0.329
S80-SYF-1	27.3	65.7	0.416

Specimens cast with concrete having f'_c of 80 MPa had smaller β_1 when compared to that of specimens having f'_c of 50MPa. Nerveless, none of these experimentally-measured β_1 values matched their theoretical counterparts. The variation between the two can be another reason explaining the differences between the computed and measured nominal capacities. Based on the above results, extending the ACI ITG-6R-10 recommendation to cover FRC beams might be valid and applicable since the conservativeness of the results was maintained.

The accuracy of the computed flexural resistances was further evaluated by adopting Shahrooz et al. [7] recommendations in which the yield stress of the idealized stress-strain relationship was taken as the stress corresponding to a strain equal to 0.005. The stress corresponding to a 0.005 strain is equal to 754 MPa for the reinforcing steel used in this study (Figure 13). By replacing the 689 MPa yield stress used in the previous analysis with f_y = 754 MPa, the computed flexure capacities were closer to the experimentally-measured values. Accordingly, the ratios of measured-to-computed nominal moment capacities ranged from 1.52 to 1.64 and from 1.54 to 1.81 for specimens with f'_c = 50 MPa and f'_c = 80 MPa, respectively.

Chapter 7: Finite Element Work

7.1 Model Description

A finite element software package, commercially known as ABAQUS, was used to carry out a nonlinear 3D finite element analysis to model the flexural behavior of four specimens considered in the experimental program. The finite element analysis was limited to specimens cast with plain concrete which were S50-NS, D50-NS, S80-NS and D80-NS. The non-linear behavior of concrete was modeled using damaged plasticity model in which the compressive and tensile behaviors were defined using the actual stress-strain curves obtained from tested cylinders. The concrete damage plasticity parameters presented in Table 18 were adopted in modeling beams with $f'_c =$ 50 and 80 MPa. Table 19 provides the parameters used to define the compressive and tensile stress strain behaviors for concrete having $f'_c =$ 50 and 80 MPa.

Table 18: concrete damage plasticity parameters for concrete having $f'_c =$ 50 and 80 MPa

Dilation Angle	Eccentricity	fb0/fc0	k	Viscosity Parameter
36	0.1	1.16	0.667	1.00E-05

Similarly, the actual stress strain response of the HSS rebars, which was obtained from the tensile test presented in Figure 13, was considered in the FE modeling. The geometry of the concrete beam was modeled using linear four-node three dimensional solid elements with reduced integration (C3D8R ABAQUS type). The 3D solid element has 3 degrees of freedom per node. The longitudinal HSS bars and the stirrups geometries were modeled using 2-node truss elements, as shown in Figure 33. Moreover, in order to take the advantage of symmetry and reduce the computational time, only one half of the beam was modeled, as shown in Figure 34. The FE results were initially verified with the experimental results for the four beams considered. The verified finite element models were then used to carry out a parametric study in which the effect of adopting different bar sizes, i.e., reinforcement ratios on the flexural behavior, was evaluated. Three reinforcement ratios (ρ) of 0.2, 0.3 and 0.75 %, were investigated using NO. 8, 10 and 16 bars, respectively.

Table 19: parameters defining the compressive and tensile behaviors for concrete having $f'_c =$ 50 and 80 MPa.

$f'_c = $ 50 MPa		$f'_c = $ 80 MPa	
Compressive Behavior	Tensile behavior	Compressive Behavior	Tensile behavior
Yield Stress (MPa)	Inelastic Strain	Yield Stress (MPa)	Inelastic Strain
48.04	0	58.5	0
58.42	0.0004	61.5	0.0001
63.42	0.0008	64.5	0.000202
64.72	0.0012	67.4	0.000307
63.54	0.0016	70.3	0.000418
60.76	0.002	73.3	0.000534
57.01	0.0024	76.2	0.000661
43.81	0.0036	79.2	0.000795
-	-	82.0	0.000935
-	-	77.7	0.0012
-	-	76.2	0.0016
-	-	72.9	0.002
-	-	68.4	0.0024
-	-	52.6	0.0036
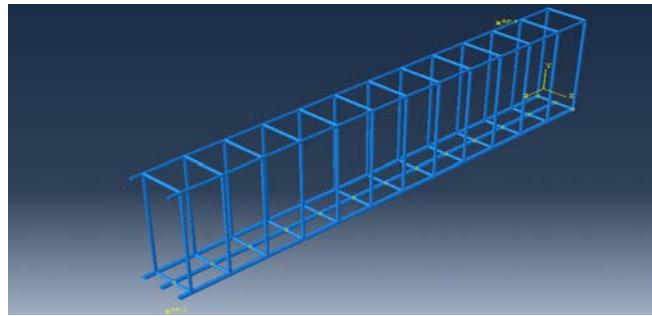
Figure 33: Beam reinforcement (Longitudinal bars and stirrups)
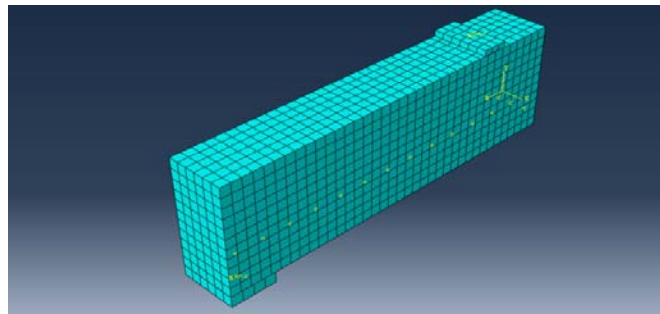
Figure 34: Assembly of the model

7.2 Model Verification

The load versus mid-span deflection predicted using the FE model is in accordance well with their counterpart experimental results as illustrated in Figure 35. The FE model successfully predicted the initial stiffness as well as its degradation trend up to failure. The FE model was also able to capture the crack distribution observed during the experiments for each of the modeled beams. Figure 36 shows a sample of the captured crack distribution in D50-NS beam based on the FE model, along with the experimentally observed crack distribution for the same specimen.
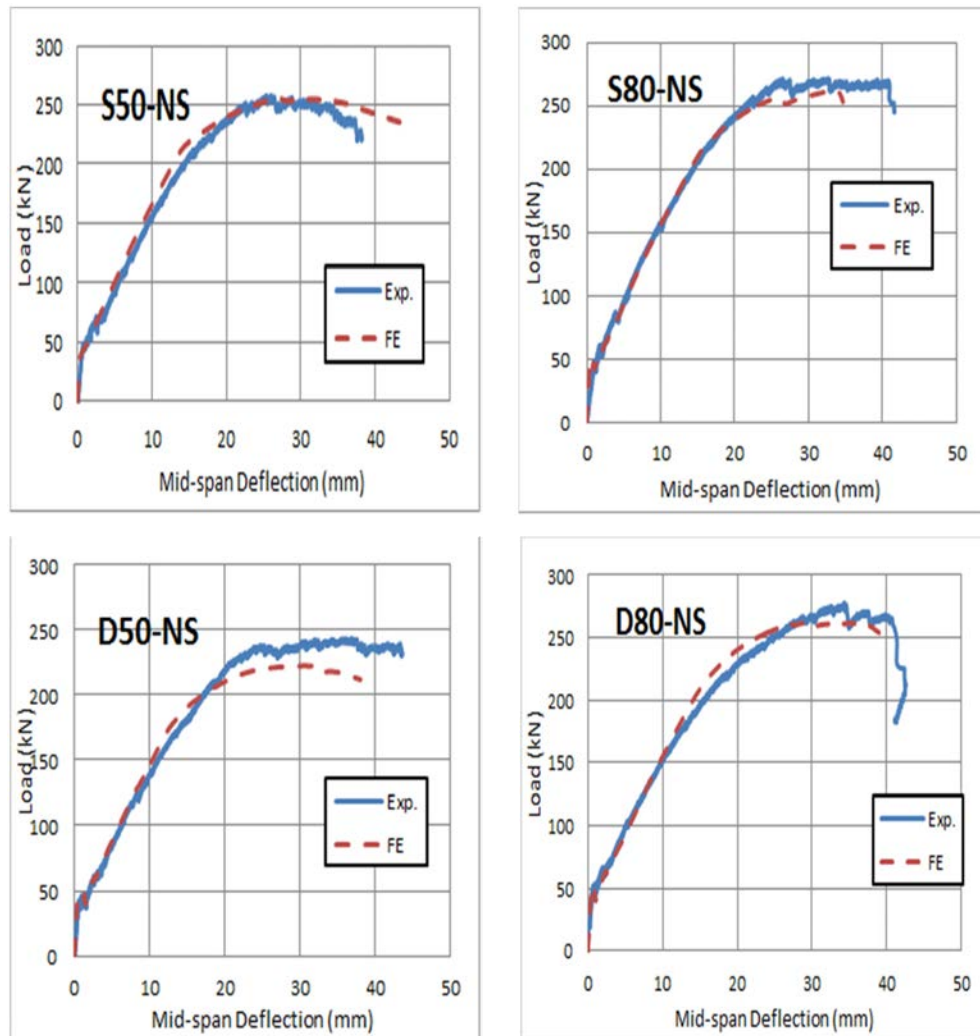
Figure 35: Comparison between experimentally and analytically (FE) generated load versus mid-span deflection responses for: S50-NS; S80-NS; D50-NS; and D80-NS

7.3 Parametric Study

The FE results for the load versus mid-span deflection responses using different tension reinforcement ratios are presented in Figures 37 (a) and (b) for specimens S50-NS and S80-NS, respectively. Results for the relatively low reinforcement ratios ($\rho = 0.2 \% \ and \ 0.3$) indicate the typical Tension-Controlled behavior at which increasing the steel reinforcement ratio resulted in increasing the load capacity in both specimens (S50-NS and S80-NS). However, at the high reinforcement ration $\rho = 0.75$ %, the behavior of the load-mid-span deflection noticeably varied, indicating the change in the section behavior from tension-controlled to compression-controlled.
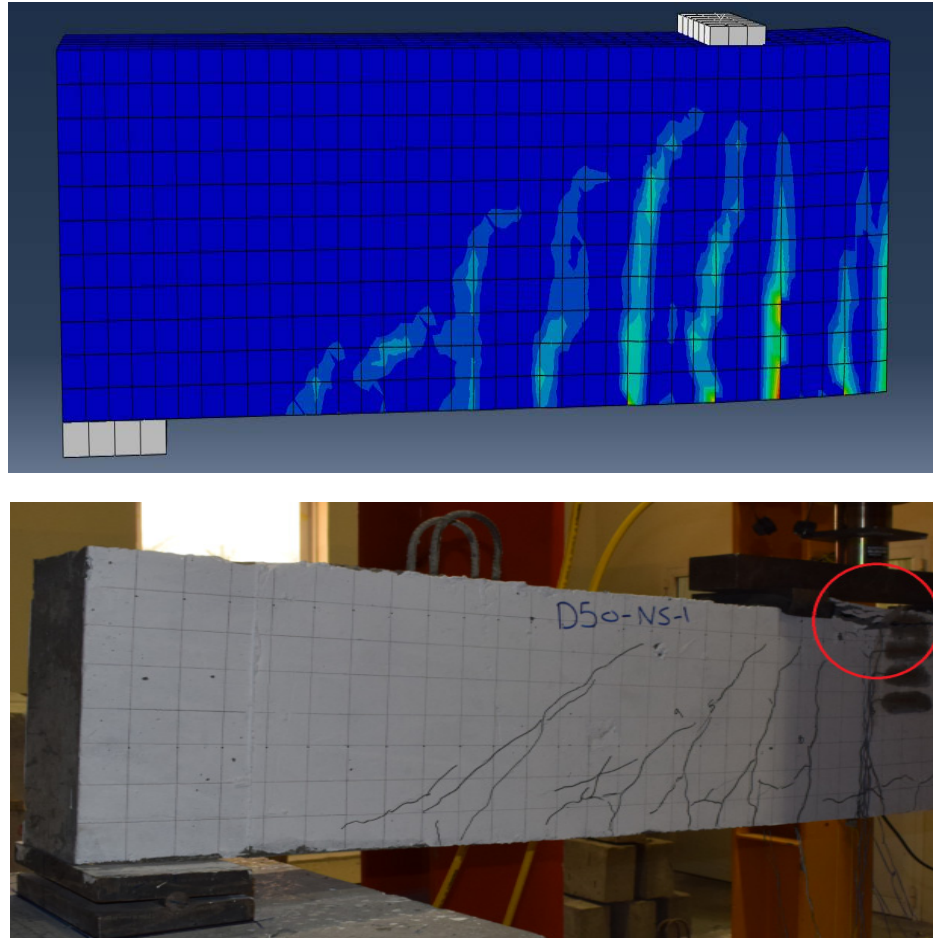
Figure 36: Comparison between the analytically (FE) developed and experimentally observed crack patterns for S50-NS specimen
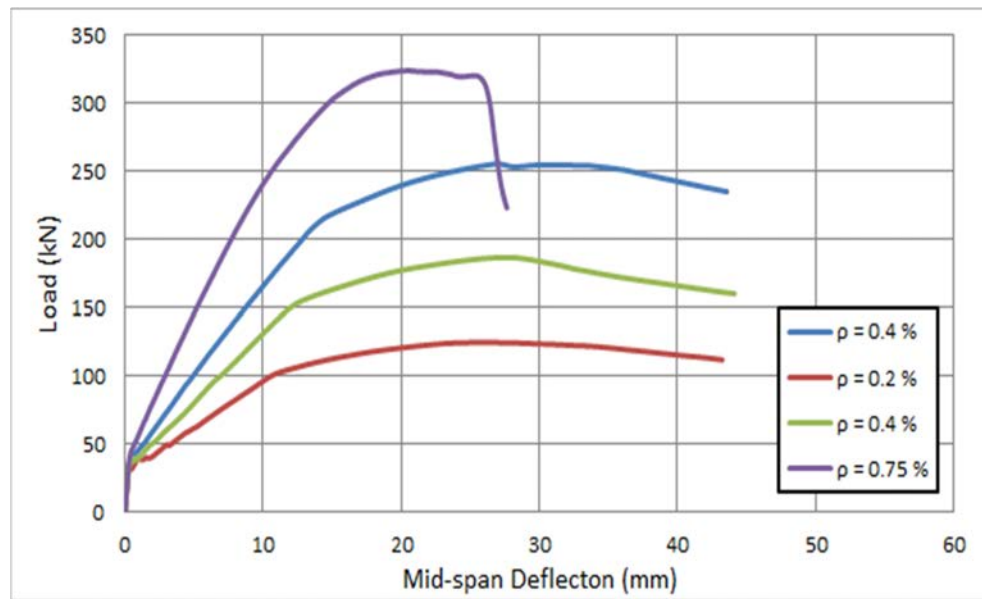
(a) S50-NS
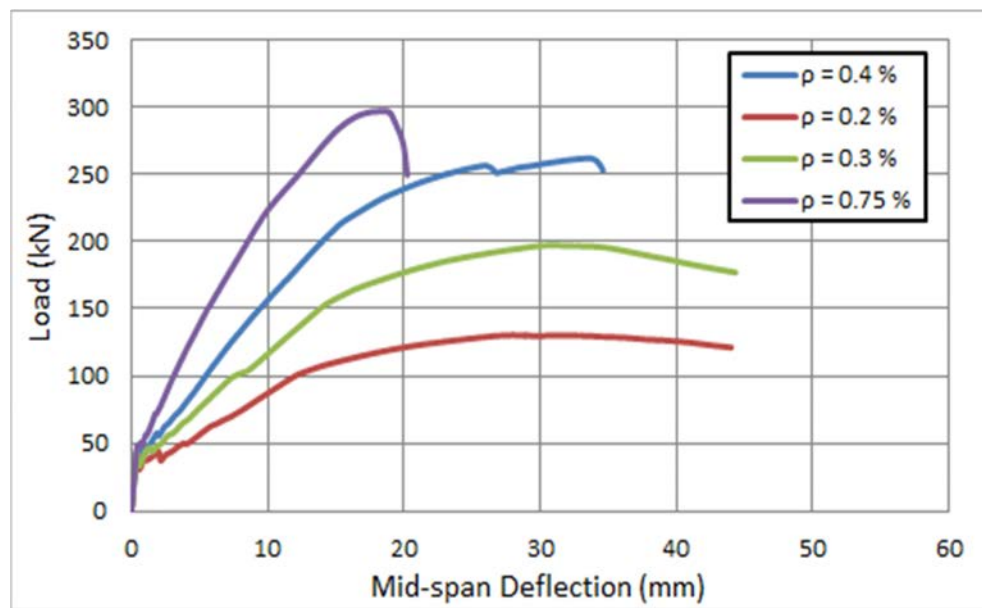
(b) S80-NS

**Figure 37: Load versus mid-span deflection responses when varying the reinforcement ratio for:
(a) S50-NS; and (b) S80-NS**

Chapter 8: Conclusions and Recommendations

8.1 Conclusions

To examine the effect of varying concrete compressive strength, compression reinforcement, steel and synthetic fibers on the flexure behavior of ASTM A1035 bar-reinforced concrete members, an experimental research program was carried out. In addition, an analytical investigation was conducted to evaluate the current design recommendations associated with the use of ASTM A1035 Grade 689 in flexural members cast with plain and fiber-reinforced concrete. A finite element model was also developed and verified using the experimental results for plain concrete specimens only. The following conclusions may be drawn:

1. The effect of fibers on the mechanical properties of concrete at material level was found to be more dominant in steel fiber-reinforced concrete than synthetic fiber reinforced concrete. Steel fiber-reinforced concrete cubes and cylinders exhibited considerably higher concrete compressive strength than the ones cast with plain concrete. In addition, due to the capability of fibers to bridge between cracks, fiber-reinforced concrete was characterized by less destructive failure modes when compared to plain concrete.

2. Increasing concrete compressive strength resulted in enhancing the flexural capacity of HSS-bar reinforced beams irrespective to the type of concrete. The highest increase percentage in the flexural capacity due to increasing concrete compressive strength from 50 to 80 MPa was recorded in specimens with steel-fiber reinforced concrete. Increasing the concrete compressive strength had insignificant contributions to the ductile and cracking behavior at different loading stages.

3. The addition of ASTM A1035 bars to the compression zone had insignificant influence on the flexural capacity and the ductile and cracking behaviors of the doubly reinforced specimens when compared to their corresponding single reinforced specimens. The ASTM A1035 bars in the compression zone did not develop sufficient stains, and therefore stresses, to cause noticeable contributions to the section behavior.

4. The overall flexural behavior of HSS bar-reinforced members can be improved by adopting steel or synthetic fiber-reinforced concrete. Specimen cast with steel fiber-reinforced concrete of $f_c' = 80$ MPa exhibited the highest load

capacity; whereas, synthetic fiber-reinforced specimen having the same high compressive strength exhibited the highest curvature ductility. The ultimate concrete compression strain at mid-span reaches up to 0.004, allowing the HSS reinforcing to develop higher strains, and therefore stresses, and thus contributes to the section capacity.

5. Specimens with fiber-reinforced concrete were characterized by an enhanced cracking behavior at service, steel-yielding and ultimate loading stages when compared to those with plain concrete. At service loading, the performance of synthetic fibers in controlling the number and depth of cracks was found to be better than that of steel fibers.

6. The performance of steel fibers in controlling the crack widths at load corresponding to longitudinal bar stress equal to $0.6f_y$, i.e., service stress varied with the concrete compressive strength. Meeting class 2 exposure crack width limit (0.33 mm) was only possible in specimens with steel fiber-reinforced concrete and with $f_c' = 80$ MPa. Synthetic fibers resulted in restraining the crack widths to meet the class 1 exposure limit and their performance was not affected by f_c'.

7. The pullout test results indicate that computing the development lengths for HSS rebars embedded in different types of concrete as per the ACI 318-08 recommendations is valid and leads to conservative estimates.

8. The load vs mid span deflection as well as the crack distribution behavior predicted using the developed FE model compared very well with their experimental counterparts. The FE model was also able to capture the transition from Tension-Controlled to Compression-Controlled behavior observed in NS specimens when increasing the reinforcement ratios.

8.2 Recommendations

The following recommendations related to the use of HSS reinforcing bars in flexural members can be considered for structural designers and future research work:

1. Steel and synthetic fibers are effective in controlling the number and depth of cracks at service loading condition, but not the crack widths. Even in case of fiber-reinforced concrete, meeting AASHTO class 2 exposure crack width limit was not possible. Therefore, more research work needs to be done to evaluate

the effectiveness of utilizing different types and percentages of fibers in controlling the crack widths, particularly at service load levels.

2. In order to incorporate the findings of the ACI-ITG-6R-10 into the ACI 318 design codes, there is a need for more research work to further document the behavior of HSS-bar reinforced concrete beams and minimize the uncertainty associated with its flexural performance.

3. The behavior of the HSS reinforcing bars embedded in FRC differs than that in plain concrete, and thus there is a need to perform a complete set of pullout tests with different bar sizes and cover thicknesses to formulate an equation that can be used to accurately calculate the development length for HSS bars embedded in FRC.

4. The developed nonlinear FE can be further utilized to perform parametric studies in which parameters affecting the performance of the HSS-bar reinforced members other than the reinforcement ratio; for example, concrete type, may be considered.

References

1. *Standard Specification for Deformed and Plain, Low-Carbon, Chromium, Steel Bars for Concrete Reinforcement*, ASTM International, West Conshohocken, PA, 2010.

2. P. M. Goodrum, B. Davis, G. B. Dadi and A. Thomas, "Case study on the effect of 690 MPa (100 ksi) steel reinforcement on concrete productivity in buildings," *Journal of Construction Engineering and Management*, vol. 139, pp. 4013025, Nov. 2013.

3. G. G. Clemena and Y. P. Virmani, "Comparing the chloride resistances of reinforcing bars," *Concrete International,* vol. 26, pp. 39-49, 2004.

4. *Building code requirements for reinforced concrete and commentary*, American Concrete Institute (ACI) Committee 318, Farmington Hills, MI, 2014.

5. *Design guide for the use of ASTM A1035/A1035M Grade 100 (690) steel bars for structural concrete*, American Concrete Institute Innovation Task Group 6, Farmington Hills, MI, 2010.

6. R. F. Mast, M. Dawood, S. H. Rizkalla and P. Zia, "Flexural strength design of concrete beams reinforced with high-strength steel bars," *ACI Structural Journal*, vol. 105, pp. 570-577, 2008.

7. B. Shahrooz, J. Reis, E. Wells, R. Miller, K. Harries and H. Russell, "Flexural members with high-strength reinforcement: behavior and code implications," *J. Bridge Eng*., vol. 19, pp. 04014003 1-7, May. 2014.

8. *Building code requirements for reinforced concrete and commentary*, American Concrete Institute (ACI) Committee 318, Farmington Hills, MI, 2011.

9. *Interim revisions to the AASHTO LFRD bridge design specifications*, 6th ed., AASHTO, Washington, DC, 2013.

10. *Report on High-Strength Concrete*, American Concrete Institute (ACI) Committee 363, Farmington Hills, MI, 2010.

11. P. K. Mehta and P. J. M. Monterio, *Concrete: Microstructure, Properties and Materials,* 3rd ed. New York: McGraw-Hill, 2006, pp. 55-77.

12. B. M. Shahrooz, R. A. Miller, K. A. Harries, and H. G. Russell, "Design of concrete structures using high-strength steel reinforcement," Transportation Research Board, Washington, DC, NCHRP Rep. 679, 2011.

13. S. Kang and J. Kim, "Investigation on the flexural behavior of UHPC considering the effect of fiber orientation distribution," *Construction and Building Materials*, vol. 28, pp. 57-65, 2012.

14. J. Thomas and A. Ramaswamy, "Mechanical properties of steel fiber-reinforced concrete," *Journal of Materials in Civil Engineering*, vol. 19, pp. 385-392, 2007.

15. J. Yang, K. Min, H. Shin and Y. Yoon, "Effect of steel and synthetic fibers on flexural behavior of high-strength concrete beams reinforced with FRP bars," *Composites Part B*, vol. 43, pp. 1077-1086, 2012.

16. B. A. Graybeal, "Flexural behavior of an ultrahigh-performance concrete I-girder," *Journal of Bridge Engineering*, vol. 13, pp. 602-610, 2008.

17. J. Xia, K. R. Mackie, M. A. Saleem and A. Mirmiran, "Shear failure analysis on ultra-high performance concrete beams reinforced with high strength steel," *Engineering Structures*, vol. 33, pp. 3597-3609, 2011.

18. K. Harries, B. Shahrooz and A. Soltani, "Flexural crack widths in concrete girders with high-strength reinforcement," *J. Bridge Eng.*, vol. 17, pp. 804–812, 2012.

19. R. J. Frosch, "Another look at cracking and crack control in reinforced concrete," *ACI Struct. J.,* vol. 96, pp. 437-442, 1999.

20. G. T. Halvorsen, "Code requirements for crack control," Concrete and concrete construction, ACI SP104, American Concrete institute, Farmington Hills, MI, pp. 275-322, 1987.

21. B. H. Oh, "Flexural analysis of reinforced concrete beams containing steel fibers," *Journal of Structural Engineering,* vol. 118, pp. 2821-2835, 1992.

22. L. Vandewalle, "Cracking behavior of concrete beams reinforced with a combination of ordinary reinforcement and steel fibers," *Materials and Structures*, vol. 33, pp. 164-170, 2000.

23. K. J. Wight and J. G. Macgregor, *Reinforced concrete mechanics and design,* 6th ed. England: Pearson, 2012, pp. 382-392.

24. G. M. Glass, "Performance of Tension Lap Splices with MMFX High Strength Reinforcing Bars." M.A. thesis, The University of Texas at Austin, Texas, United States, 2007.

25. J. B. Johnson, "Bond strength of corrosion resistant steel reinforcement in concrete." M.A. thesis, Virginia Polytechnic Institute and State University, Blaksburg, Virginia, United States, 2010.

26. *Bond and development of straight reinforcing bars in tension*, American Concrete Institute (ACI) ACI 408-R03, Farmington Hills, MI, 2003.

27. M. Khandaker and A. Hossain, "Bond characteristics of plain and deformed bars in lightweight pumice concrete," *Constr. Bulid. Mater.*, vol. 22, pp. 1491-1499, 2008.

28. K. Holschemacher, D. Weibe and S. Klotz, "Bond of reinforcement in ultra high-strength concrete," SP228-34, American Concrete Institute, Farmington Hills, MI, 2005.

29. H. Yalciner, O. Eren and S. Sensoy, "An experimental study on the bond strength between reinforcement bars and concrete as a function of concrete cover, strength and corrosion level," *Cement and Concrete Research*, vol. 42, pp. 643-655, 2012.

30. S. H. Chao, A. A. Naaman and G. J. Aprra-montesions, "Bond behavior of reinforcing bars in tensile strain-hardening fiber-reinforced cement composites," *Struct. J. ACI*, vol. 106, pp. 897-906, 2009.

31. T. Horiguchi, H. Saeki and Y. Fujita, "Evaluation of pullout test for estimating shear, flexural, and compressive strength of fiber reinforced silica fume concrete," *Mater. J. ACI*, vol. 85, pp. 126-132, 1988.

32. K. Mackie, A. Mirmiran, J. Xia and M. A. Saleem, "Development length of high-strength steel rebar in ultrahigh performance concrete," *Journal of Materials in Civil Engineering*, vol. 25, pp. 991-998, 2013.

33. V. Afroughsabet and T. Ozbakkaloglu, "Mechanical and durability properties of high-strength concrete containing steel and polypropylene fibers," *Construction and Building Materials*, vol. 94, pp. 73-82, 2015.

34. K. Hannawi, H. Bian, W. Prince-Agbodjan and B. Raghavan, "Effect of different types of fibers on the microstructure and the mechanical behavior of ultra-high performance fiber-reinforced concrete," *Composites Part B: Engineering*, vol. 86, pp. 214-220, 2016.

35. J. Thomas and A. Ramaswamy, "Mechanical properties of steel fiber-reinforced concrete," *Journal of Materials in Civil Engineering*, vol. 19, pp. 385-392, 2007.

36. Y. Ding and W. Kusterle, "Compressive stress–strain relationship of steel fibre-reinforced concrete at early age," *Cement and Concrete Research*, vol. 30, pp. 1573-1579, 2000.

37. F. Bencardino, L. Rizzuti, G. Spadea and R. N. Swamy, "Stress-strain behavior of steel fiber-reinforced concrete in compression," *Journal of Materials in Civil Engineering*, vol. 20, pp. 255-263, 2008.

38. L. F. A. Bernardo and S. M. R. Lopes, "Neutral axis depth versus flexural ductility in high-strength concrete beams," *Journal of Structural Engineering*, vol. 130, pp. 452-459, 2004.

Appendix A

Plots of Load versus Mid-span Deflection for the second set of specimens are shown in Appendix A.
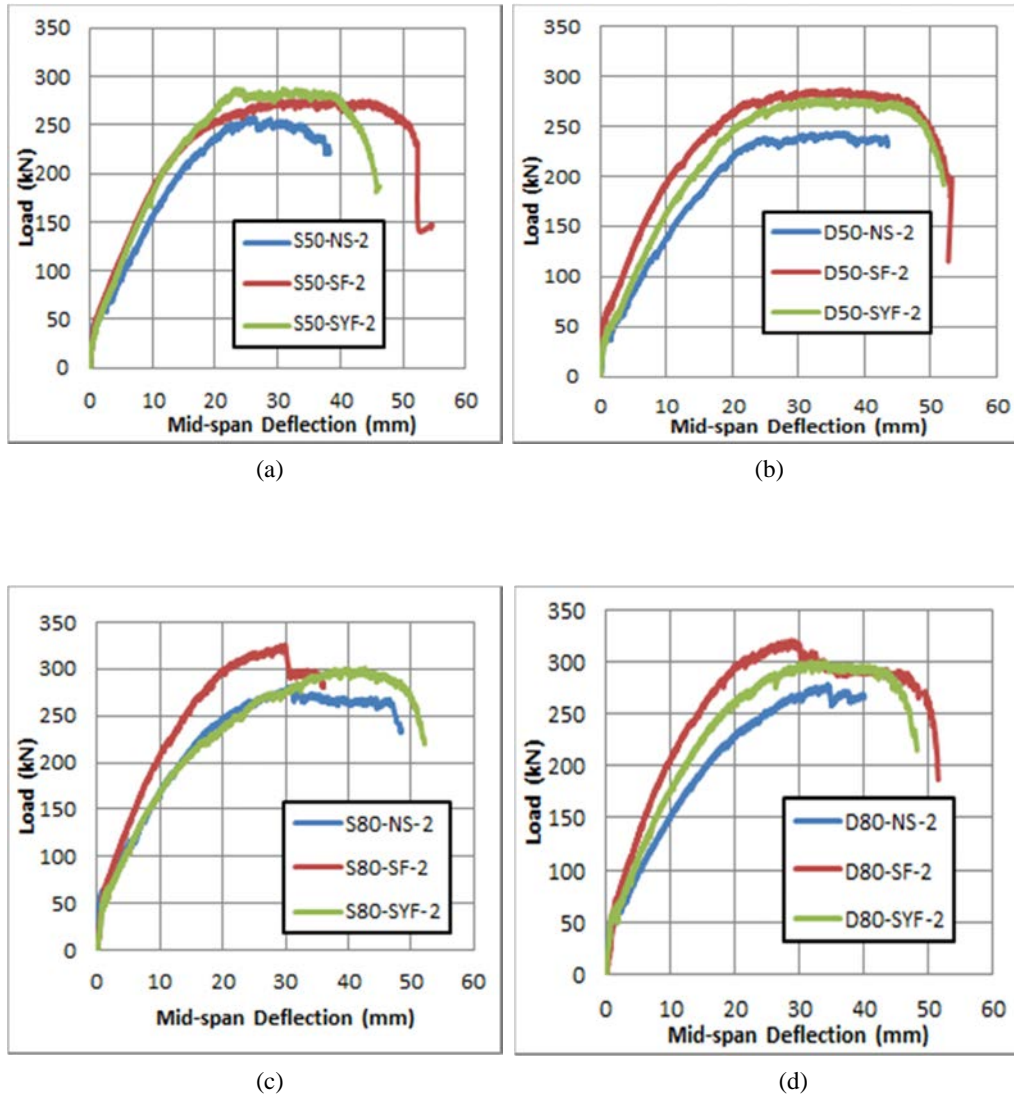
Figure 38: Load versus mid-span deflection responses for the tested beams: (a) S50-(NS, SF, and SYF)-2; (b) S80-(NS, SF, and SYF)-2; (c) D50-(NS, SF, and SYF)-2; (d) D80-(NS, SF, and SYF)-2

Appendix B

The crack patterns of the remaining specimens (whose crack patterns were not provided in the report) at: service load; steel yielding load, and ultimate load are provided in the appendix.
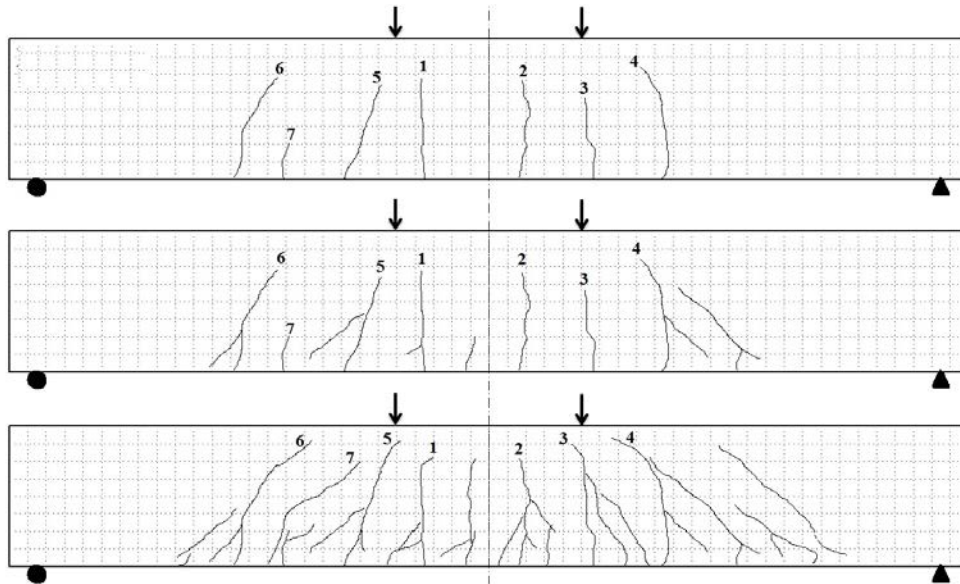

Figure 39: D50-NS-1
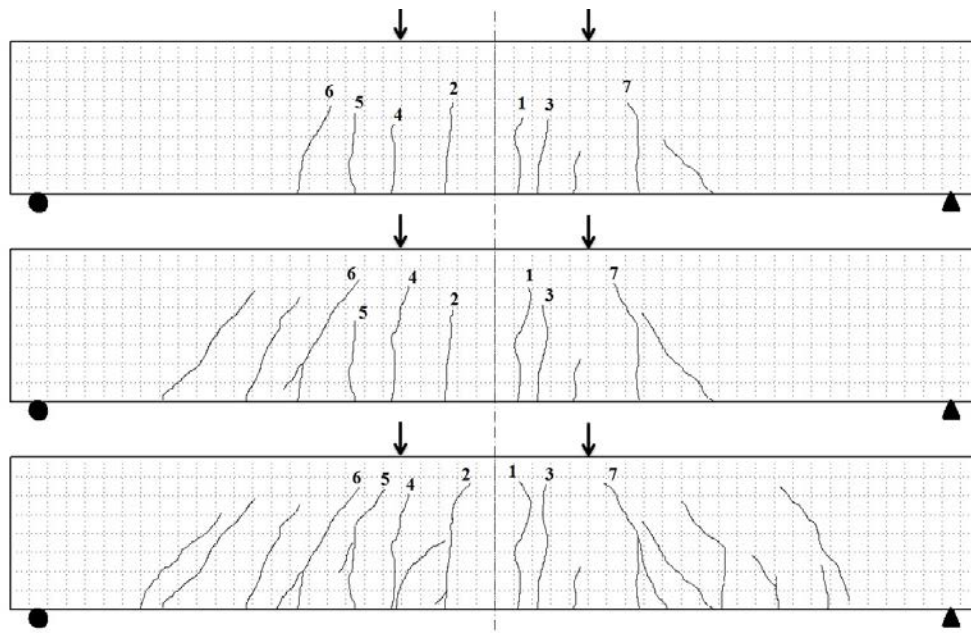
Figure 40: D50-SF-1
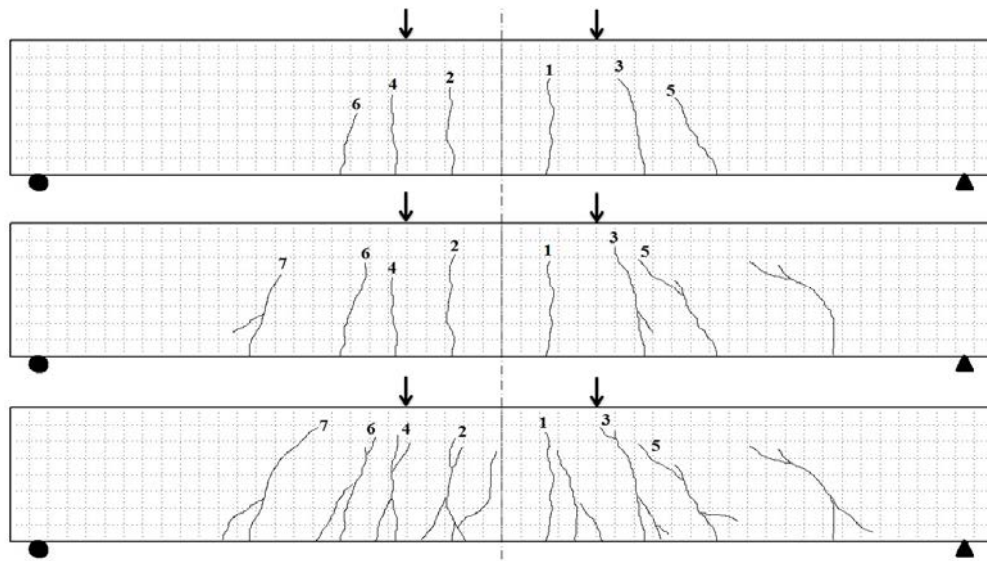
Figure 41: D50-SYF-1
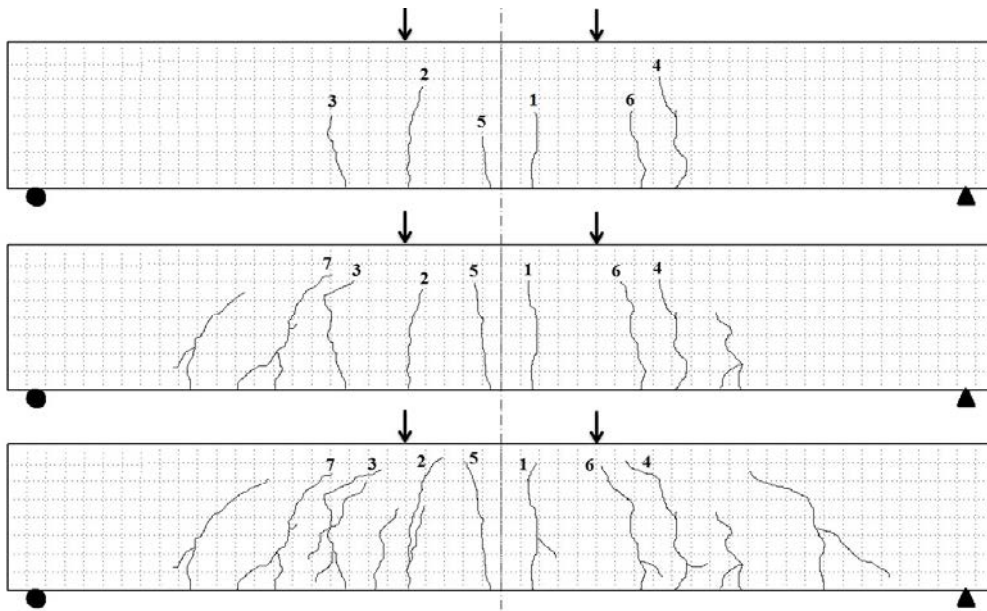
Figure 42: D80-NS-1
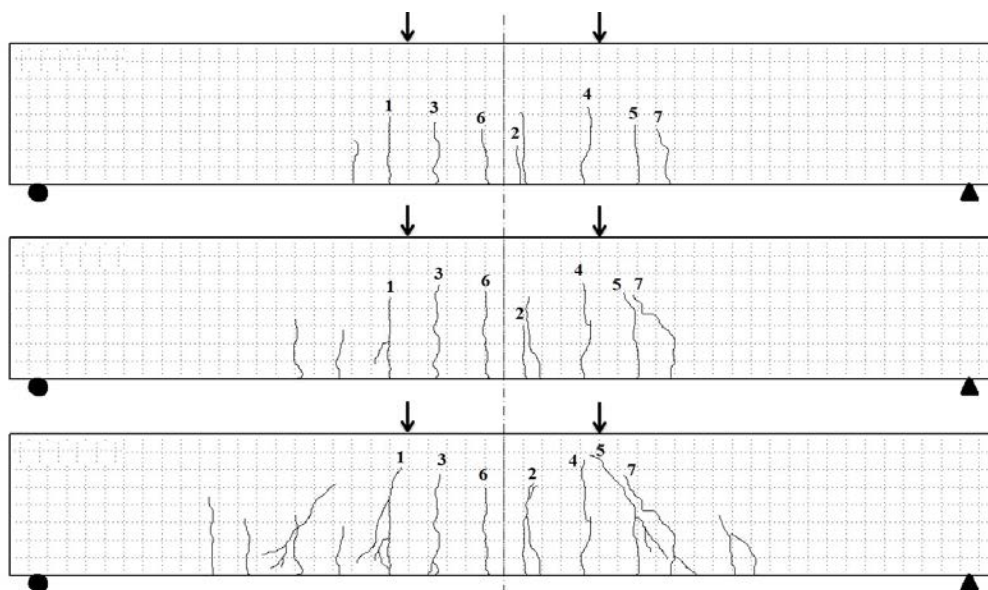
Figure 43: D80-SF-1
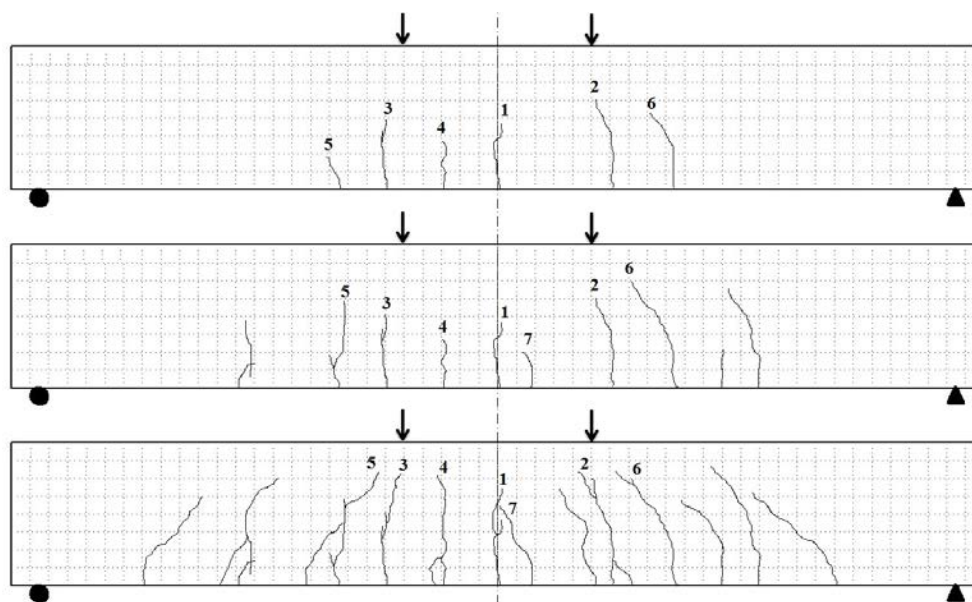
Figure 44: D80-SYF-1
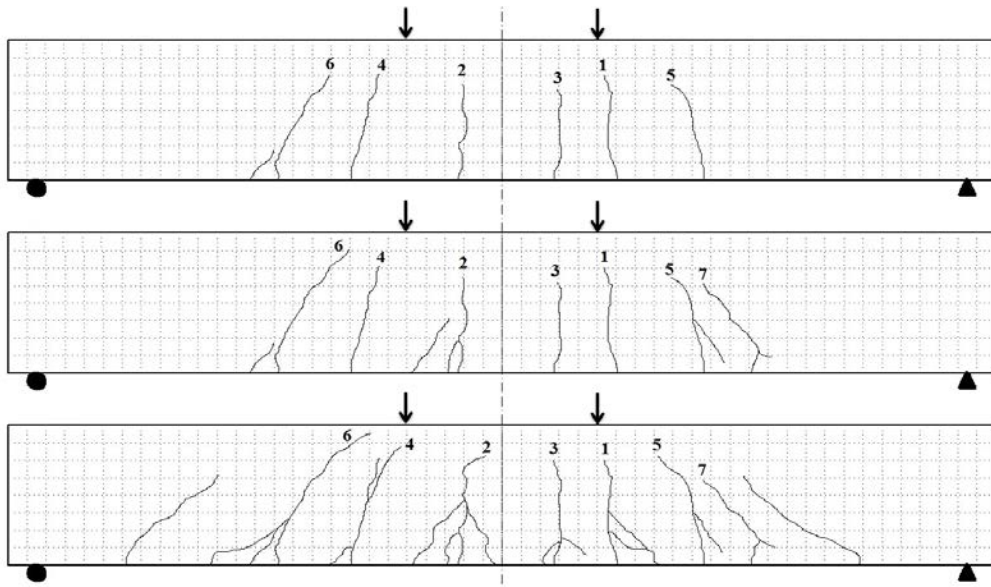
Figure 45: S50-NS-2
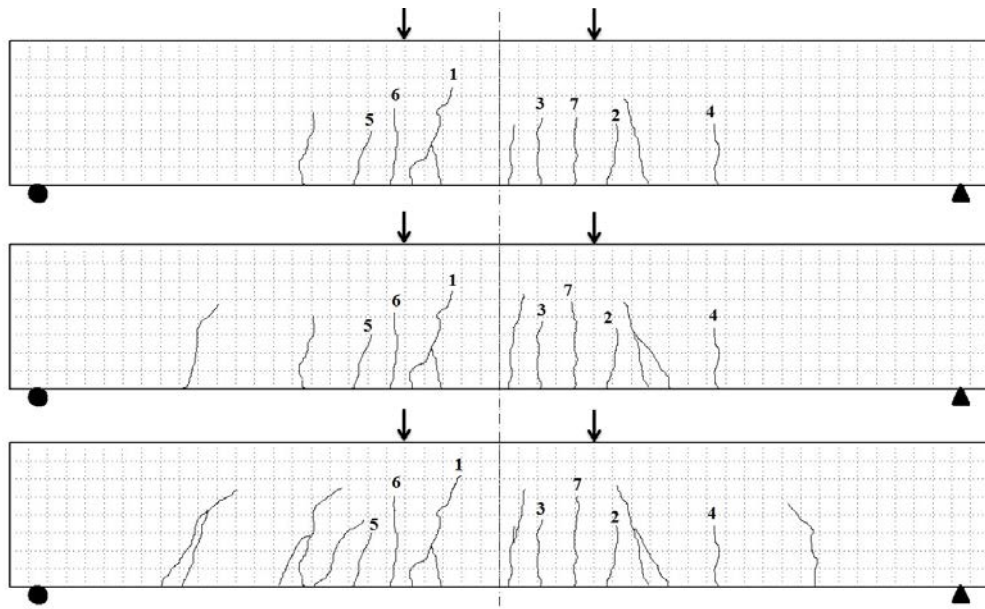
Figure 46: S50-SF-2
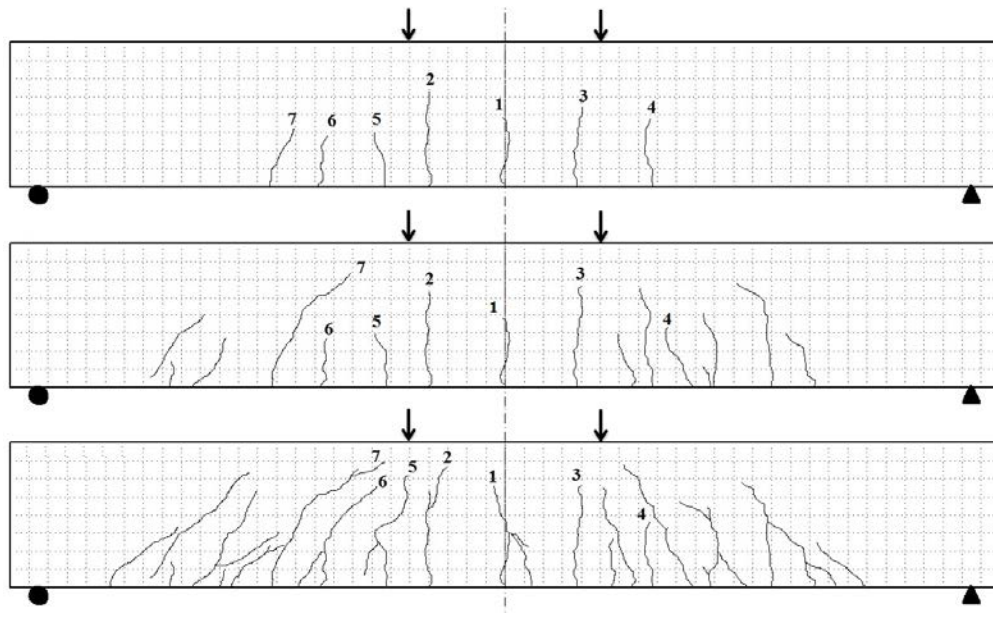
Figure 47: S50-SYF-2
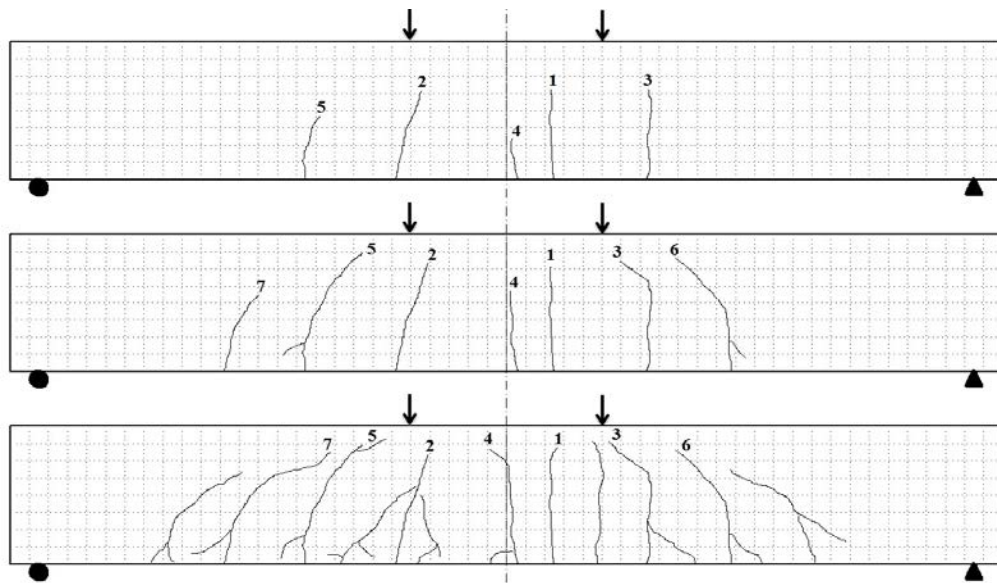
Figure 48: S80-NS-2
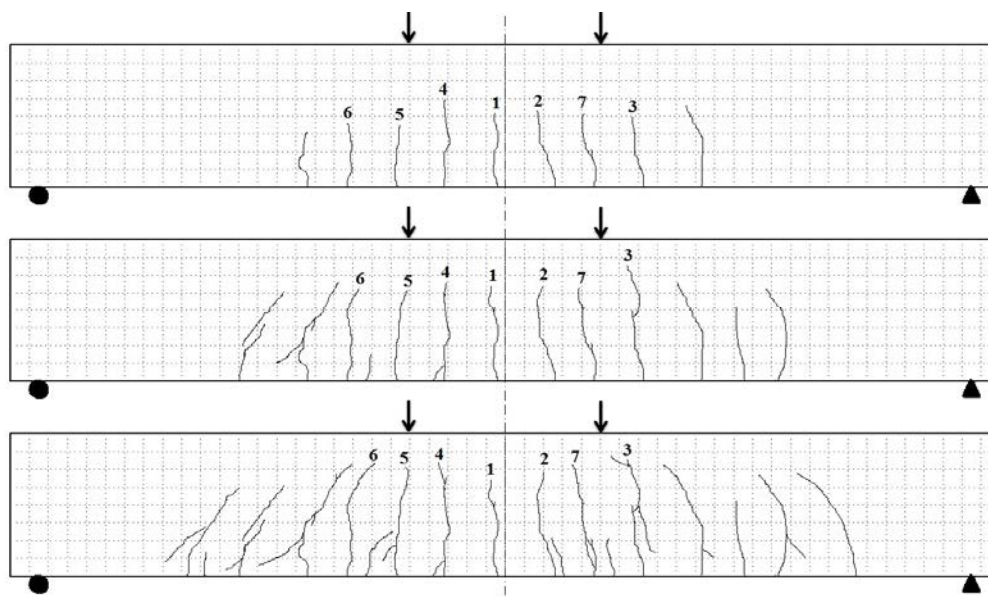
Figure 49: S80-SF-2
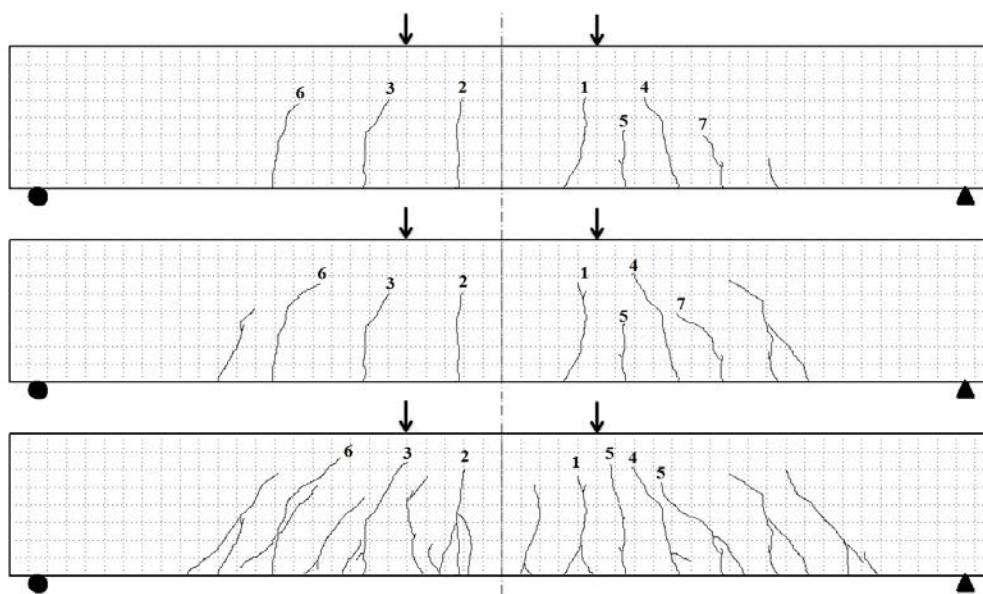
Figure 50: S80-SYF-2
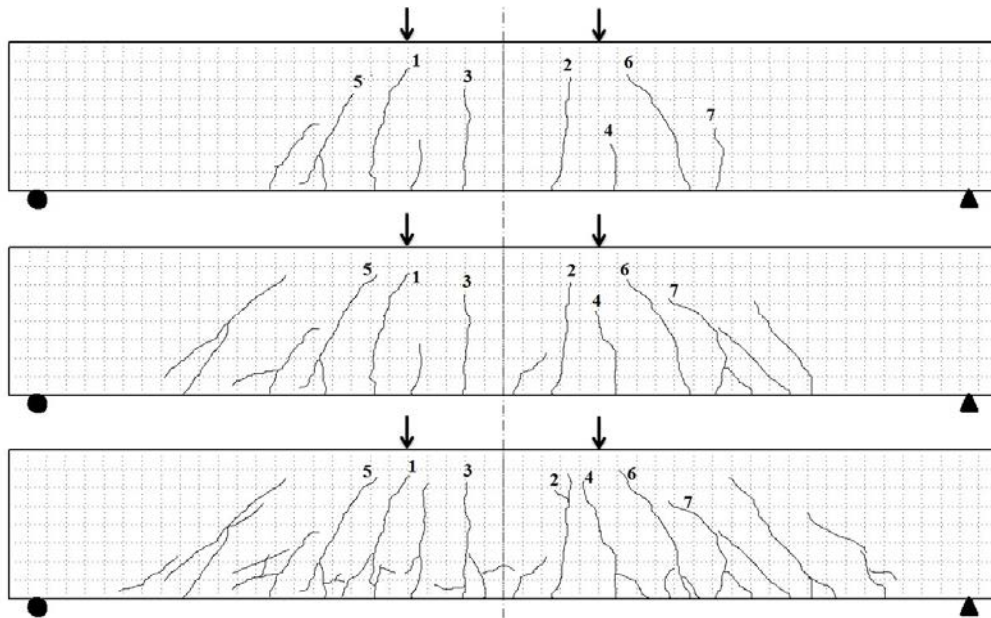
Figure 51: D50-NS-2
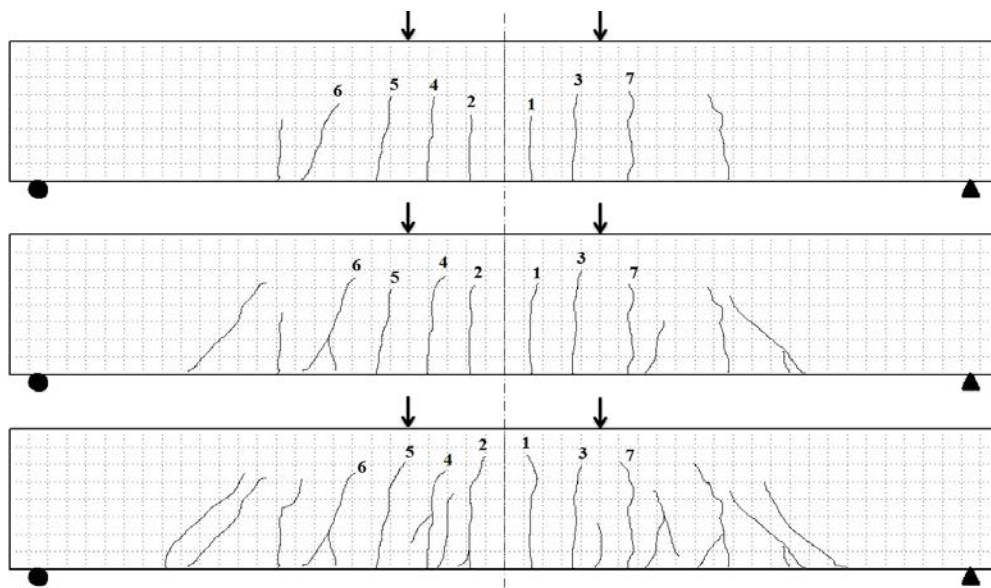
Figure 52: D50-SF-2
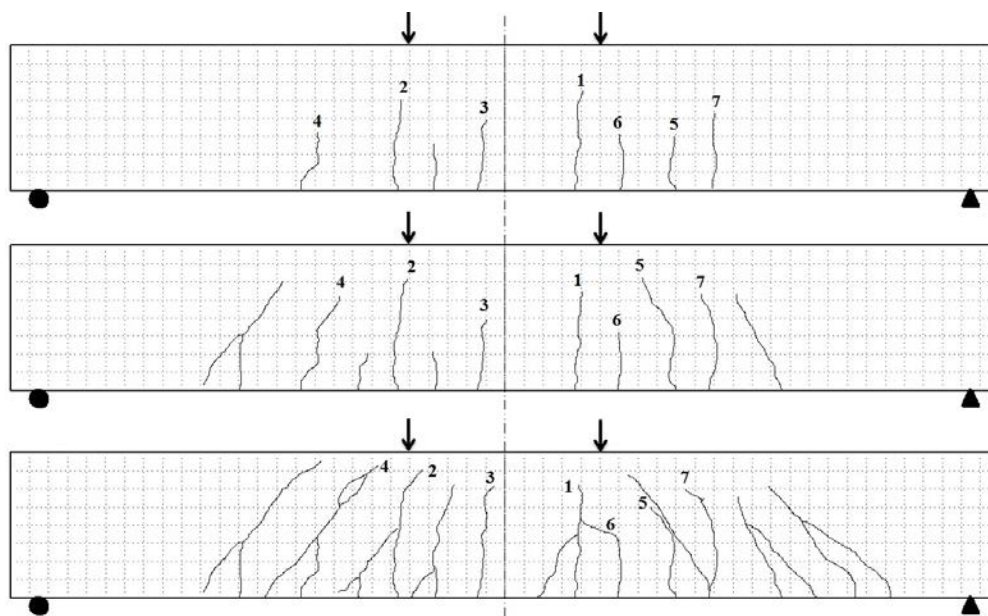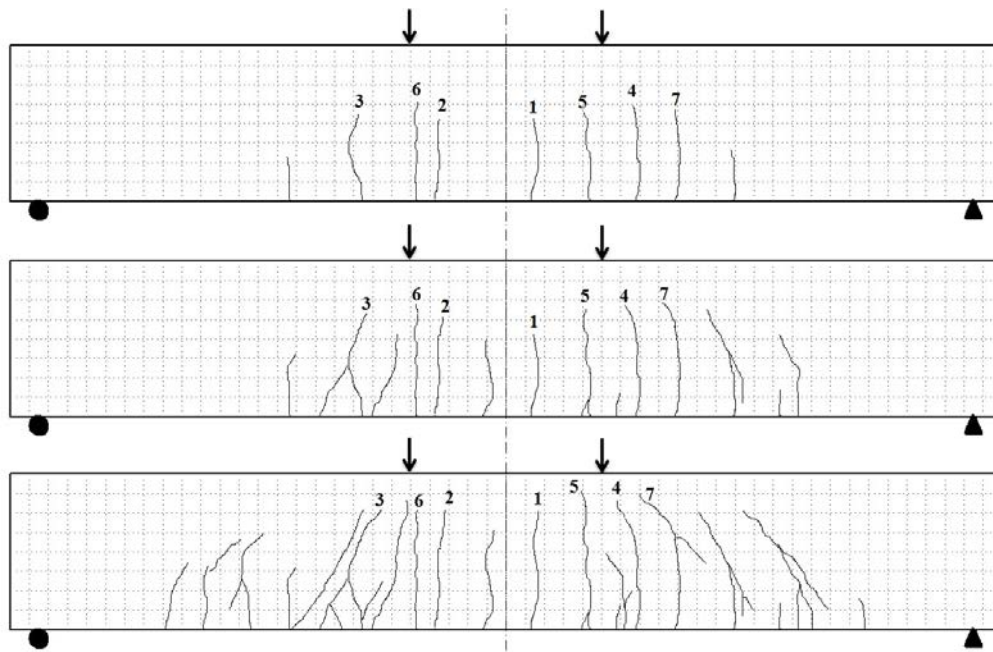
Figure 53: D50-SYF-1
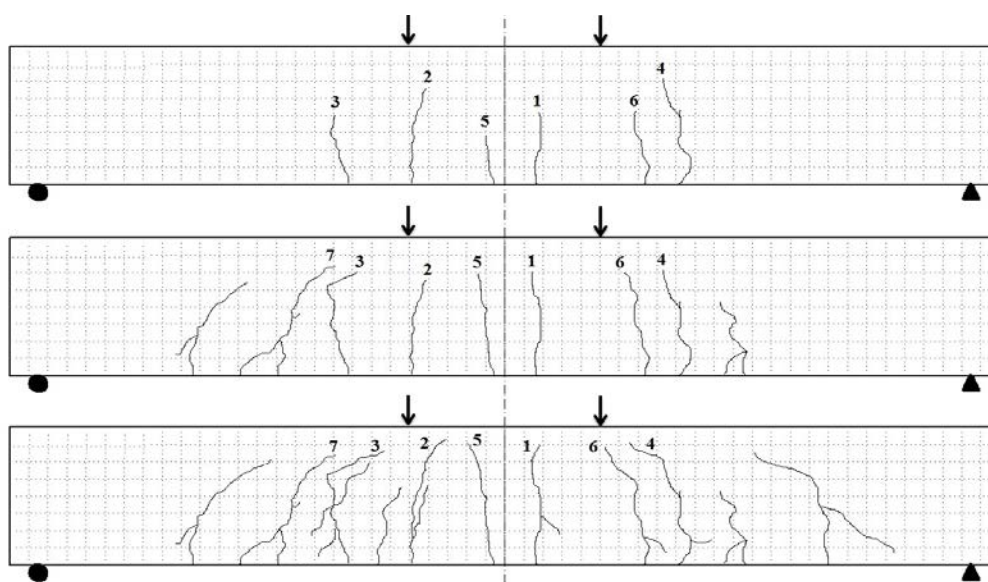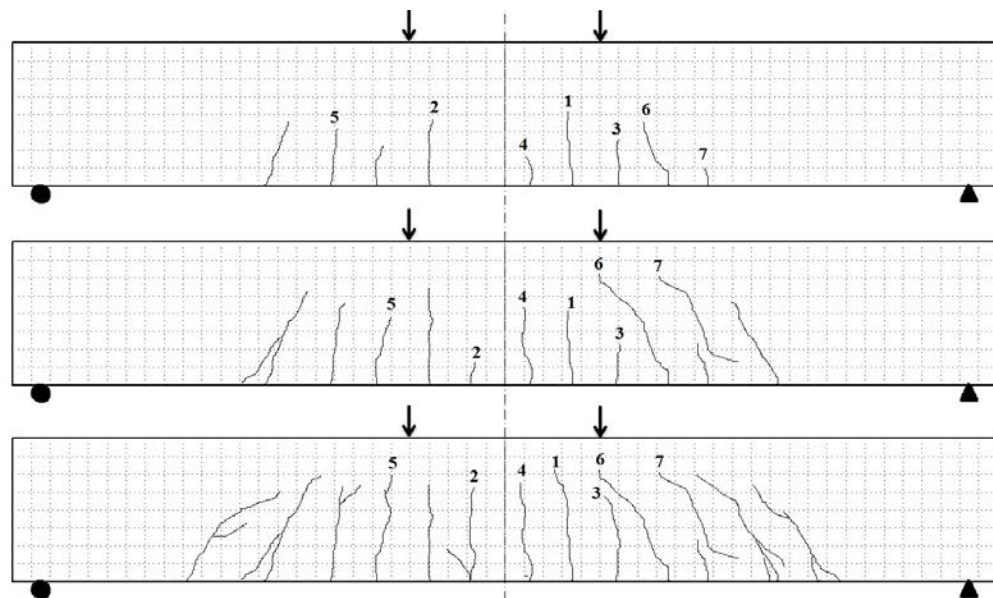

Figure 54: D80-NS-2

Figure 55: D80-SF-2

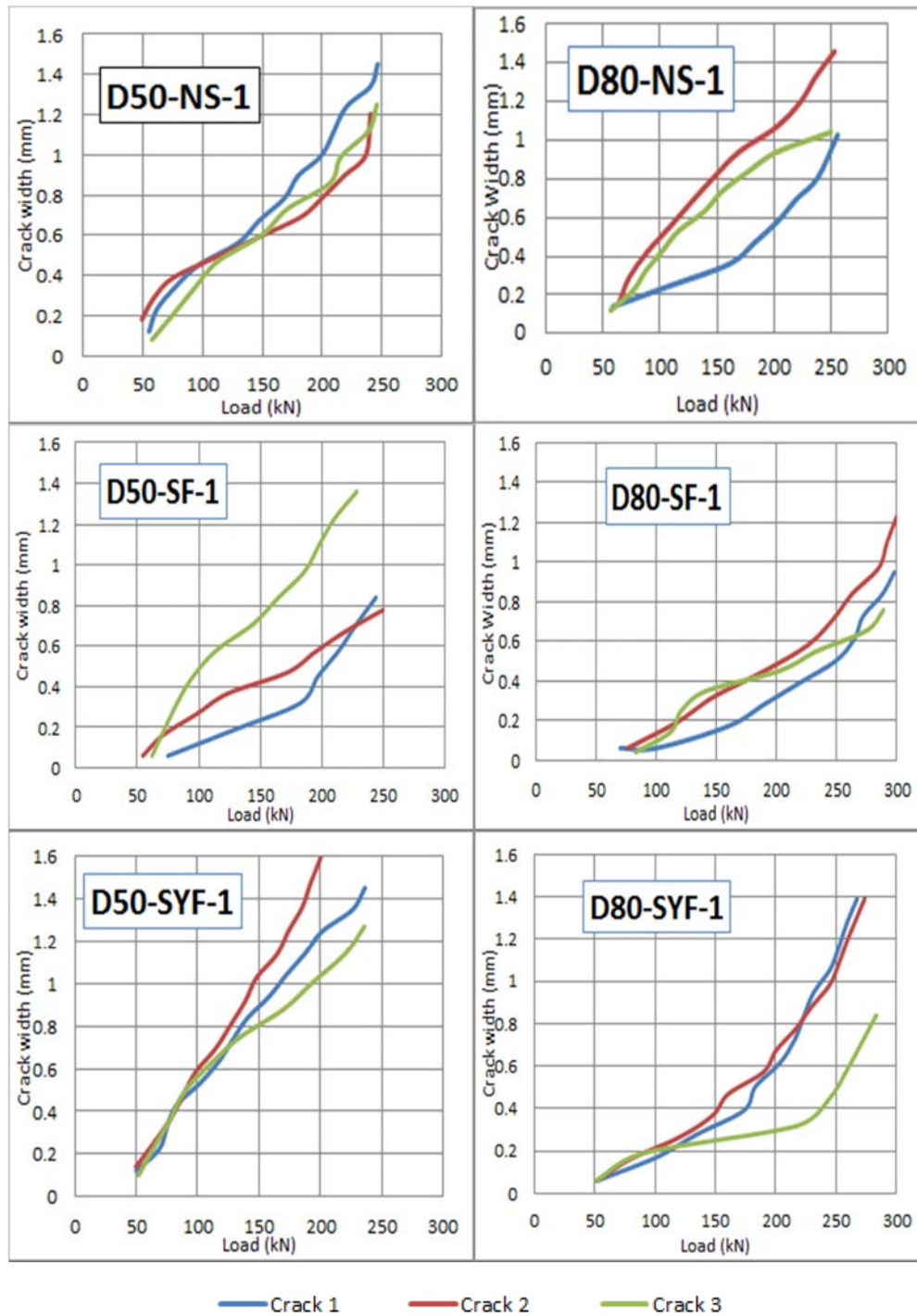**Figure 56: D80-SYF-2**

Appendix C

Figure 57: Crack width-load responses for D50-(NS, SF, and SYF)-1; and D80-(NS, SF, and SYF)-1
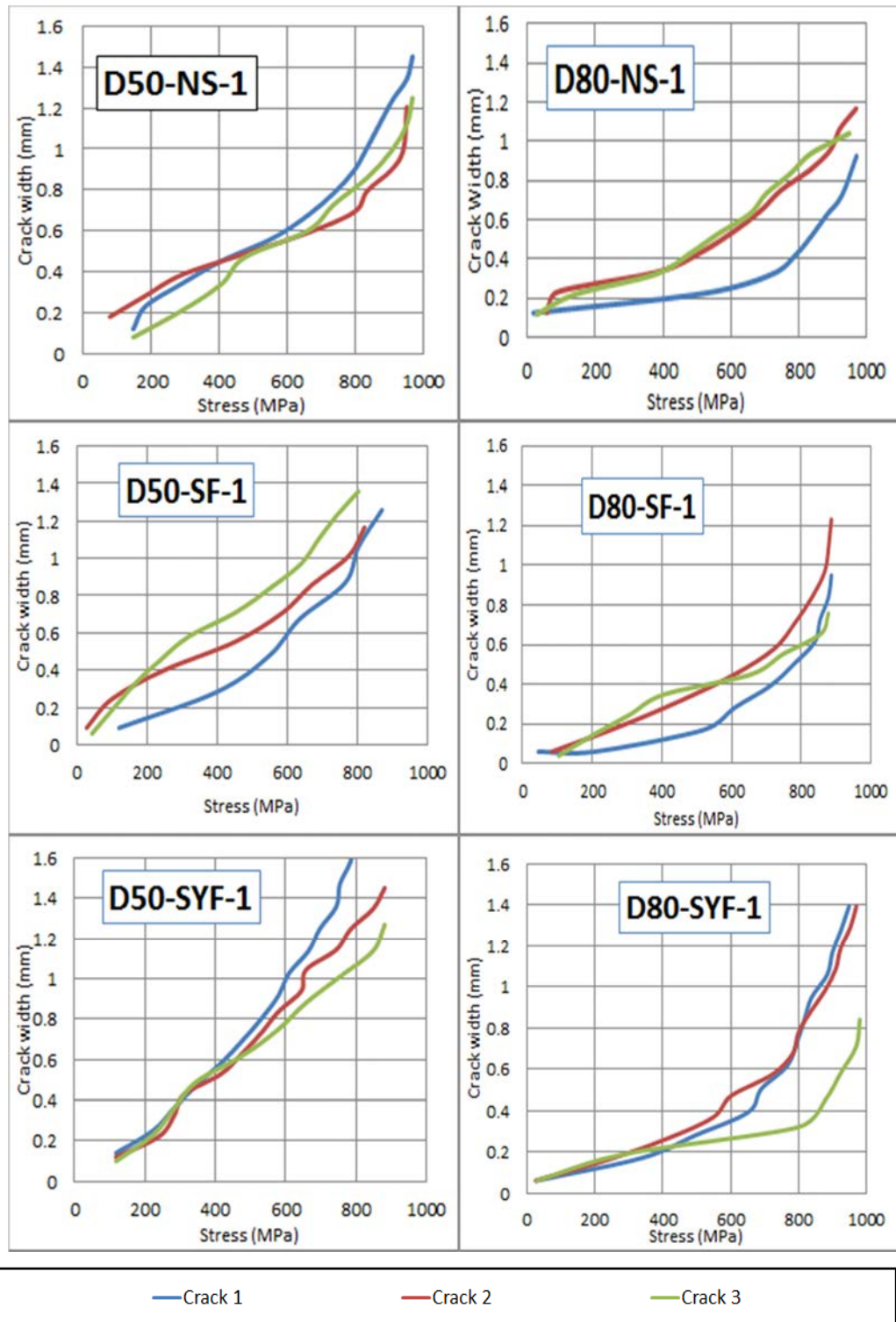
Figure 58: Crack width-stress in longitudinal reinforcement responses for D50-(NS, SF, and SYF)-1; and D80-(NS, SF, and SYF)-1
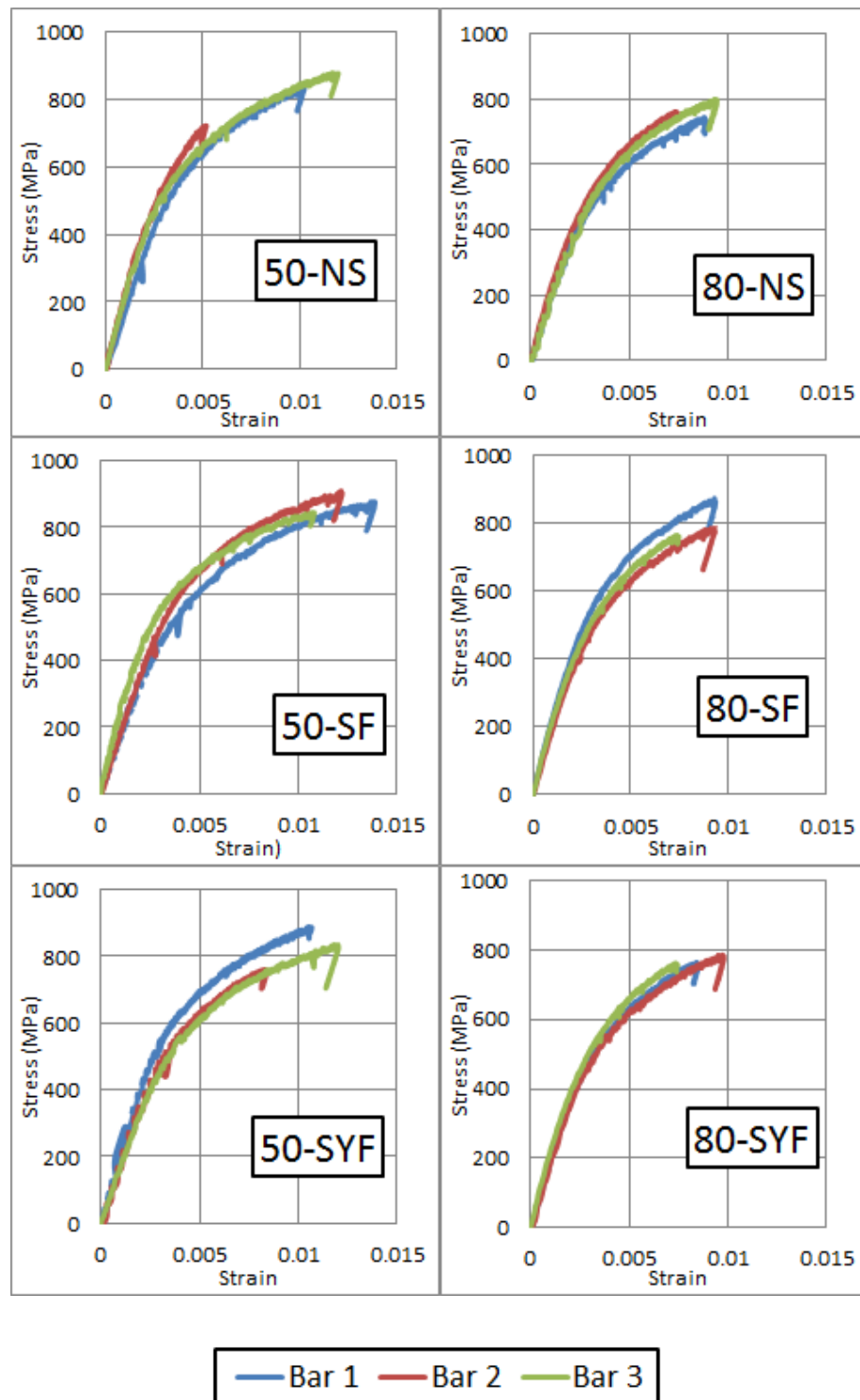
Appendix D

Figure 59: Load versus slip responses for the three HSS bars embedded in: 50-NS, 80-NS; 50-SF; 80-SF; 50-SYF; and 80-SYFpulltout blocks

Vita

Saif Maad Aldabagh was born in Baghdad, Iraq, on 5th of November, 1992. He received his high school diploma from Al Shola Private School in Sharjah in 2010. He graduated with a bachelor's degree in Civil Engineering (Cum laude) in 2014 from the American University of Sharjah, United Arab Emirates. He is currently a graduate research assistant at the department of Civil Engineering, at the American University of Sharjah. His research interests include large-scale experimental testing, composite materials and nonlinear finite element analysis.